

## ABSTRACT

Title of Document:

DEVELOPMENT OF ADVANCED  
NUMERICAL MODELS FOR VARIABLE  
GEOMETRY MICROCHANNEL HEAT  
EXCHANGERS

Long Huang, Doctor of Philosophy, 2014

Directed By:

Reinhard Radermacher, Professor  
Department of Mechanical Engineering

Air-to-refrigerant microchannel heat exchangers (MCHXs) are now extensively used in the heating, ventilation, air-conditioning and refrigeration (HVAC&R) industry. Numerical models are favored in the research and development process due to the fast calculation speed and lower cost as opposed to prototype development and testing. More recently, the evolving simulation and manufacturing capabilities have given the engineers new opportunities in pursuing complex and cost-efficient novel heat exchanger designs. Advanced heat exchanger modeling tools are desired to explore geometries out of conventional boundaries of design.

The current research and development of MCHXs has reached a plateau, in that, the optimum designs cannot be further improved with the limited number of geometry related design variables currently used. Freeing up the current MCHX uniform geometry restriction would lead to novel designs that address various design and applications objectives, such as performance enhancement, material reduction and space constraints.

This thesis presents the research, development and comprehensive validation of advanced heat exchanger models for microchannel heat exchangers. These new models include unprecedented modeling capabilities, with extensive consideration of various

underlying heat transfer and fluid flow phenomena. The proposed microchannel heat exchanger models are capable of simulating variable geometry microchannel heat exchangers with variable tubes, ports and fins while accounting for effects such as heat conduction, combined heat and mass transfer as well as air and refrigerant flow maldistribution, thus distinguishing itself as the cutting edge modeling tool in the open literature.

The models are validated against 247 MCHX experimental data points obtained from open literature, in-house laboratories and industry partners. This is the most comprehensive validation of microchannel heat exchanger models in open literature, including eight different fluids and eighteen different geometries. The validated model is then coupled with a multi-objective genetic algorithm to optimize the variable geometry heat exchangers to minimize material and envelope volume. The optimization study shows up to 35 percent reduction in material and 43 percent savings in envelope volume for the same performance compared to a baseline conventional geometry design. This research will help engineers to develop creative microchannel heat exchangers ultimately resulting in improved systems efficiency at lower costs.

DEVELOPMENT OF ADVANCED NUMERICAL MODELS FOR VARIABLE  
GEOMETRY MICROCHANNEL HEAT EXCHANGERS

By

Long Huang

Dissertation submitted to the Faculty of the Graduate School of the  
University of Maryland, College Park, in partial fulfillment  
of the requirements for the degree of  
Doctor of Philosophy  
2014

Advisory Committee:  
Dr. Reinhard Radermacher (Chair/Advisor)  
Dr. Christopher Cadou  
Dr. Jelena Srebric  
Dr. Bao Yang  
Dr. Amir Riaz  
Dr. Vikrant Aute

© Copyright by  
Long Huang  
2014

## Acknowledgements

I'd like to express my sincere gratitude to my advisor, Dr. Reinhard Radermacher for offering me the opportunity to carry out this thesis research at the Center for Environmental Energy Engineering. I benefited greatly from his advice, motivation, immense knowledge and innovative thoughts. I am also grateful to my committee members: Dr. Christopher Cadou, Dr. Jelena Srebric, Dr. Bao Yang, Dr. Amir Riaz and Dr. Vikrant Aute.

I would like to thank all CEEE students and staff for their continuous support during my stay at University of Maryland. A special thank you to Vikrant Aute, for his dedication in helping and pushing me to achieve the goals in my thesis research. I would also like to thank Hongtao Qiao for sharing his experience and knowledge with no reservations. Many thanks to Moon Soo Lee, Khaled Saleh and Daniel Bacellar for working with me on the CFD related projects. In addition, I'd like to acknowledge the support of Daikin Industries Ltd., for providing geometry details and experimental data for the heat exchangers referred in this thesis.

I thank my parents for their faith in me and their encouragement on pursuing this Ph.D. None of this would be possible without the love and patience from them. At the end, I'd like to express my appreciation to Qian Deng. Thank you for sharing your journey of life with me, as an excellent landscape architect, the fellow roadtripper and most importantly, my best friend and my wife.

## TABLE OF CONTENTS

1 Introduction.....	1
1.1 Background and Motivation .....	1
1.2 Literature Review of Steady State Heat Exchanger Modeling.....	6
1.2.1 Microchannel heat exchanger .....	6
1.2.2 Flow mal-distribution and header modeling.....	8
1.2.3 Heat conduction in heat exchanger core .....	12
1.2.4 Fluted tube coaxial heat exchanger.....	15
1.3 Summary of Background.....	18
1.4 Research Objectives.....	21
1.5 Completed Tasks and Thesis Organization.....	23
1.5.1 A model for air-to-refrigerant microchannel heat exchangers with variable tube and fin geometries.....	23
1.5.2 Microchannel heat exchanger modeling under dry, wet and partially wet surface conditions accounting for tube-to-tube heat conduction.....	24
1.5.3 A computational fluid dynamics and effectiveness-NTU based co-simulation approach for flow mal-distribution analysis in microchannel heat exchanger headers .....	25
1.5.4 Air flow distribution and design optimization of variable geometry microchannel heat exchangers.....	25
1.5.5 A finite volume coaxial heat exchanger model with moving boundaries and modifications to correlations for two-phase flow in fluted annuli.....	26

2 A Model for Air-to-Refrigerant Microchannel Heat Exchangers With Variable Tube and Fin Geometries.....	28
2.1 Concept of Variable Geometry .....	29
2.1.1 In-tube heat transfer and pressure drop.....	32
2.1.2 Air flow mal-distribution .....	33
2.1.3 Refrigerant flow mal-distribution .....	33
2.1.4 Heat conduction through fins.....	34
2.1.5 Material saving.....	34
2.1.6 Design requirements .....	35
2.2 Modeling Details.....	36
2.2.1 Basic solving methodology.....	36
2.2.2 Heat transfer equation at control volume.....	40
2.2.3 Three-stream effectiveness-NTU method.....	43
2.2.4 Wet surface condition .....	44
2.2.5 Hydraulic equation.....	45
2.2.6 Segment sub-division.....	45
2.3 Model Validation .....	46
2.3.1 Conventional geometry condenser data .....	49
2.3.2 Conventional geometry CO <sub>2</sub> gas cooler/condenser data.....	52
2.3.3 Variable geometry condenser data from industrial partner.....	55
2.3.4 Validation summary.....	57
2.4 Summary.....	58

3 Microchannel Heat Exchanger Modeling Under Dry, Wet And Partially Wet Surface Conditions Accounting For Tube-To-Tube Heat Conduction .....	60
3.1 Modeling Details.....	60
3.1.1 Basic solving methodology.....	60
3.1.2 Air-to-surface heat and mass transfer .....	62
3.1.3 Governing equations for refrigerant side control volume.....	69
3.2 Air-to-Fin Heat and Mass Transfer Model Comparison with CFD Simulation .....	71
3.2.1 CFD simulation.....	71
3.2.2 Dry fin surface comparison.....	73
3.2.3 Wet fin surface comparison .....	76
3.3 Model Validation .....	80
3.3.1 Validation results .....	80
3.3.2 Model comparison: effect of fin conduction.....	86
3.4 Summary.....	87
4 A Computational Fluid Dynamics and Effectiveness-NTU Based Co-Simulation Approach For Flow Mal-Distribution Analysis in Microchannel Heat Exchanger Headers .....	89
4.1 Effectiveness-NTU Based Segmented Microchannel Tube Model.....	89
4.2 CFD Header Modeling Details .....	94
4.3 CFD Header Model and Effectiveness-NTU Based Heat Exchanger Model Co-Simulation Methodology .....	94
4.4 Ten-Tube Microchannel Heat Exchanger Case Study.....	97
4.4.1 Heat exchanger modeling details.....	97

4.4.2 CFD header model .....	99
4.4.3 Results and discussions.....	100
4.5 Validation Against Experimental Data .....	107
4.5.1 Heat exchanger modeling details.....	107
4.5.2 CFD header model .....	108
4.5.3 Results and discussions.....	111
4.6 Summary .....	116
5 Air Flow Distribution and Design Optimization of Variable Geometry Microchannel Heat Exchangers .....	118
5.1 Automotive Condenser Optimization .....	118
5.1.1 R134a condenser optimization.....	120
5.1.2 R290 condenser validation.....	125
5.2 CO <sub>2</sub> Gas Cooler Optimization .....	127
5.3 Prediction of Air Flow Mal-distribution.....	131
5.4 Summary .....	135
6 A Finite Volume Coaxial Heat Exchanger Model With Moving Boundaries and Modifications to Correlations for Two-Phase Flow in Fluted Annuli.....	137
6.1 Model Description .....	137
6.1.1 Model overview .....	137
6.1.2 Segment level heat transfer model.....	140
6.1.3 Phase change tracking methods .....	142
6.2 Study on Segment Insertion/Sub-division Methods .....	150
6.3 Two-Phase Fluted Tube Annuli Correlation.....	155

6.4 Experimental Validation of Numerical Model and Proposed Correlation Formulations .....	161
6.5 Summary .....	166
7 List of Major Contributions and Future Work.....	168
7.1 Major Contributions.....	168
7.2 List of Publications .....	170
7.3 Future Work .....	172
References.....	174

## LIST OF TABLES

Table 1-1 Literature review of existing MCHX model and comparison with proposed model.....	20
Table 2-1 Condenser and gas cooler experimental data summary .....	48
Table 2-2 Geometry details of manufacture provided CG-MCHXs.....	50
Table 2-3 Selected correlations and correction factors for conventional geometry condenser validation.....	50
Table 2-4 Selected correlations and correction factors for conventional geometry CO <sub>2</sub> gas cooler/condenser validation .....	53
Table 2-5 Geometry details of manufacture provided VG-MCHXs .....	55
Table 2-6 Selected correlations and correction factors for industrial partner provided condenser data.....	56
Table 2-7 Validation summary and comparison of three approaches.....	58
Table 3-1 Summary of experimental data.....	80
Table 3-2 Selected correlations and correction factors for conventional and variable geometry evaporator data.....	83
Table 3-3 Validation summary and comparison of fin conduction assumptions.....	87
Table 4-1 Case study MCHX geometry parameters .....	98
Table 4-2 Summary of selected heat transfer and pressure drop correlations .....	98
Table 4-3 R134a automotive MCHX specifications.....	108
Table 5-1 Summary of selected heat transfer and pressure drop correlations .....	119
Table 5-2 Design variables of R134a microchannel condenser.....	122

Table 5-3 Comparison of baseline and optimized R134a variable geometry condenser design .....	124
Table 5-4 Comparison of baseline and optimized R290 variable geometry condenser design .....	126
Table 5-5 Summary of selected heat transfer and pressure drop correlations .....	127
Table 5-6 Design variables of CO <sub>2</sub> microchannel gas cooler .....	129
Table 5-7 Comparison of baseline and optimized CO <sub>2</sub> variable geometry gas cooler design .....	130
Table 6-1 Parameters of water-to-refrigerant CHX .....	150
Table 6-2 Fluid-dependent parameter based on Kandlikar (1991) .....	161
Table 6-3 Geometric parameters of brine-to-refrigerant fluted tube CHX.....	162
Table 6-4 Test conditions of brine-to-refrigerant fluted tube CHX.....	163
Table 6-5 Selected correlations for brine-to-refrigerant fluted tube CHX .....	163

## LIST OF FIGURES

Figure 1-1 Microchannel tube cross-section.....	1
Figure 1-2 Microchannel heat exchangers.....	2
Figure 1-3 Coaxial heat exchangers.....	2
Figure 1-4 Fluted tube design.....	6
Figure 2-1 Standard configuration MCHX.....	30
Figure 2-2 Variable geometry MCHX.....	30
Figure 2-3 Standard multi-slab MCHX.....	31
Figure 2-4 Variable geometry multi-slab MCHX.....	32
Figure 2-5 Example of refrigerant side computation sequence for a 35 tube MCHX.....	38
Figure 2-6 Air flow propagation example.....	39
Figure 2-7 Solution methodology for proposed model.....	40
Figure 2-8 Port segment of proposed model.....	41
Figure 2-9 Control volume configuration.....	41
Figure 2-10 Validation of conventional geometry condensers.....	52
Figure 2-11 Validation of conventional geometry CO <sub>2</sub> gas coolers/condensers.....	54
Figure 2-12 Validation of variable geometry condensers.....	57
Figure 3-1 Air side discretization.....	61
Figure 3-2 Solution methodology for proposed model.....	62
Figure 3-3 Adiabatic fin tip air/fin segment.....	64
Figure 3-4 Prescribed temperature air/fin segment.....	65
Figure 3-5 Partially wet adiabatic fin tip air/fin segment.....	68
Figure 3-6 Partially wet prescribed temperature air/fin segment.....	69

Figure 3-7 Refrigerant side control volume.....	69
Figure 3-8 CFD Computational domain a) Boundaries; b) Mesh view of top tube .....	72
Figure 3-9 Fin temperature distribution: top wall 350.15 [K], bottom wall 350.15 [K] ..	74
Figure 3-10 Air temperature distribution: top wall 350.15 [K], bottom wall 350.15 [K]	75
Figure 3-11 Fin temperature distribution: top wall 340.15 [K], bottom wall 350.15 [K]	76
Figure 3-12 Air temperature distribution: top wall 340.15 [K], bottom wall 350.15 [K]	76
Figure 3-13 Fin temperature distribution: top wall 278.15 [K], bottom wall 278.15 [K]	77
Figure 3-14 Air temperature and humidity ratio distribution: top wall 278.15 [K], bottom wall 278.15 [K].....	78
Figure 3-15 Fin temperature distribution: top wall 278.15 [K], bottom wall 280.15 [K]	78
Figure 3-16 Air temperature and humidity ratio distribution: top wall 278.15 [K], bottom wall 280.15 [K].....	79
Figure 3-17 Validation of conventional geometry condensers.....	82
Figure 3-18 Validation of variable geometry condensers.....	82
Figure 3-19 Validation of microchannel evaporators.....	85
Figure 4-1 MCHX top level illustration and tube level view .....	91
Figure 4-2 Refrigerant flow distribution top level solver flow chart.....	93
Figure 4-3 MCHX face view and co-simulation concept illustration.....	95
Figure 4-4 Proposed co-simulation solving methodology .....	96
Figure 4-5 Ten-tube MCHX inlet header mesh .....	100
Figure 4-6 Pressure contours, velocity magnitude contours and mass flow distributions of the ten-tube hot water MCHX case studies.....	103

Figure 4-7 Pressure contours, velocity magnitude contours and mass flow distributions of the ten-tube R134a microchannel condenser case studies .....	106
Figure 4-8 Cross-section view of R134a automotive condenser inlet header .....	109
Figure 4-9 R134a automotive microchannel condenser inlet header mesh .....	111
Figure 4-10 Comparison between experimental data and simulated results.....	113
Figure 4-11 Pressure contours, velocity magnitude contours and mass flow distributions of the R134a automotive microchannel condenser validation case (Refrigerant inlet pressure=979 [kPa], inlet temperature=338 [K], mass flow rate=29.5 [g/s]).....	115
Figure 5-1 Model validation for a conventional geometry automotive condenser.....	120
Figure 5-2 Top-bottom velocity distribution profile.....	121
Figure 5-3 Optimization results of R134a condenser under uniform air flow.....	123
Figure 5-4 Optimization results of R134a condenser under non-uniform air flow .....	124
Figure 5-5 Optimization results for R290 condenser under uniform air flow .....	125
Figure 5-6 Optimization results of R290 condenser under non-uniform air flow .....	127
Figure 5-7 Capacity validation for conventional geometry CO <sub>2</sub> gas cooler.....	128
Figure 5-8 Optimization results of CO <sub>2</sub> gas cooler under uniform air flow .....	130
Figure 5-9 Optimization results of CO <sub>2</sub> gas cooler under non-uniform air flow .....	131
Figure 5-10 Air flow distribution for variable geometry microchannel heat exchanger	132
Figure 5-11 Air distribution solving methodology .....	133
Figure 5-12 Optimization results of CO <sub>2</sub> gas cooler under uniform and non-uniform air flow distribution.....	134
Figure 6-1 Fluted tube geometry.....	138
Figure 6-2 Model main solving methodology .....	139

Figure 6-3 Segment insertion techniques.....	144
Figure 6-4 Parallel flow configuration segment insertion method .....	146
Figure 6-5 Counter flow configuration segment insertion method.....	147
Figure 6-6 Segment subdivision method .....	149
Figure 6-7 Sensitivity study of heat load on number of segments, parallel flow case (No segment insertion/subdivision) .....	152
Figure 6-8 Comparison of segment insertion methods on heat load deviations, parallel flow case.....	152
Figure 6-9 Comparison of segment insertion methods on computation time, parallel flow case.....	153
Figure 6-10 Sensitivity study of heat load on number of segments, counter flow case (No segment insertion/subdivision) .....	154
Figure 6-11 Comparison of segment insertion/subdivision methods on heat load deviations, counter flow case .....	155
Figure 6-12 Comparison of segment insertion methods on computation time, counter flow case.....	155
Figure 6-13 Comparison between simulation and experimental heat load for brine-to-refrigerant condenser .....	164
Figure 6-14 Comparison between simulation and experimental pressure drop for brine-to-refrigerant condenser .....	165
Figure 6-15 Comparison between simulation and experimental heat load for brine-to-refrigerant evaporator.....	165

Figure 6-16 Comparison between simulation and experimental pressure drop for brine-to-refrigerant evaporator..... 166

## NOMENCLATURE

$A$	surface area [m <sup>2</sup> ]
$Bo$	boiling number [dimensionless]
$C$	heat capacity rate [W·K <sup>-1</sup> ]
$C^*$	heat capacity rate ratio [dimensionless]
$C_0$	connection number [dimensionless]
$C_p$	specific heat [J·kg <sup>-1</sup> ·K <sup>-1</sup> ]
$D$	diameter [m]
$DP$	pressure drop [Pa]
$e$	flute depth [m]
$F$	frictional loss coefficient [dimensionless]
$F_{fl}$	fluid-dependent parameter [dimensionless]
$Fr$	Froude number [dimensionless]
$G$	mass flux [kg·s <sup>-1</sup> ·m <sup>-2</sup> ]
$H$	header
$h$	enthalpy [J·kg <sup>-1</sup> ]
$ID$	inner diameter [m]
$k$	thermal conductivity [W·m <sup>-1</sup> ·K <sup>-1</sup> ]
$L$	fin height [m]/length [m]
$\dot{m}$	mass flow rate [kg·s <sup>-1</sup> ]
$NTU$	number of transfer units [dimensionless]
$Nu$	Nusselt number [dimensionless]
$P$	perimeter [m]/pressure [Pa]

$p$	flute pitch [m]
Pr	Prandtl number [dimensionless]
$Q$	heat transfer rate [W]
$R$	absolute thermal resistance [ $\text{K}\cdot\text{W}^{-1}$ ]
Re	Reynolds number [dimensionless]
$r^*$	radius ratio [dimensionless]
$S$	stream
$T$	temperature [K]
$\Delta T$	temperature difference [K]
$U$	heat transfer coefficient [ $\text{W}\cdot\text{m}^{-2}\cdot\text{K}^{-1}$ ]
$u$	velocity [ $\text{m}\cdot\text{s}^{-1}$ ]
$V$	volume [ $\text{m}^3$ ]
We	Weber number [dimensionless]
$x$	position [m] or quality [dimensionless]
$\Delta x$	distance [m]

***Greek letters***

$\alpha$	local heat transfer coefficient [ $\text{W}\cdot\text{m}^{-2}\cdot\text{K}^{-1}$ ]
$\alpha_d$	local mass transfer coefficient [ $\text{m}\cdot\text{s}^{-1}$ ]
$\delta$	thickness [m]
$\varepsilon$	effectiveness [dimensionless]
$\eta$	fin efficiency [dimensionless]

$\theta$	excess temperature [K]/ helix angle [ $^{\circ}$ ]
$\mu$	dynamic viscosity [Pa·s]
$\rho$	density [ $\text{kg}\cdot\text{m}^{-3}$ ]
$\omega$	humidity ratio [ $\text{kg vapor} \cdot \text{kg dry air}^{-1}$ ]
$\varphi$	two-phase multiplier [dimensionless]

### *Subscripts*

c	cross-section
CBD	convective boiling dominant
cond	condensation
cr	critical point
e	end
eff	effective
evap	evaporation
g	gas
h	hydraulic
i	intermediate
in	Inlet
inner	inner port
l	liquid
lo	liquid only
max	maximum

min	minimum
NBD	nucleate boiling dominant
o	total
out	outlet <sup>o</sup>
ref	refrigerant
wall	tube wall

# 1 INTRODUCTION

## 1.1 Background and Motivation

Air-to-refrigerant heat exchangers (HXs) are an essential component of almost all air-conditioning, refrigeration and heat pumping systems. Tube-fin heat exchangers (TFHXs) and microchannel heat exchangers (MCHXs) are the most common types of air-to-refrigerant HXs. MCHXs are gaining grounds in HVAC&R industry due to their high material utilization and enhanced heat transfer performance. Typically, MCHXs employ flat tubes with 1-2.5 mm hydraulic diameter flow channels (Kandlikar, 2007) as shown in Figure 1-1. Several MCHX configurations are shown in Figure 1-2.

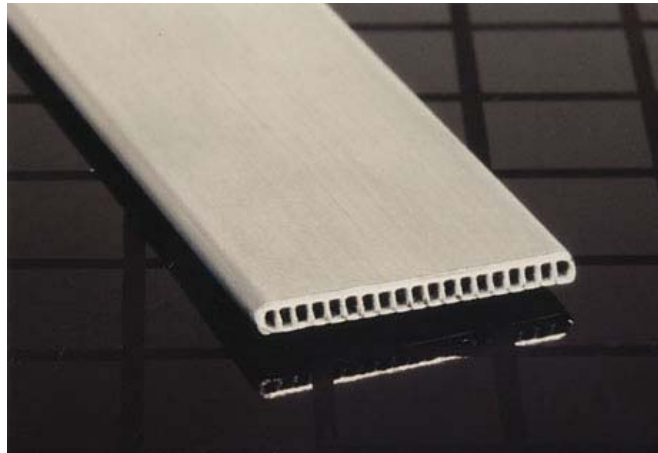


**Figure 1-1 Microchannel tube cross-section**  
([http://www.nsf.gov/pubs/2002/nsf01168/nsf01168ff\\_photo\\_02.htm](http://www.nsf.gov/pubs/2002/nsf01168/nsf01168ff_photo_02.htm))



**Figure 1-2 Microchannel heat exchangers**

<https://www.sanhuaeurope.com/es/en/products/sanhua-mche/micro-channel-heat-exchanger-mche>

In addition to the air-to-refrigerant heat exchangers, fluid-to-fluid heat exchangers are also applied extensively in water source heat pump systems and secondary-loop systems serving as evaporators, condensers and heat recovery units. One type of fluid-to-fluid heat exchanger is the coaxial tube (tube-in-tube) heat exchanger. It consists of one inner tube and one or more outer flow channel(s), coaxial heat exchangers as shown in Figure 1-3 is the most common fluid-to-fluid heat exchangers.



**Figure 1-3 Coaxial heat exchangers**

<http://www.packless.com/catalog/CategoryListView.aspx?id=10>

Numerical simulations save significant engineering time as compared the traditional time-consuming HX development approach of designing and testing prototypes, and are thus extensively applied in design and performance evaluation. The emerging needs of simulation based research and development of new generation of HXs is an opportunity for HX modeling research. With the aid of advanced HX simulation tools, the engineers are able to simulate the most flexible designs of HXs, which would allow the engineers to further push the HX technology envelope.

There are two types of HX models: steady-state models, which focus on accurate performance prediction, or transient models that aim at control logic development for the system. The focuses of this research are on steady state models of variable geometry air-to-refrigerant MCHXs and fluid-to-fluid fluted tube CHXs.

Most of earlier MCHX modeling efforts focus on fast prediction of the overall performance using lumped control volume while ignoring certain important phenomena such as phase distribution and tube-to-tube conduction within the MCHX. Recent studies have tried to tackle some of the complicated phenomena by means of time-consuming simulation methods based on refined control volumes. In general, previous MCHX modeling work aimed at either the overall performance and/or only one of the important phenomena but overlooked a) simultaneous effects b) capability of designing improved geometries c) validity of the assumptions and calculation speed and (d) generalization to different applications such as evaporators and condensers and different working fluids. Furthermore, none of the previous work focused on novel and generalized heat exchanger configurations such as arbitrary geometric parameters while considering most of the important factors using refined control volume.

MCHXs use headers to mix and distribute the working fluid into individual microchannels. The uneven flow distribution (i.e., mal-distribution) leads to system capacity degradation is one of the challenges in the adoption of MCHXs. Mueller & Chiou (1988) concluded that there are four types of flow mal-distribution and the causes are: 1) mechanical design of headers and the inlet ducts; 2) self-induced mal-distribution caused by the heat transfer process; 3) gas-liquid flow phase separation in headers; 4) fouling and corrosion. While the fouling and corrosion effects are extremely challenging to predict numerically, the modeling of the first three effects have been attempted using simplified assumptions. There lacks an unified approach than can predict the actual flow behavior in the header, at the same time, can study the fluid flow into each individual microchannel ports, with no restrictions of header dimensions, fluid phase, heat transfer and phase change in the headers and tubes.

The heat conduction within the heat exchanger is a detrimental effect. The traditional mitigation approach in tube-fin heat exchangers (TFHXs) to such is to perform fin cuts to avoid conduction from tube to tube. For MCHXs considering the geometric and heat transfer characteristics, one should look at the heat conduction between refrigerant passes. A comprehensive conduction model would address the heat conduction while considering all three possible surface conditions: dry, wet and partially wet.

The current research and development of conventional geometry MCHXs has reached a plateau that the designs cannot be improved through optimization given the limited number of design variables. The flow distribution and heat conduction issues have been addressed up to some extent, but the solutions to such issues are sparse. The

variable geometry microchannel heat exchanger (VG-MCHX) concept, studied in this research, could be one of the potential solutions to expand the application envelope of the MCHX technology. Such an innovative design allows the MCHXs to have variable fin types, fin densities, tube heights, tube widths, port widths and heights, tubes per bank, tube vertical spacing and horizontal spacing etc. In addition to the variable physical parameters, the positions of tubes, fins and fin cuts are specified individually. Such designs can mitigate the negative effects by means of geometric variation. Last but not the least, VG-MCHX designs can be easily customized to meet certain design requirements. An advanced VG-MCHX model is desired to assist the engineers in exploring the optimum designs with enhanced heat transfer and reduced material cost.

The modern designs of CHX apply the fluted tube as the inner tube (shown in Figure 1-4) which has significant heat transfer enhancement. A CHX is comprised of one or more inner tube(s) and one outer tube. The size and design of the CHXs varies in different applications. In general, refrigerant flows through the outer tube while water or brine flows through the inner tube(s). Counter-flow configuration is favored in most of the designs because of its high efficiency compared to parallel-flow configuration. Helical wound configurations are commonly adopted in CHX designs due to its advantage of compactness and better heat transfer coefficients. However, a large pressure gradient is introduced as compared to the straight tube CHX arrangement. Since the heat transfer performance of CHX is significantly related to the inner tube design, various tube types have been used in CHX products such as smooth tube, micro-finned tube, corrugated tube and fluted tube, etc. Most of previous CHX models are based on lumped models or moving boundary models, which are simplified and lack

several details and accuracy. A detailed CHX model is needed to simulate various flow conditions, flow configurations, coil configurations and tube geometries. Due to the limited data on two-phase flow in such heat exchanger geometries, there are no suitable two-phase correlations to simulate the heat transfer and pressure drop of refrigerant in the fluted outer annulus. Considering the substantial difference in geometry and flow behavior between straight tube and fluted tube, new two-phase fluted tube annulus correlation formulations are necessary in order to accurately predict the thermal and hydraulic performance of CHXs with fluted tube geometry.



**Figure 1-4 Fluted tube design**  
(<http://www.packless.com/products/condenser-coils.htm>)

## **1.2 Literature Review of Steady State Heat Exchanger Modeling**

### **1.2.1 Microchannel heat exchanger**

The development of HX simulation models started in the early 60s of the twentieth century. The heat exchanger model developed by Herman (1962) is one of the earliest effort that integrated mathematical heat exchanger models and computer technology. Most of the MCHX simulation models sprung up after year 2000 when such type of heat exchanger was widely adopted in automotive radiator and condenser applications, as well as gas coolers in supercritical CO<sub>2</sub> cooling systems. The fundamental set of equations used in the previous MCHX models can be categorized

into two classes: energy equations and effectiveness-NTU equations (Kays & London, 1984). Energy equation method employs energy conservation laws in the control volume. In general, these equations are solved iteratively to obtain the outlet conditions of the fluids. Alternatively, effectiveness-NTU method, which does not require iteration, can be employed. Both methods require estimation of fluid properties, heat transfer coefficients and heat transfer areas.

Yin *et al.* (2001) developed a finite-volume first principles based CO<sub>2</sub> gas cooler model. Empirical correlations were used to predict the heat transfer coefficients, pressure drop and fin efficiency. The model is shown to predict capacity within 2 percent of the experimental values. Kim & Bullard (2001), Yun *et al.* (2007) and Jin *et al.* (2011) presented several CO<sub>2</sub> microchannel evaporator models for automotive applications. Energy and mass conservation principles are applied under wet surface condition. In their presented validation, these evaporator models yield to less than 10% deviation on overall heat capacity. However, the condensation prediction of Kim & Bullard's model has a Root Mean Square (RMS) error of 13.1% and the sensible heat capacity prediction's mean deviation by Yun *et al.* is 17.3%. These indicate that the dehumidification phenomenon is not sufficiently captured in these two CO<sub>2</sub> evaporator models. Although the same model discretization approach and fundamental equations were applied, Jin's model reported lower RMS error of the calculated condensation rate ( $\pm 8.2\%$ ). The use of separate air-side heat transfer correlations for dry and wet conditions could be the main contribution to this improvement. Asinari *et al.* (2004) studied the heat conduction effect based on a microchannel gas cooler model. The

model adopted a hybrid finite-volume and finite-element approach to model the fin performance.

Effectiveness-NTU method is proven to be an efficient and robust method and has been used in many of the MCHX models (Jiang, 2003; Schwentker *et al.*, 2005; Shao *et al.*, 2009; Brix *et al.*, 2009; Brix *et al.*, 2010; García-Cascales *et al.*, 2010; Tuo *et al.*, 2012). Schwentker *et al.* (2005) and García-Cascales *et al.* (2010) discretized the model on a per tube base. The heat transfer and pressure drop in the ports are assumed uniform within the tube. The R134a and R410A condenser experimental validations demonstrated that such approach is computationally fast and accurate. Brix *et al.* (2009, 2010) performed parametric studies on refrigerant mass flow rate, quality distribution and air-side flow distribution based on a simplified MCHX model. The control volume (segment-by-segment) has been refined from tube to single port in two of the recent publications (Shao *et al.*, 2009 and Ren *et al.*, 2013). The serpentine type microchannel condenser model by Shao *et al.* (2009) is the first MCHX model that adopted port-by-port calculation. Three dimensional heat conduction terms are integrated into the fundamental equation set. However, the effectiveness-NTU method applied in this model is derived based on the no heat loss assumption. In addition, the fin efficiency correlation used in this model is developed based on adiabatic fin tip assumption. The heat conduction formulation is contradictory to the assumption of effectiveness-NTU method and the fin efficiency correlations.

### 1.2.2 Flow mal-distribution and header modeling

The refrigerant distribution in parallel flow MCHX has been experimentally studied. Several refrigerants and different header geometries have been tested by researchers. Most of the previous researches are focused on flow distribution

improvement with different header shapes and inlet arrangements. Cho *et al.* (2003) identified that the header orientation was the most important factor affecting flow distribution in MCHXs. A study on phase separation and distribution in headers has been published by Vist & Pattersen (2004). The authors proposed using a short inlet tube to enhance the vapor and liquid distribution in the headers. Hrnjak (2004) presented three methods for the study of mal-distribution: infrared imaging, frost accumulation and exit air temperature profile. To reduce the mal-distribution, he suggested placing the inlet and outlet header on the opposite side of the heat exchanger with single-phase fluid and creating a misty flow with extremely small droplet sizes in the headers with two-phase fluid. Poggi *et al.* (2009) studied single-phase flow behavior in a vertical header. The experimental test showed that the pressure drop in the flow channels is greater than the header pressure drop by a ratio of 10. Severe flow maldistribution was not found in this test for single-phase HydroFluoroEther 7100 and water. Ren and Hrnjak (2013) correlated the single-phase pressure drop in D shaped headers of both heat exchanger inlet and outlet. The correlation is capable of predicting the pressure difference between each channels. Jin (2006) observed that the quality mal-distribution was more severe than the mass flow mal-distribution. Hwang *et al.* (2007) recommended placing the inlet connecting tube in the center of the horizontal header to improve the liquid distribution. Byun and Kim (2011) tested a parallel flow microchannel evaporator with vertical headers with R410A. Significant improvement of flow distribution was obtained while placing the inlet at the top instead of using a middle inlet. Also, they concluded that top and bottom outlets are better compared to a middle outlet. Zou and Hrnjak (2013a, 2014b) presented flow visualization

experiments of R134a and R410A distribution in vertical header. The best flow distribution in Zou and Hrnjak's test was at high mass flow rate and low quality where the flow is in the churn and separated regimes.

Extensive simulation efforts on microchannel heat exchanger modeling using the effectiveness-NTU method and the energy balance method can be found in the open literature. These models use empirical correlations for the calculation of header and tube pressure drop. It is often a challenge to match the predicted and experimentally measured pressure drop due to the limitation on the applicability of the correlations and the high uncertainty in experimental pressure measurement. It should be noted that there is no correlation specifically developed for pressure drop in MCHX headers.

Flow mal-distribution in finned tube heat exchangers has been modeled by Domanski (2003). He developed a simulation model with the capability of solving flow mal-distribution in different circuits. One-dimensional air mal-distribution can be accounted for in this model. Kim *et al.* (2009) studied the effect of non-uniform air flow distribution based on a cycle simulation model of a residential R410A heat pump system. It was concluded that the control of individual refrigerant circuit flow rates would benefit the evaporator performance significantly when the airflow mal-distribution is severe. Brix *et al.* (2010) developed a two-tube MCHX model and then conducted a parametric study of refrigerant flow distribution profile to evaluate its impact on the MCHX's performance. Brix *et al.* investigated the effect of the non-uniform airflow distribution on the local UA value and studied the coupled influence of refrigerant-side and air-side mal-distribution. Tuo *et al.* (2012) presented an evaporator model that considered both refrigerant flow distribution and detailed header

pressure drop. In Tuo's header pressure drop formulation, contraction loss, expansion loss, pressure loss due to tube protrusion, frictional loss, momentum loss as well as gravity effect are taken into account. The simulated pressure drop between inlet and outlet header is validated against experimental data within 12 percent deviation. The iterative flow distribution calculation method and correlation based header pressure drop prediction approach were also adopted by Ren *et al.* (2013) in a port-by-port MCHX model.

Zhang and Li (2003) conducted a CFD study on flow distribution in a plate-fin heat exchanger by simulating the entire heat exchanger domain. Based on the modeling effort, the authors concluded that applying modified headers with a two-stage-distributing structure could reduce the mal-distribution effect. Lalot *et al.* (1999) reported 7-25% performance degradation for different types of heat exchangers based on the numerical CFD simulation results. Fei and Hrnjak (2004) modeled the two-phase flow in a header using the Eulerian model. Deviations of the experimental data and simulation results were presented. The actual droplet diameter, void fraction, the effect of flow expansion and re-circulation cannot be well captured by the presented model. Habib *et al.* (2008) correlated flow mal-distribution parameter of a HX using air as tube-side fluid. CFD simulation is performed with different air flow velocities and nozzle geometries in order to formulate a correlation. The paper also showed that adding a second header could lead to a 50 percent decrease in the mass flow rates' standard deviation. Poggi *et al.* (2009) presented a CFD simulation of single-phase flow in header and validated the model with experimental result of a vertical header. Saleh *et al.* (2012a) developed a three-dimensional single phase flow header CFD model as

a part of the header optimization package. In order to simulate the pressure drop in tubes, the porous jump interior condition is applied to connect the inlet header and outlet. The CFD header model was then used to develop metamodelling for use in approximation assisted optimization. Compared to previous CFD modeling effort, the application of the porous jump condition allowed the model to take the tubes into account while being computationally less expensive compared to full heat exchanger CFD simulation. The limitation of this approach is that the air-to-refrigerant heat transfer in the tubes could not be modeled. In a later publication by Saleh *et al.* (2012b), the optimized header designs are integrated with the heat exchanger model by Jiang *et al.* (2006) to perform a heat exchanger level optimization.

The air-side flow distribution is assumed to be uniform or taken as an input profile in previous heat exchanger models. Brix *et al.* (2010) studied the air-flow maldistribution effect on refrigerant flow distribution. Brix *et al.* proposed that the air maldistribution effect can be compensated by a suitable phase distribution in the header. For tube-fin heat exchangers, air velocity distribution has been experimentally measured by Kirby *et al.* (1988) and Aganda *et al.* (2000). Computational Fluid Dynamics (CFD) simulation was carried out by Yashar *et al.* (2011, 2014) for tube-fin heat exchangers as well. However, the application of air velocity distribution in MCHX models is sparse due to the limitation of experimental testing.

### 1.2.3 Heat conduction in heat exchanger core

Many researchers have experimentally investigated the TFHX performance degradation induced by heat conduction. For TFHXs, there are two types of heat conduction, longitudinal conduction in the refrigerant flow direction and tube-to-tube conduction through the fins. Heat conduction in the fluid flow direction is negligible

for most applications (Shah & Sekulic, 2003). The main concern is the tube-to-tube conduction through the fins due to the temperature difference. Chiou (1978) studied the two-dimensional heat conduction effect on crossflow plate fin heat exchangers. Chiou introduced a dimensionless conduction effect factor to determine the significance of two-dimensional conduction. Chiou's numerical study found the largest conduction effect factor when the ratio of heat capacity rate is one. Heun & Crawford (1994) analyzed the fin conduction effect on multi-pass crossflow heat exchangers. They assumed that the temperature distributions on the fins are one-dimensional. They concluded that capacity degradation due to fin conduction is more severe for low fin conduction resistance and large air-side conductance cases. Romero-Mendez *et al.*, (1997) studied the tube-to-tube heat conduction in a single-row plate-fin heat exchanger. They identified up to 20 percent performance degradation due to fin conduction. Payne & Domanski (2002) showed significant performance impact comparing continuous fin evaporator with fin-cut evaporator. Through numerical study for TFHXs, similar conclusions can also be found in Kou & Yuan (2007), Ranganayakulu, *et al.* (1997) and Zilio, *et al.* (2007) that the performance always deteriorates for all kinds of flow conditions and all geometric arrangements. Singh *et al.* (2008) proposed two different models (resistance model and conduction model) to tackle for the fin conduction problem. Resistance model only concerns the immediate neighboring tubes for a given tube. The adiabatic fin tip assumption is used for obtaining air-to-tube heat transfer. The conduction term is introduced as a correction on the wall temperature. Conduction model solves the heat conduction term using Fourier heat diffusion equation which

consumes significant amount of time. Singh concluded that resistance model achieve the same amount of accuracy as the conduction model with much less computational effort.

MCHX fins are separated by tubes within the MCHX bank. Unlike tube-fin heat exchangers, multi-bank MCHXs are assembled using separate banks where the fins are separated between banks in the air-flow direction. The concern of tube-to-tube heat conduction in MCHX is the large temperature difference between flow passes. Asinari *et al.* (2004) studied the two-dimensional fin conduction effect on CO<sub>2</sub> microchannel gas coolers using a finite-volume and finite-element hybrid approach. They concluded that the overall heat exchanger performance prediction using simplified fin tip assumption is similar to the discretized approach they used. However, the adiabatic fin tip assumption is not accurate when the neighboring tubes have large temperature difference. The heat conduction in the air-flow direction is found to be negligible in Asinari's work. Shao *et al.* (2009) proposed a model for serpentine microchannel condensers that accounts for three dimensional conduction. They used a correction term similar to the Singh *et al.* (2008) approach to consider fin conduction. Adiabatic fin tip based fin efficiency was applied in these models which conflicts with the assumption made in the tube-to-tube conduction formulation. Martínez-Ballester *et al.* (2011) also applied similar methodology to account for tube-to-tube heat conduction through fins. They also found the heat conduction in air-flow direction is minor compared to the transverse direction. In addition, Martínez-Ballester *et al.* (2011) found that the air-side temperature variation between the tubes is quite small except the region near the tube. Based on the above observations, Martínez-Ballester *et al.* (2013a) discretized the fin into three regions in the vertical direction. An analytical solution was derived based on

the one-dimensional fin conduction assumption. The discretization of the three regions is based on a proposed parameter, the fin height ratio. When the fin height ratio varies from 0 to 50 percent, 5 percent performance deviation was found. Considering the model validation reports a 5 percent accuracy of capacity prediction, the selection of fin height ratio was crucial to the accuracy of the model. However, there is no physics based guideline on the selection of such parameter. Martínez-Ballester *et al.* (2013b) compared the fin conduction model of Martínez-Ballester *et al.* (2013a) with Singh *et al.* (2008) approach. No computational saving and accuracy improvement were found through the case study. Ren *et al.* (2013) model divided one fin surface and the air-flow into two sections in order to accommodate the port-segment discretization of the model. The fin conduction problem was solved separately for the two sections of the fin. The separation of air stream should not have much impact on the overall heat exchanger capacity prediction. However, separate air-flow propagation in one flow passage affects local heat transfer calculation when the wall temperature difference is significant between top and bottom of the fin.

Among the reviewed MCHX models, Jiang (2003) and Ren *et al.* (2013) were applied to evaporator application. Jiang (2003) model assumes the fin tip is adiabatic. Temperature difference based model by Ren *et al.* (2013) cannot account for the mass transfer. The validation was conducted against a fully dry evaporator without dehumidification.

#### 1.2.4 Fluted tube coaxial heat exchanger

Garimella *et al.* (1990) is one of the earliest papers that investigated the heat transfer characteristics of single phase flow in spirally-fluted tube. Srinivasan & Christensen (1992) performed extensively experiment to correlate the single phase heat

transfer and pressure drop in the fluted tube. Garimella & Christensen (1995a, 1995b and 1997) provided a comprehensive review of the heat transfer and hydraulic performance of single phase flow in both inner tube and the annulus. Garimella & Christensen (1997) concluded that the enhancement of frictional factor is 1.1 to 2, in laminar flow regime and up to 10 in turbulent flow regime as compared to smooth tube. The typical Nusselt number values on the annulus side of a fluted CHX are 4-20 times that of the smooth annulus side when the flow is laminar. In the turbulent flow regime, the increase in Nusselt number increases 1.1-4 times. Arnold *et al.* (1993) provided detailed guidelines as well as heat transfer and pressure drop correlations for designing single-phase fluted tube CHX. Gregorig (1954) illustrated the concept of heat transfer enhancement of condensation on a ridged or fluted surface, where the vapor-liquid interface to take on a non-uniform curvature. The surface tension effect pushes the condensate from the flute crest to into through where a thin film region is created at the crest. Rousseau *et al.* (2000, 2003) also pointed out that micro-circulation of liquid phase leads to the replacement of cold liquid with hotter liquid near the surface. Since CHXs are generally serving as condenser/evaporator in refrigeration and heat pump system which have two-phase flow on the annulus side, two-phase heat transfer and pressure drop correlations are essential parts in the simulation model. However, such correlations are not available in the published literature.

Experimental investigations (Rennie *et al.*, 2005; Kumar *et al.*, 2006) have been conducted in the past to evaluate the performance of CHXs under various operating conditions, tube types and flow configurations. However, there is limited research published on the steady state numerical modeling of CHX. Kumar *et al.* (2008)

performed a numerical study for a helically coiled CHX under different flow conditions. New correlations have been proposed for both pressure drop and heat transfer in the smooth outer tube of helical CHX. Rennie (2004) numerically modeled a helically coiled CHX with different tube diameter ratios and mass flow rates in the annulus based on a finite volume computational fluid dynamics (CFD) code. The inner tube heat transfer coefficient was validated against literature data. Rennie (2004) reported that the thermal resistance on the annular side is the dominant factor of the heat exchanger's overall thermal resistance. Zhu *et al.* (2010) conducted a numerical investigation of laminar film condensation on a vertical fluted tube. The simulation results agreed with experimental data, however, no new correlation was proposed as a result of the simulation work.

Rousseau *et al.* (2000, 2003) presented a simulation model for fluted tube water heating condensers. To the best of our knowledge, the Rousseau *et al.* model is the only analytical CHX model available in the open literature. Their moving boundary three-zone modeling approach is based on effectiveness-NTU algorithm and uses correlations for local heat transfer and pressure drop calculations. Rousseau's model is limited to predicting the performance of fluted tube condenser with superheated inlet and fixed outlet subcooling. On the annulus side, smooth round tube heat transfer (Shah, 1979) and pressure drop (Traviss *et al.*, 1973) correlations are adopted to predict refrigerant flow characteristics in the condensation region. The correlations are further modified by using two enhancement factors. The first enhancement factor accounts for the enhancement of helical tube as compared to straight tube. The second enhancement factor accounts for the difference between standard tube surface and fluted surface. As

mentioned earlier, there are no correlations in the open literature that were specifically developed for two phase flow in fluted tube annuli. Such correlations are necessary in order to accurately predict the thermal and hydraulic performance of CHXs with fluted tube geometry.

### **1.3 Summary of Background**

Microchannel heat exchanger numerical modeling is a fast growing research field. The reviewed MCHX models are summarized in Table 1-1. The literature survey suggested there lacks of new capabilities in developing new generation of MCHXs. Moreover, there are several significant gaps in the prediction of current MCHX designs. Previously, all the modeling efforts were dedicated to predict the performance of conventional uniform geometry MCHXs. The context of uniform geometry refers to a MCHX having the same geometry parameters such as number of tubes per bank, tube vertical spacing, fins per inch (FPI), port diameter etc. The current research and development of MCHXs has reached the plateau that the optimum designs cannot be further improved with limited number of design variables. The flow distribution and heat conduction issue can be simulated but the solutions are sparse. To further expand the MCHX technology envelope, variable geometry microchannel heat exchanger concept could be one of the potential solutions. Such an innovative design allows the MCHXs to have variable fin types, fin densities, tube heights, tube widths, port widths and heights, tubes per bank, tuber vertical spacing and horizontal spacing. In additional to the variable physical parameters, the positions of tubes, fins as well as fin cuts can be specified individually. The variable geometry designs are aimed at not only reduction of thermal resistances and material use, but also minimization of negative effects such as air and refrigerant flow mal-distribution, fin conduction between each

section of MCHXs. The current MCHX models do not have the capabilities to account for these variable parameters. A generalized MCHX model that accounts for any geometric combinations and accounts for these heat transfer and fluid flow phenomena is desired.

**Table 1-1 Literature review of existing MCHX model and comparison with proposed model**

Model	Variable Geometry	Control Volume	Application	Validated Refrigerant
Yin et al. 2001	No	Tube-Segment	Gas Cooler	CO2
Jiang. 2003		Tube-Segment	Condenser/Evaporator	Water
Asinari et al. 2004		Tube-Segment	Gas Cooler	CO2
Schwentker et al. 2006		Tube-Segment	Condenser	R134a
Shao et al. 2009		Port-Segment	Condenser	R290
Brix et al. 2009, 2010		Tube-Segment	Evaporator	CO2
Fronk and Garimella 2010		Tube-Segment	Gas Cooler	CO2
Garcia-Cascales et al. 2010		Tube-Segment	Condenser	R134a, R410A
Tuo et al. 2012		Tube-Segment	Evaporator	R134a
Martinez-Ballester et al. 2013		Tube-Segment	Condenser/Gas Cooler	R410A, CO2
Ren et al. 2013		Port-Segment	Condenser/Evaporator	R410A, CO2

The heat conduction between tubes can cause substantial performance degradation of MCHXs. The models reviewed are either extremely time consuming or based on bold hypothesis. None of the available models correctly accounts for heat conduction effect under wet surface condition, not to mention the partially wet condition. The investigation of such problem requires a fast yet fundamentally correct model to account for various conditions including dry, wet and partially wet surfaces.

The refrigerant and air flow mal-distribution effects have been validated to be the major factors that influence the thermal and hydraulic characteristics of MCHXs. Current modeling approaches only concern the flow differences between tubes. However, none of previous models have the capability to obtain the flow distribution among microchannel ports in the air flow direction. The mal-distribution induced by heat transfer difference in the air flow direction can be much more severe than the transverse direction between tubes. The header modeling is another important aspect of flow distribution prediction. The current CFD models do not connect the header modeling with the air-to-refrigerant heat transfer on the tube side, which neglect one of the most importance mal-distribution causes. It is necessary to have an approach that can predict the fluid flow behavior accurately while accounts for the heat transfer and pressure drop in heat exchangers' tubes. Lastly, air-flow distribution is now based on velocity distribution input profiles. The VG-MCHX design concept opens up an immerse opportunity for air distribution predictions. The air flow distribution can be approximated with empirical correlations through an iterative approach.

Another vast research focus is the coaxial heat exchanger modeling. Although CHXs are used widely in commercial HVAC&R applications, the detailed modeling effort is sparse, especially fluted tube CHXs. A finite-volume CHX model with moving boundaries can significantly improve the prediction accuracy. In addition, the development of fluted annuli two-phase correlations is necessary such that the CHX model can be applied for two-phase applications.

#### **1.4 Research Objectives**

The proposed work concerns itself with steady state modeling of air-to-refrigerant microchannel heat exchangers and fluid-to-fluid coaxial heat exchangers.

The first part focuses on developing a first-principles based model for a variable geometry microchannel heat exchanger with the most design flexibility and comprehensive consideration of thermal and hydraulic phenomenon within the heat exchanger. In addition to microchannel heat exchanger modeling, the second part focuses on the detailed modeling of coaxial heat exchangers which is also an essential part for HVAC&R applications.

The proposed microchannel model development will result in the most advanced microchannel heat exchanger simulation tool available, and feature the following capabilities:

- Model for variable geometric parameters including tube, port and fin dimensions, as well as locations of tubes and fins
- Fin performance analysis under dry, wet and partially wet conditions, accounting for tube-to-tube conduction through the fins
- Accurate prediction of fluid flow behavior in headers and heat transfer process in tubes
- Capable of predicting fluid distribution in two-dimensions at per port level
- Ability to predict the variable geometry impact on air flow distribution

Secondly, the modeling of coaxial heat exchangers focuses on the following:

- Modeling coaxial heat exchanger with different geometric configurations, flow arrangements and surface types with greater accuracy
- Being able to track the phase change for both fluids in finite volumes

- Improved prediction of two-phase heat transfer and pressure drop in fluted tube annuli

Finally, a comprehensive experimental validation is conducted for the proposed heat exchanger models. The performance enhancement and material cost saving potential of variable geometry heat exchanger is explored through design optimization.

## **1.5 Completed Tasks and Thesis Organization**

The thesis is divided into five research thrusts based on the proposed research objectives.

### **1.5.1 A model for air-to-refrigerant microchannel heat exchangers with variable tube and fin geometries**

A generalized finite volume-based model to simulate MCHXs with variable tube and fin geometries using a three-stream UA-AMTD method is presented in Chapter 2. MCHXs with variable geometry can have different port dimensions, tube sizes and fin surfaces within the heat exchanger core and can have single or multiple tube banks. These novel MCHX designs can further enhance the heat exchanger performance and improve its material utilization. A comprehensive literature review reveals that there is no experimental or numerical investigation of such innovative designs nor is there a modeling approach that can handle such flexible geometries. The model is validated against 227 experimental data points for eight different fluids, and eighteen MCHX geometries, including four different variable geometry microchannel condensers. This validation effort is the most comprehensive MCHX model validation presented in open literature.

### 1.5.2 Microchannel heat exchanger modeling under dry, wet and partially wet surface conditions accounting for tube-to-tube heat conduction

A literature survey suggests that there lacks a unified air-to-surface heat and mass transfer modeling approach for MCHXs, especially under dehumidifying condition with tube-to-tube heat conduction. In Chapter 3, I present an air-to-fin heat and mass transfer model for MCHX operating under dry, wet and partially wet conditions. Typically, there are two boundary conditions for the fins in MCHX. The adiabatic fin tip boundary condition is applied to the extended fins on top and bottom of the microchannel slab. The second boundary condition is the prescribed surface temperature, applicable to a fin bounded by two tubes. The proposed fin analysis method accounts for both boundary conditions and tube-to-tube conduction. The modeling approach is capable of locating the boundary between dry and wet surface if a fin is partially wet. The model is verified against simulation results for air-to-surface heat transfer on a fin obtained using a commercially available Computational Fluid Dynamics (CFD) package. A new finite volume MCHX model is developed using the proposed fin analysis method. The model is capable of predicting the performance of a variable geometry MCHX (VG-MCHX) under both dry and dehumidifying conditions, and is validated against experimental data. The proposed model allows for the most comprehensive and accurate analysis of microchannel evaporators and condensers. The model is validated against experimental data, including 20 evaporator data points in addition to the condenser and gas cooler validation presented in Chapter 2. The proposed model allows for the most comprehensive and accurate analysis of microchannel evaporators and condensers.

### 1.5.3 A computational fluid dynamics and effectiveness-NTU based co-simulation approach for flow mal-distribution analysis in microchannel heat exchanger headers

Refrigerant flow mal-distribution is a practical challenge in most microchannel heat exchangers (MCHXs) applications. Geometry design, uneven heat transfer and pressure drop in the different microchannel tubes are three main reasons leading to the flow mal-distribution. To efficiently and accurately account for these three effects, a new MCHX co-simulation approach is proposed in Chapter 4. The proposed approach combines a detailed header simulation based on CFD and a robust effectiveness-based finite volume tube-side heat transfer and refrigerant flow modeling tool. The co-simulation concept is demonstrated on a ten-tube MCHX case study. Gravity effect and uneven airflow effect were numerically analyzed using both water and condensing R134a as the working fluids. The approach was validated against experimental data for an automotive R134a condenser. The inlet header was cut open after the experimental data had been collected. The detailed header geometry was reproduced using the proposed CFD header model. Good prediction accuracy was achieved compared to the experimental data. The presented co-simulation approach is capable of predicting detailed refrigerant flow behavior in MCHX header while accurately predicts the overall heat exchanger performance.

### 1.5.4 Air flow distribution and design optimization of variable geometry microchannel heat exchangers.

Variable geometry refers to the use of variable tube and port dimensions, variations in fin type and fin density in different sections of the heat exchanger core. The locations of individual tubes and fins can also vary, especially in multi-slab configurations. The goals of this new concept are heat transfer enhancement, material

savings and fulfilling special design and application requirements. Chapter 5 presents studies on the design optimization of variable geometry MCHXs based on a validated simulation tool. The optimization study investigates an automotive R134a and R290 condenser and a CO<sub>2</sub> gas cooler in air-conditioning systems. The objective of the study is to evaluate the potential cost and performance benefits of variable geometry microchannel heat exchangers compared to conventional fixed geometry microchannel heat exchangers used today. The optimization objectives are maximize capacity and to reduce cost. The optimization study shows a 35 percent reduction in material and 43 percent savings in envelope volume for a variable geometry gas cooler for the same performance compared to a baseline conventional geometry design. An iterative approach is proposed to calculate the air flow mal-distribution due to heat exchanger's geometry variation. Optimum designs using the calculated air flow distribution are compared with designs that assume uniform air distribution. The comparison showed 3% difference for the best material saving case found. It is important to consider the impact of geometry variations on air flow distribution and the heat exchanger designs. The optimization study reveals the potential of the variable geometry MCHX and motivates engineers to pursue such innovative designs.

#### 1.5.5 A finite volume coaxial heat exchanger model with moving boundaries and modifications to correlations for two-phase flow in fluted annuli

Coaxial Heat Exchangers (CHXs) are now used extensively in heat pump and refrigeration systems. The design of such systems requires estimation of CHX's thermal and hydraulic performance. Chapter 6 presents a generalized finite volume CHX model that is capable of simulating single-phase and two-phase flow with a smooth or fluted inner tube. The concepts of segment insertion and subdivision

(moving boundary within the segment) are adopted in this model to track the phase change point along the flow channel. This allows for reliable model accuracy even with a lower number of discretized finite volumes, thereby reducing computation time. For the segment insertion and subdivision functions, four different approaches are provided in order to achieve the best accuracy and least computational effort under various flow configurations and fluid conditions. The simulation model can be applied to straight and helical tubes with choices of smooth, grooved and fluted tube surface. Empirical single-phase and two-phase correlations from the literature are adopted in the proposed model for the applicable surfaces. At present, there are no correlations for two-phase flow in fluted tube annuli, in the open literature. This paper proposes modifications to existing two-phase fluted surface heat transfer and pressure drop correlation formulations by applying empirical two-phase flow multipliers onto existing fluted tube single phase correlations. The solving methodology of this model requires the heat exchanger geometry, flow configuration, inlet states, as well as mass flow rates of the fluids to solve for the outlet conditions, heat load, pressure drop and charge of the CHX. Coupled with non-linear equation solver, the model can also provide the required mass flow rate for a specific superheat/subcooling on either side of the CHX. The model and modified correlations are validated against experimental data of brine-to-refrigerant fluted tube condenser and evaporator used in a heat pump application.

## 2 A MODEL FOR AIR-TO-REFRIGERANT MICROCHANNEL HEAT EXCHANGERS WITH VARIABLE TUBE AND FIN GEOMETRIES

Having the benefit of high material utilization and enhanced heat transfer efficiency, air-to-refrigerant MCHXs have been widely used in the automotive industry. More recently, they are also being used in the stationary HVAC&R industry. Compared to the traditional time-consuming heat exchanger product development approach of designing and testing prototypes, numerical simulation tools are now extensively used in the performance evaluation and design of MCHX as well as other air-to-refrigerant heat exchangers. Previously, all modeling efforts were dedicated to predict the performance of conventional uniform geometry MCHXs. The term “uniform geometry” refers to a MCHX having the same geometry parameters, such as number of tubes per bank, tube vertical spacing, tube height and width, fins per inch (FPI), port diameter and number of ports. The current research and development of MCHXs have reached the stumbling block that the optimum designs cannot be further improved with the limited number of design variables currently available.

To further expand the MCHX technology envelope, the variable geometry microchannel heat exchanger (VG-MCHX) concept can be a potential solution. This is an innovative design that allows the MCHXs to have variables in fin types, fin densities, tube height, tube widths, port widths and heights, tubes per bank, tube vertical spacing, and horizontal spacing. This design is in some way analogous to variable geometry tube and fin heat exchangers (Singh *et al.* 2009) that are widely used as indoor units in air-conditioning and heat pumping applications. Singh *et al.* (2009) proposed a tube-fin heat exchanger model with arbitrary fin sheet. Singh *et al.* model accounts for variable tube diameters, variable tube locations, variable tube pitches, and variable

number of tubes per bank as well as variable location of fin cuts. The model is validated with a R410A condenser using four different tube diameters. In addition to the variable physical parameters, the positions of tubes and fins can be specified individually. The variable geometry designs are aimed at not only the reduction of thermal resistances and material use, but also the minimization of negative effects such as air and refrigerant flow mal-distribution, tube-to-tube conduction between each section of MCHXs and frost accumulation. The current MCHX models do not have the capability to account for these variable parameters. This paper presents a model which is able to simulate the most flexible MCHX designs with variable geometry, and would allow the engineers to further push the MCHX technology envelope.

The chapter introduces a generalized condenser and gas cooler model for MCHX with variable geometric parameters. The model is capable of simulating single-slab and multi-slab MCHXs with variable fins, variable tubes and variable ports. For multi-slab cases, the location of each slab can be specified in a three-dimensional Cartesian grid. In addition, the geometries of each slab can be varied. A three-stream UA-AMTD method is developed in the proposed model to account for different air side condition and geometric parameters above and below the port-segment. The model is validated with 227 data points, using eight different fluids, under a wide range of testing conditions.

## **2.1 Concept of Variable Geometry**

The conventional MCHXs have a uniform fin, tube, port configuration as shown in Figure 2-1 and is termed here as the standard configuration. The manufacturing processes for such a design are well established. However, the development of new generation MCHXs is restricted by such uniformity. For a specific application, the

optimum MCHX designs can be further extended with adaptive geometry to achieve the best HX performance or the most suitable design. The proposed VG-MCHX model is applicable to but not limited to the sample configuration shown in Figure 2-2. Similarly, a traditional multi-slab MCHX as shown in Figure 2-3 has both the slabs aligned and they have the same dimensions. Whereas a multi-slab VG-MCHX as presented in Figure 2-4 can have variable dimensions and locations for both the slabs.

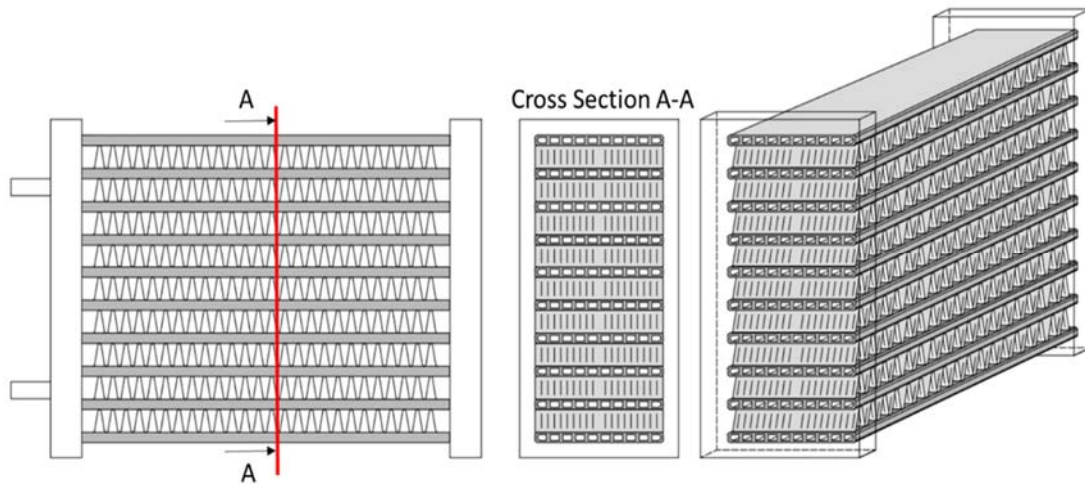


**Figure 2-1 Standard configuration MCHX**

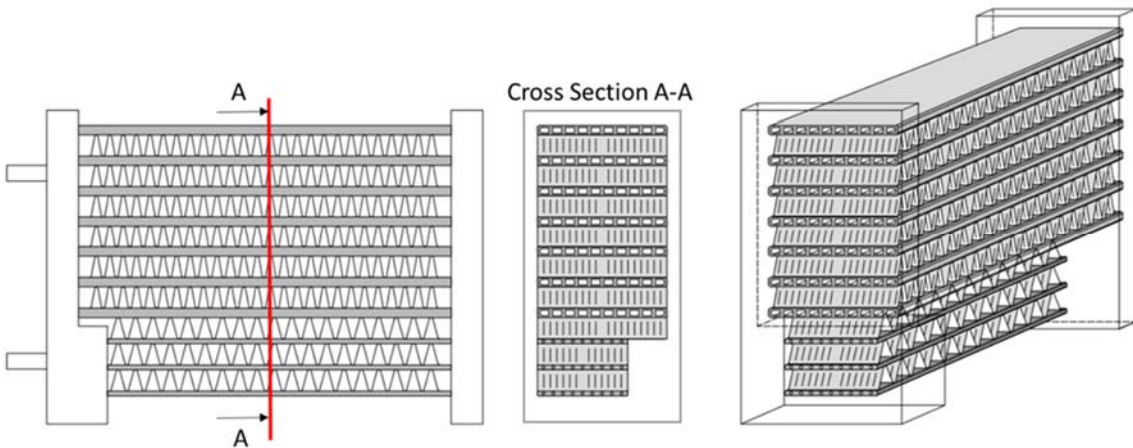


**Figure 2-2 Variable geometry MCHX**

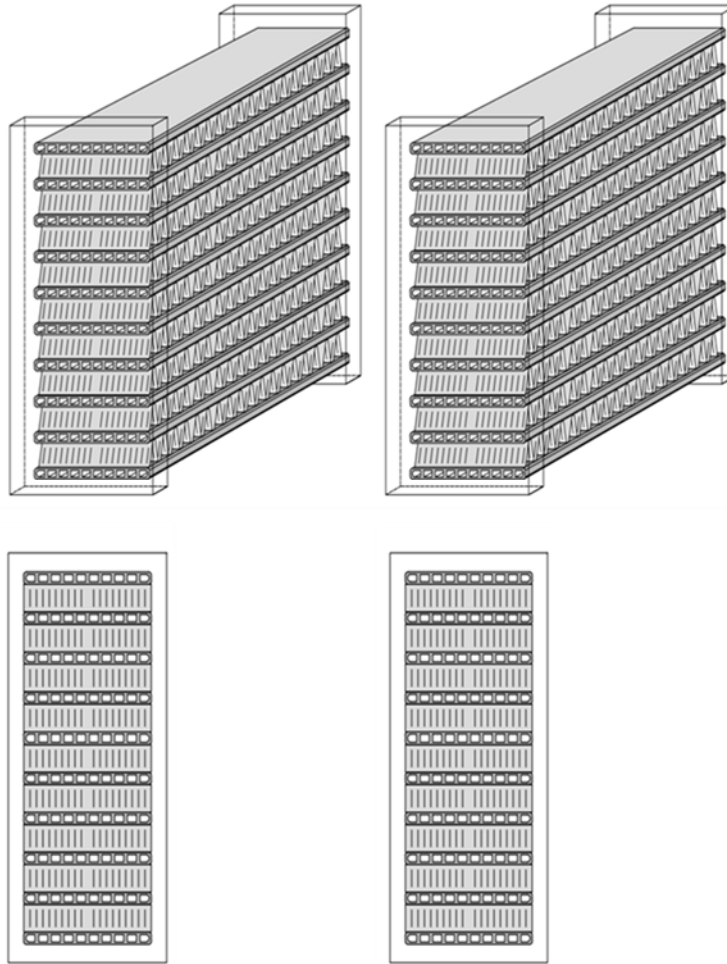
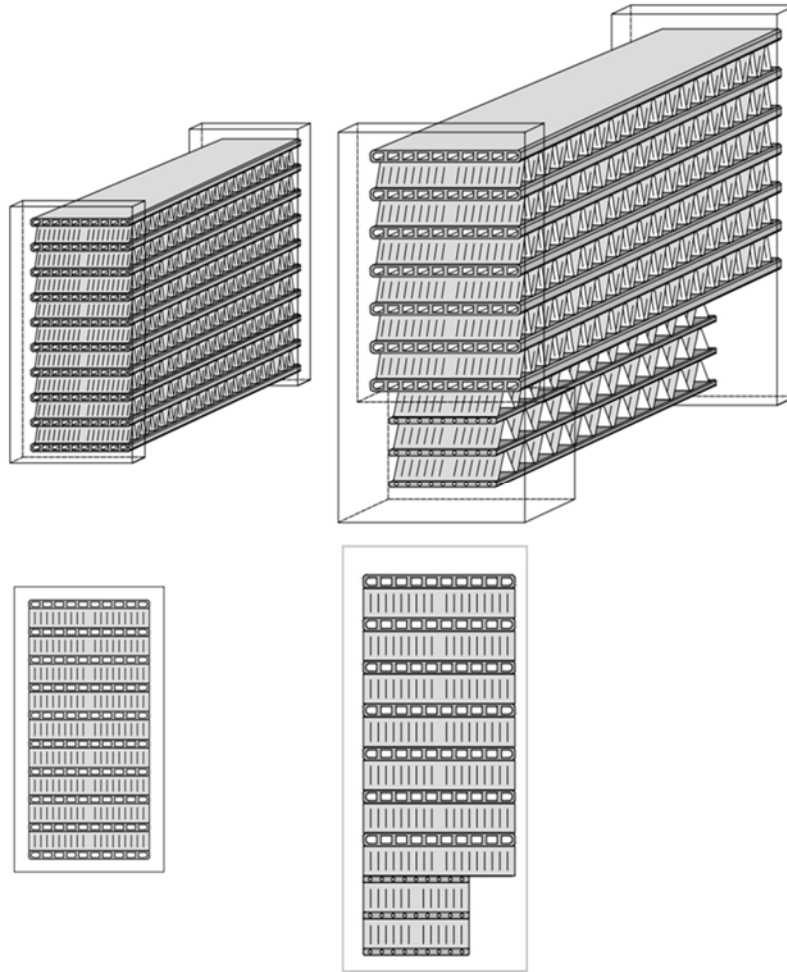


Figure 2-3 Standard multi-slab MCHX



**Figure 2-4 Variable geometry multi-slab MCHX**

There are several geometric parameters that can be varied within a VG-MCHX. The variable geometry can be developed to mitigate detrimental effects such as air and refrigerant flow mal-distribution, to enhance performance and to reduce cost. The remainder of this section will focus on these aspects and propose the corresponding variable geometry solutions.

### 2.1.1 In-tube heat transfer and pressure drop

Extensive experimental studies of in-tube heat transfer and pressure drop along with the developed correlations have led to much better understanding of the port design. In most MCHX applications, there are multiple flow passes with varying number of tubes,

resulting in variable refrigerant mass flux. A proper port design for each tube pass can lead to a better balance between the maximization of heat transfer and minimization of pressure drop.

### 2.1.2 Air flow mal-distribution

Air side mal-distribution on heat exchanger face is a practical problem in almost all heat exchanger applications. Several experimental studies have been carried out to map the velocity distribution on coil face (Kirby *et al.*, 1988, Aganda *et al.*, 2000). Yashar *et al.*, (2011, 2014) conducted numerical simulation of air flow distribution using CFD. The air flow mal-distribution is one of the causes of refrigerant side mal-distribution. It essentially leads to un-desired approach temperature distribution and thus performance degradation. To reduce the mal-distribution effect, the fin type, fin height and fin density can be appropriately chosen for different sections of the MCHX. The new designs with variable fin geometry can reduce the air side resistance and air flow mal-distribution while maintaining acceptable pressure drop.

### 2.1.3 Refrigerant flow mal-distribution

Mueller and Chiou (1988) summarized four types of refrigerant flow mal-distribution: mechanical design of headers and the inlet connecting tubes; self-induced flow mal-distribution caused by the heat transfer process; refrigerant phase separation in headers; fouling and corrosion. To minimize the header-to-tube refrigerant flow mal-distribution, cross-section areas of each tube can be adjusted for a better balance of mass flux and frictional pressure drop in tubes. There is no previous literature that studied the refrigerant distribution into different ports within a tube. Since the air inlet state is different from the first port to the last port of a given tube in the air flow direction, the heat transfer difference from air to different ports would also cause

refrigerant-side maldistribution. A variable port size profile can improve the refrigerant flow distribution in two-dimensions, from tube to tube and from port to port.

#### 2.1.4 Heat conduction through fins

The negative impact of tube-to-tube conduction due to temperature difference has been studied numerically and experimentally for tube-fin heat exchangers. The typical solution is to cut the fin between tube banks such that this effect is eliminated in air flow direction. Although there are several models in the literature that account for MCHX fin conduction (Asinari *et al.*, 2004; Martínez-Ballester *et al.*, 2013a, 2013b; Ren *et al.*, 2013), there is no discussion about this effect and the solution in actual MCHX applications. In the case of MCHXs, the depth is typically very small in the air flow direction. For multi-slab MCHX applications, the fin is generally not continuous between each slabs. Thus, fin cut between slabs is not necessary. Multi-pass MCHX is a common practice in most of the MCHX designs. Refrigerant merges into the intermediate header from the tubes in the upstream pass, mixes, and is then distributed into the downstream pass. The neighboring tubes between the two passes would have the largest surface temperature difference. In this case, either a traditional fin cut can be performed or a sparse fin density can be applied between the two tubes to minimize the fin conduction effect.

#### 2.1.5 Material saving

Counter flow arrangement is the most commonly used arrangement in heat exchanger designs. The purpose of such design is to maintain a certain heat transfer potential throughout the entire HX. Even with counter flow configuration, there are still certain sections within an MCHX that are oversized. In other words, there is potential for achieving the same performance with lower heat transfer area and hence reduced

cost. Also, for specific designs, such as condenser, the last pass normally serves as a sub-cooler to ensure that the exiting refrigerant is always in the liquid phase. Smaller tube size and lower fin density can be used in these sections to achieve material savings.

#### 2.1.6 Design requirements

Ling *et al.* (2013) presented a residential separate sensible and latent cooling system. A four-bank microchannel condenser is used in the design. The outlet air through the de-superheating region of first bank is supplied to desiccant wheel for regeneration purpose. Different from the traditional inline configuration, the first bank is located separately from the other three banks. The proposed model was used in the prototype design process to simulate such arrangement. Also, the superheated region has a dedicated suction fan. The air velocity difference on the heat exchanger surface was also accounted for. It should also be mentioned that, the radiator and condenser arrangement in automotive applications is a common design that has different sizes of MCHXs in the air flow direction. An optimum relative location and size can be determined with the assist of the proposed variable geometry microchannel condenser model.

This section summarized several potential VG- MCHX applications above based on literature review and general knowledge of MCHX designs. In the remainder of the section, the modeling details of the proposed model is described and a comprehensive validation of both standard geometry and variable geometry condensers and gas coolers is presented.

## 2.2 Modeling Details

### 2.2.1 Basic solving methodology

In this section, a segment-by-segment microchannel heat exchanger model is developed based on three-stream energy equation. The purpose of this model is to provide fast yet accurate overall performance prediction. The proposed model in this section provides initial wall temperature guess for the detail conduction analysis described in Chapter 3. The model can be also coupled with the refrigerant distribution model described in Chapter 4. to account for flow maldistribution effect. The following assumptions are made:

- Steady state model
- Geometry
  - Tubes share one-half of top fin and a one-half of bottom fin
  - Segment can be sub-divided to track the exact phase change point
- Heat Transfer
  - Adiabatic at the center of the fin
  - Uniform port inner wall temperature
  - The thermo-physical properties and heat transfer coefficients are evaluated based on the inlet of each segment/sub-divided segment
- Fluid flow
  - Thermally and hydro-dynamically fully developed flow
  - Refrigerant is well-mixed in the intermediate header
  - Refrigerant flow is assumed to be equally distributed into the tubes
  - Negligible momentum pressure drop

- Horizontal air flow with user specified air-flow distribution on heat exchanger face

The refrigerant side calculation sequence is based on the refrigerant flow direction. The headers are categorized into inlet headers, intermediate headers and outlet headers. There can be more than one inlet and outlet header. The calculation starts by means of all the downstream tubes of inlet header. Once all the inlet streams are solved, the solver proceeds to intermediate headers. For each intermediate header, if all of its upstream tubes are solved, the refrigerant is mixed within it. After the calculation of header pressure drop, the refrigerant is then distributed into the downstream tubes. Finally, there will be a check for all outlet headers' upstream tubes. If all the outlet headers' upstream tubes' calculations are solved, the tube outlet conditions would be used in the following outlet header pressure drop calculation. This completes one iteration of the refrigerant side calculation. To illustrate the refrigerant side solving sequence, a four pass automotive condenser (Eisele, 2012) is presented in Figure 2-5. For this particular pass configuration, the refrigerant side solving sequence is H-a, S-1, H-b, S2, H-c, S-3, H-d, S-4, H-e. The proposed model assumes no heat transfer in header. Only the pressure drop is calculated for all the headers.

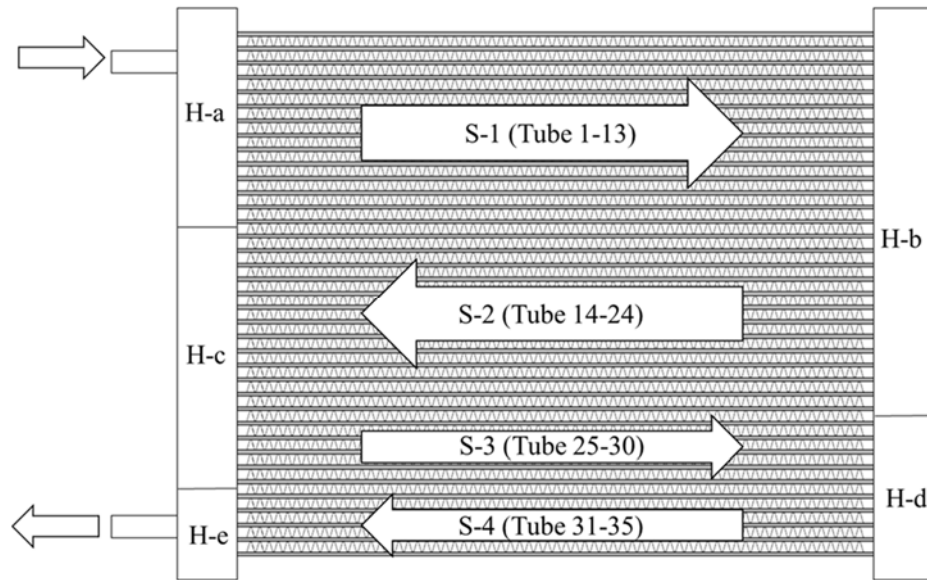


**Figure 2-5 Example of refrigerant side computation sequence for a 35 tube MCHX**

The air-side propagation is conducted iteratively. The initial guess of air inlet conditions for all the tubes is air inlet state at MCHX face. For ports within a tube, the air-side condition is immediately passed to the next port in air flow direction. However, after each iteration, the air-side enthalpy residuals at both tube level and port level are checked. Figure 2-6 illustrates a typical VG-MCHX air-side propagation from upstream Tube 1 and 2 to downstream Tube 3. To account for the complexity of the variable geometry MCHXs, all the tubes and fins are located on a Cartesian grid. For each tube and associated fins, the locations of the four corner points are processed in the solver to find neighboring tube in the air-flow direction. In Figure 6, a portion of the outlet air from Tube 1 and 2 that facing Tube 3 is mixed then passed to Tube 3. The remainder of Tube 1 and 2's outlet air streams will keep flowing in the air flow direction until they hit the corresponding air side downstream tube(s) or the boundary (outlet) of the MCHX. In the proposed model, air velocity distribution on heat exchanger face can be either assumed uniform or unevenly distributed based on a velocity profile input.

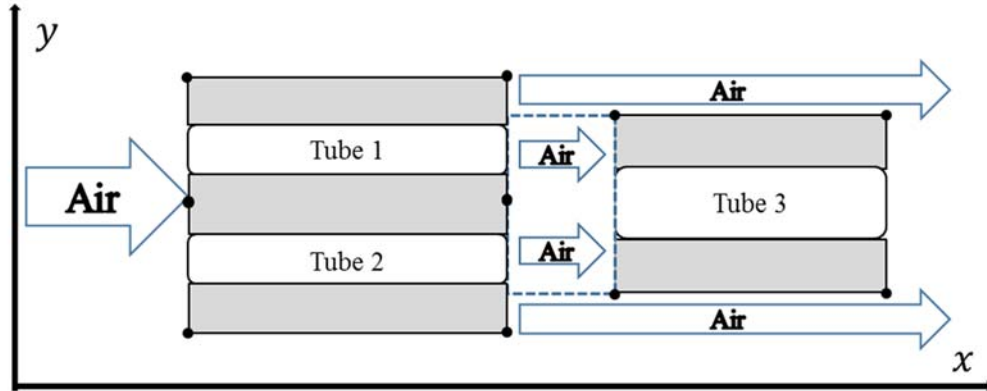


**Figure 2-6 Air flow propagation example**

The top level solution methodology is presented in Figure 2-7. The air-side Heat Transfer Coefficients (HTCs) are calculated on a per port base. All the open literature on air-side heat transfer correlations report overall heat transfer coefficient for the entire HX envelope. In the case of variable geometry MCHX, at each port, the geometry and air-side state are propagated to the entire MCHX to calculate air-side heat transfer coefficient. Such approximation is used in this model to apply empirical correlations because empirical correlations (especially air-side) are typically developed for an entire heat exchanger. Further CFD analysis can be carried out to investigate the air-side heat transfer coefficient variation with the heat exchanger core. It should also be noted that, in between of every iteration, the per port three-dimensional air HTCs are updated based on the updated air side conditions. The same approach is also applied to fin efficiency calculations.

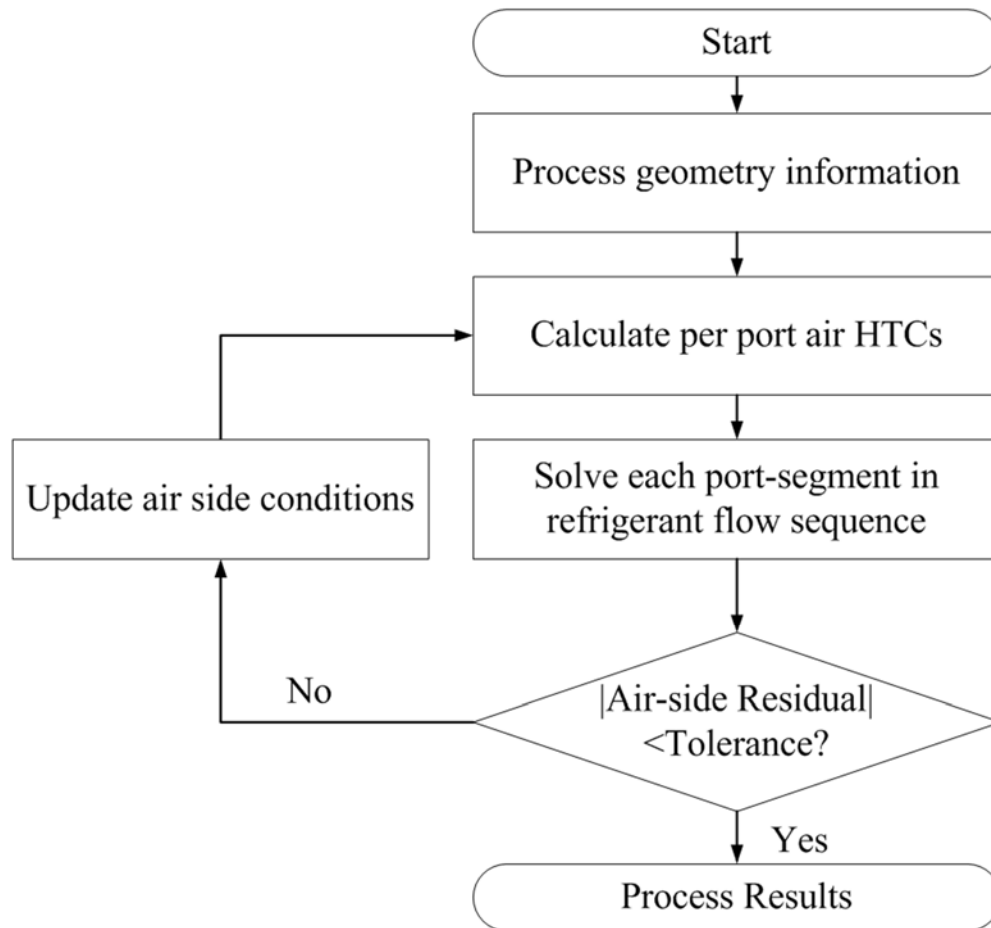


**Figure 2-7 Solution methodology for proposed model**

### 2.2.2 Heat transfer equation at control volume

In the air flow direction, the tube is divided into control volumes based on individual ports as shown in Figure 2-8. In the refrigerant flow direction, the ports are divided into segments. Figure 2-9 presents the configuration of one control volume (port-segment) in the proposed model. Since the fins on top and bottom could be different (e.g., fin type and fin density), there are two air streams (top and bottom) and one refrigerant stream. Considering the major contribution of overall heat transfer resistance is from the air-side, it is logical to assume that the inner port wall temperature is uniform within the control volume. Conservation of energy is applied to each control volume as described next.

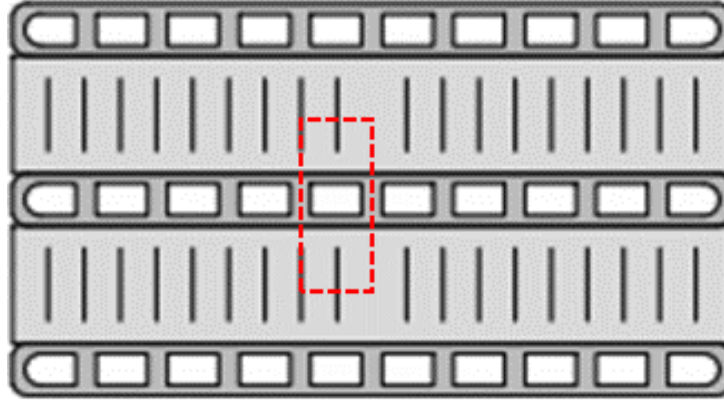


**Figure 2-8 Port segment of proposed model**

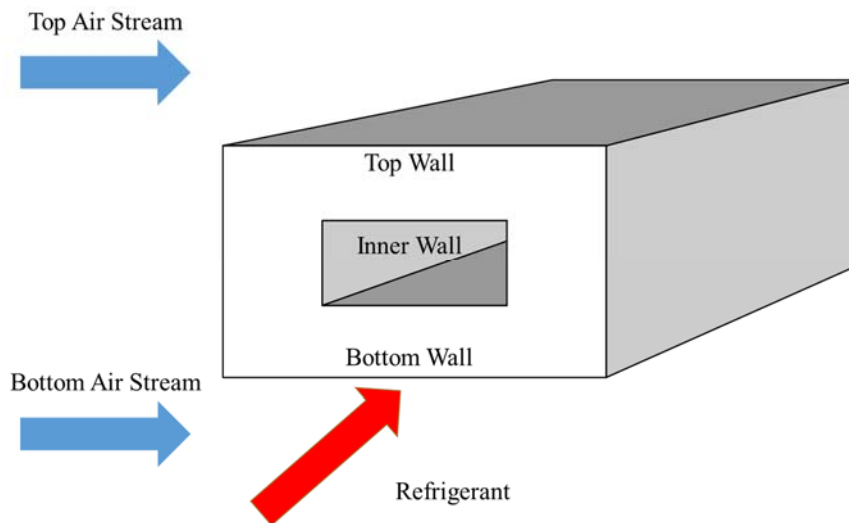


**Figure 2-9 Control volume configuration**

Equation (2-1) defines the heat transfer from refrigerant to inner wall.

$$\dot{m}_{ref}(h_{ref,in} - h_{ref,out}) = U_{ref} A_{inner} (T_{ref} - T_{wall,inner}) \quad (2-1)$$

Where  $T_{ref}$  is the average refrigerant temperature in the control volume. For two-phase flow, refrigerant inlet temperature is applied to avoid additional iteration.

Equation (2-2) defines the heat conduction from inner tube wall to outer tube walls.

$$U_{ref} A_{inner} (T_{ref,in} - T_{wall,inner}) = \frac{kA_{inner,top}}{\Delta x_{top}} (T_{wall,inner} - T_{wall,top}) + \frac{kA_{inner,bot}}{\Delta x_{bot}} (T_{wall,inner} - T_{wall,bot}) \quad (2-2)$$

Where  $\Delta x_{top}$  and  $\Delta x_{bot}$  are the distance between outer walls to inner wall for rectangular port case. For round port cases, these are calculated based on the distances from top and bottom point of the round ports to the top and bottom tube walls.  $A_{inner,top}$  and  $A_{inner,bot}$  are defined as the inner wall surface areas facing top tube wall and bottom tube wall.

Equation (2-3) and (2-4) define the heat transferred from outer wall to top air and bottom air through the fins.

$$\frac{kA_{inner,top}}{\Delta x_{top}} (T_{wall,inner} - T_{wall,top}) = U_{air,top} (A_{p,top} + \eta_{fin,top} A_{s,top}) \cdot (T_{wall,top} - T_{air,top}) \quad (2-3)$$

$$\frac{kA_{inner,bot}}{\Delta x_{bot}} (T_{wall,inner} - T_{wall,bot}) = U_{air,bot} (A_{p,bot} + \eta_{fin,bot} A_{s,bot}) \cdot (T_{wall,bot} - T_{air,bot}) \quad (2-4)$$

The air side energy conservation is defined in equation (2-5) and (2-6).

$$U_{air,top} (A_{p,top} + \eta_{fin,top} A_{s,top}) \cdot (T_{wall,top} - T_{air,top}) = \dot{m}_{air,top} (h_{air,top,out} - h_{air,top,in}) \quad (2-5)$$

$$U_{air,bot} (A_{p,bot} + \eta_{fin,bot} A_{s,bot}) \cdot (T_{wall,bot} - T_{air,bot}) = \dot{m}_{air,bot} (h_{air,bot,out} - h_{air,bot,in}) \quad (2-6)$$

The heat transfer coefficients, heat transfer areas, and fin efficiencies as well as air-side properties are calculated separately for the top air and bottom air to account for the variable geometric parameters. It should be noted that, AMTD method is applied to all the equations instead of LMTD method. It is found that the AMTD method is computationally faster and more robust than the LMTD method. Since the control

volume is at per port level, there is negligible difference on capacity prediction between the two methods.

Within a segment/sub-divided segment, there are six unknowns: top air outlet enthalpy, bottom air outlet enthalpy, refrigerant outlet enthalpy, inner port wall temperature, top tube wall temperature and bottom tube wall temperature. Equation (2-1) to (2-6) are solved simultaneously to find these six unknowns. This equation set can be generally applied to both single-phase and two-phase refrigerant flow. For two-phase flow, empirical refrigerant side heat transfer correlations typically require heat flux as an input. In this case, the heat transfer coefficient is determined iteratively.

### 2.2.3 Three-stream effectiveness-NTU method

For verification and comparison purpose, a single-phase three-stream effectiveness-NTU method developed by Baclic *et al.* (1982) is implemented. Based on known fluid inlet properties, calculated heat transfer coefficients and areas, the heat capacity and Number of Transfer Unit (NTU) can be obtained. The outlet states of refrigerant and two air streams can be then solved using analytical equation sets in the three-stream effectiveness-NTU methods. The equations are lengthy and are not presented in this paper for brevity. For the details of the equations, the reader is referred to Baclic *et al.* (1982).

For the segments/sub-divided segment with two-phase refrigerant flow inside the channel, since the minimum heat capacity on both sides would always be the heat capacity of the air stream, heat transfer between refrigerant and air streams can be solved in a modified effectiveness-NTU formulation.

The effectiveness for top and bottom of the control volume can be calculated based on equation (2-7) and (2-8).

$$\varepsilon_{top} = 1 - \exp(-NTU_{top}) \quad (2-7)$$

$$\varepsilon_{bot} = 1 - \exp(-NTU_{bot}) \quad (2-8)$$

Then, air outlet temperatures are obtained using equation (2-9) and (2-10).

$$T_{air,top,out} = T_{air,top,in} - \varepsilon_{top}(T_{air,top,in} - T_{ref,in}) \quad (2-9)$$

$$T_{air,bot,out} = T_{air,bot,in} - \varepsilon_{bot}(T_{air,bot,in} - T_{ref,in}) \quad (2-10)$$

Once the air side outlet conditions are solved, the overall capacity is calculated based on equation (2-11).

$$Q = \dot{m}_{air,top}(h_{air,top,out} - h_{air,top,in}) + \dot{m}_{air,bot}(h_{air,bot,out} - h_{air,bot,in}) \quad (2-11)$$

Based on conservation of energy, refrigerant outlet enthalpy is obtained.

$$h_{ref,out} = h_{ref,in} - Q / \dot{m}_{ref} \quad (2-12)$$

Both energy equation method and three-stream effectiveness-NTU method are validated and compared.

#### 2.2.4 Wet surface condition

When the heat transfer surface temperature is below the air dew point, dehumidification occurs. In this case, both sensible heat load and latent heat load should be considered while calculating the air-to-surface heat and mass transfer.

$$q = \alpha(T_s - T_{air}) + \alpha_d(\omega_s - \omega_{air})h_{fg} \quad (2-13)$$

To simplify the dehumidification problem, we can correlate the heat transfer coefficient  $\alpha$  with the mass transfer coefficient  $\alpha_d$  assuming Lewis number equals to one. Lewis number is defined as:

$$Le^{2/3} = \frac{\alpha}{C_{p,air}\alpha_d} \quad (2-14)$$

Such that we can represent the driving potential for simultaneous heat and mass transfer using enthalpy difference.

$$q = \alpha_d (h_s - h_{air}) \quad (2-15)$$

Taken the average of inlet and outlet enthalpy as the air enthalpy in above equation. The energy conservation on the air side becomes:

$$\alpha_d (A_p + \eta_{fin} A_s) \cdot (h_s - h_{air}) = \dot{m}_{air} (h_{air,out} - h_{air,in}) \quad (2-16)$$

For the proposed model, top air and bottom air are treated separately. Equation (2-16) is applied to the top and/or side(s) if the respective mean fin temperature(s) are/is found to be lower than dew point temperature. The air side mass balance is shown in equation (2-17).

$$\alpha_d (A_p + \eta_{fin} A_s) \cdot (\omega_s - \omega_{air}) = \dot{m}_{air} (\omega_{air,out} - \omega_{air,in}) \quad (2-17)$$

Known air outlet enthalpy and air outlet humidity ratio, the air outlet temperature can be calculated.

### 2.2.5 Hydraulic equation

For each port-segment, the refrigerant frictional pressure drop is calculated based on empirical correlations. The model ignores momentum pressure drop to avoid additional iteration to obtain the outlet condition of each control volume. The pressure drop calculation is independent of the heat transfer calculation. The prediction of frictional pressure drop in headers and expansion/contraction pressure drop between header and tubes are also based on empirical pressure drop correlations.

### 2.2.6 Segment sub-division

At the phase change point, the heat transfer and pressure drop characteristics changes intensely. Thus, even with a finite-volume approach, it is essential to locate

the phase change point. This accounts for the different heat transfer and pressure drop calculations in the varied phases. Once heat transfer and hydraulic equations of the control volume are solved, the outlet refrigerant phase is then compared to the inlet phase. If there is a phase transition in the port-segment, this port-segment would be further sub-divided in the refrigerant flow direction in order to locate the phase change point. The segment sub-division function is implemented based on the HX model developed by Jiang *et al.* (2006). The method can be generally applied to both evaporation and condensation applications. Up to two-phase change points can be located within a port-segment.

### **2.3 Model Validation**

The validation of proposed model against experimental data is presented in this section. Section 2.3.1 discusses the model validation with data points from the literature. The data points include condenser applications in automotive, air-conditioning and refrigeration using pure refrigerants. Section 2.3.2 discusses the model validation for CO<sub>2</sub> gas coolers/condensers. In section 2.3.3, the model is validated using industrial partner supplied data points for four different conventional geometry condensers and four variable geometry condensers. The refrigerants validated in this sub-section are pure refrigerant (R32) and refrigerant mixture (R410A). All the results presented are here are obtained using UA-AMTD method described in Section 2.3.2. Validation is also conducted using three-stream effectiveness-NTU method presented in Section 2.3.3 for additional verification. In addition, in our calculations all conventional geometry condenser cases are simulated using Schwentker *et al.* (2006) model for comparison purposes. Schwentker's MCHX model is a typical effectiveness-NTU based model that employs tube-segment approach. This model is computationally

faster but lacks VG-MCHX modeling capability. The thermophysical properties of refrigerants were calculated using the NIST REFPROP 9.1 (Lemmon et al., 2013).

An overview of experimental data points used for validation is summarized in Table 2-1. Eight different fluids, eighteen MCHX geometries, 227 data points are validated in this effort. 196 data points out of the validated data points have experimental energy balance within five percent. In the presented validation, these 196 data points are shown in the figures and are accounted for in the statistics. The average of air side and refrigerant side capacity is taken as the reference experimental capacity. Data points with low mass flux values are for refrigerator condenser applications. The low dew point temperature data points are under demist operation in automotive applications. Also, a wide range of reduced pressures is covered not only for non-CO<sub>2</sub> cases but also for super-critical CO<sub>2</sub> gas coolers and sub-critical CO<sub>2</sub> condensers. Clearly, most of empirical correlations are not applicable to the low mass flux cases, high air velocity cases and supercritical CO<sub>2</sub> cases.

**Table 2-1 Condenser and gas cooler experimental data summary**

Refrigerant	R1234yf, R134a, R152a, R290 (Propane), R32, R410A, R717 (Ammonia), CO <sub>2</sub>
Mass flux [kg/m <sup>2</sup> s]	12-1045
Dew point temperature [C]	19-69
Reduced pressure	0.11-0.6 (Non-CO <sub>2</sub> Cases); 0.93-1.95 (CO <sub>2</sub> Cases)
Air frontal velocity [m/s]	1.2-5
Number of slabs	1-5
Number of conventional geometry condenser data points	120
Number of conventional geometry CO <sub>2</sub> gas cooler/condenser data points	84
Number of variable geometry condenser data points	23
Total number of data points validated	227
Total number of data points presented (Experimental energy imbalance less than 5%)	196

For all the cases, Churchill correlation is used to calculate single-phase refrigerant side pressure drop. Gnielinski correlation is applied in single-phase refrigerant side heat transfer prediction. The heat transfer and pressure drop correlations are tuned when the applied correlation is not applicable to the working conditions or the heat exchanger geometry is not within the valid parameter ranges. The heat transfer and pressure drop correction factors for each validation data sets will be presented in the following sections. Huang *et al.* (2014) studied the sensitivity of two-phase heat transfer and pressure drop empirical correlations. The correlations are sensitive to the type of fluids, the working conditions as well as the prediction of the fluids. In numerical simulations, the pressure drop predictions are typically yield to

larger error as compared to capacity predictions. This is due to the fact that there are very limited pressure drop correlations available in the literature. However, it should be noted that the pressure drop prediction do not have significant effect on capacity prediction, especially for CO<sub>2</sub> gas cooler cases operating at high pressure level. The authors share these findings with the readers such that the model and validation efforts can be useful to real engineering applications.

### 2.3.1 Conventional geometry condenser data

In this section, the model is validated against data points from five different data sources and twelve different geometries. The tested fluids are R134a, R152a, R290, R32, R410A, R717 and R1234yf. The header of automotive condenser tested by Eisele (2012) was cut open to obtain detailed port and header geometry. For four industrial partner provided CG-MCHXs and Eisele (2012)'s condenser, the dimensions of both intermediate port (i) and end port (e) are used in model. The geometry information for the four CG-MCHXs is given in Table 2-2. For Schwentker's model, the port dimension is assumed uniform. The pressure data from Eisele (2012) is not sufficient for validation. Thus, the pressure drop validation for this data set is not presented. A summary of correlations and correction factors used in this validation is available in Table 2-3. For Hoehne and Hrnjak (2004) data, the refrigerant mass flux in the serpentine type heat exchanger is around 150 [kg/m<sup>2</sup>s], which is within the correlation's valid range. However, the mass flux ranges from 12 to 40 [kg/m<sup>2</sup>s] for the one-pass and two-pass cases. For these cases, the empirical correlations under-predict both heat transfer and pressure drop. Thus, we applied the corrected factors. For the one-pass condenser case with closed ports, we only modeled for the open ports.

**Table 2-2 Geometry details of manufacture provided CG-MCHXs**

Heat exchanger	Number of tubes	Number of main section tubes	Fin type	Tube type	Port type
CG-MCHX-A	26	23	Fin-A	Tube-A	Port-A (i,e)
CG-MCHX-B	23	23	Fin-B	Tube-B	Port-B (i,e)
CG-MCHX-C	34	34	Fin-B	Tube-B	Port-B (i,e)
CG-MCHX-D	67	67	Fin-B	Tube-B	Port-B (i,e)

**Table 2-3 Selected correlations and correction factors for conventional geometry condenser validation**

Data source	Heat transfer correlation (Correction factor)		Pressure drop correlation (Correction factor)
	Air side	Refrigerant side two-phase	Refrigerant side two-phase
Eisele, 2012	Chang (1.4)	Shah (1.0)	Homogeneous (1.0)
Hoehne & Hrnjak, 2004, R290, Serpentine	Chang (1.0)	Shah (1.0)	Friedel (1.0)
Hoehne & Hrnjak, 2004, R290, TwoPass	Chang (1.5)	Traviss (1.5)	Lockhart–Martinelli (1.0)
Hoehne & Hrnjak, 2004, R290, OnePassOpen	Chang (1.5)	Traviss (2.0)	Lockhart–Martinelli (2.0)
Hoehne & Hrnjak, 2004, R290, OnePassClosed	Chang (1.5)	Traviss (3.0)	Lockhart–Martinelli (3.0)
Litch & Hrnjak, 1999, R717, Serpentine	Chang (1.0)	Shah (1.0)	Homogeneous (1.0)
Litch & Hrnjak, 1999, R717, Two Pass	Chang (1.0)	Shah (1.0)	Homogeneous (0.77)
Jin & Hrnjak, 2012	Chang (1.0)	Shah (1.0)	LockhartMartinelli (1.0)
CG-MCHX-A	Fin-A correlation (1.0)	Traviss (1.0)	Friedel (1.0)
CG-MCHX-B	Fin-B correlation (1.0)	Shah (1.0)	Lockhart–Martinelli (1.0)
CG-MCHX-C	Fin-B correlation (1.0)	Shah (1.0)	Lockhart–Martinelli (1.5)
CG-MCHX-D	Fin-B correlation (1.0)	Shah (1.0)	Lockhart–Martinelli (1.5)

The comparisons of simulated heat loads and pressure drops against experimental data are presented in Figure 10. 77 data points out 90 yield to absolute heat load deviations less than five percent. The average absolute deviation between experimental data and simulated results is 21.5%.

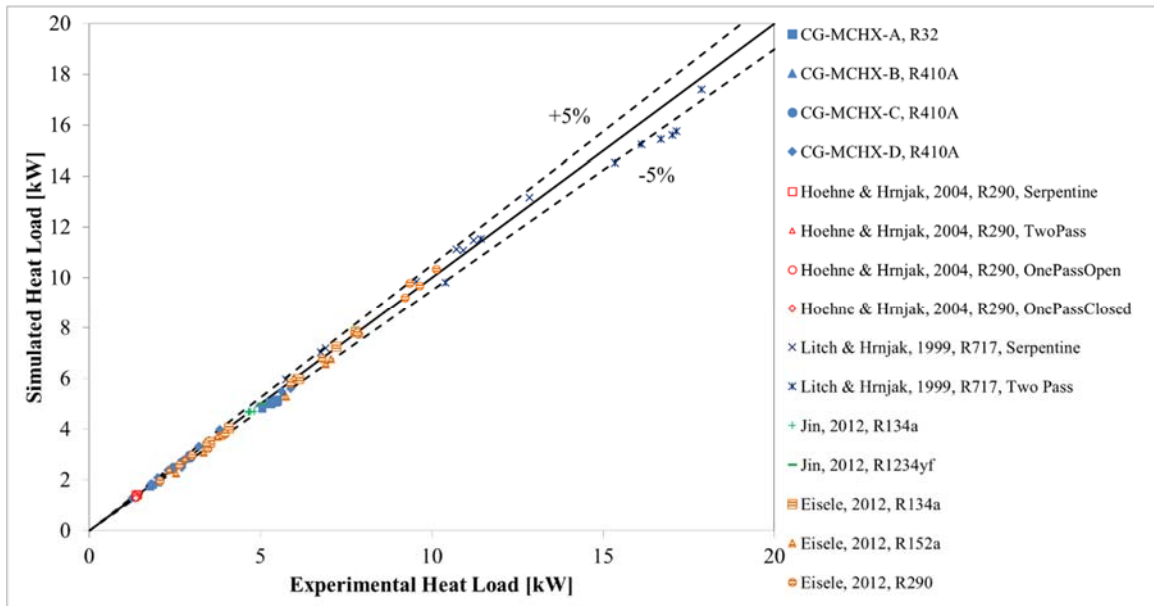


**Figure 2-10(a) Heat load validation of conventional geometry condensers**

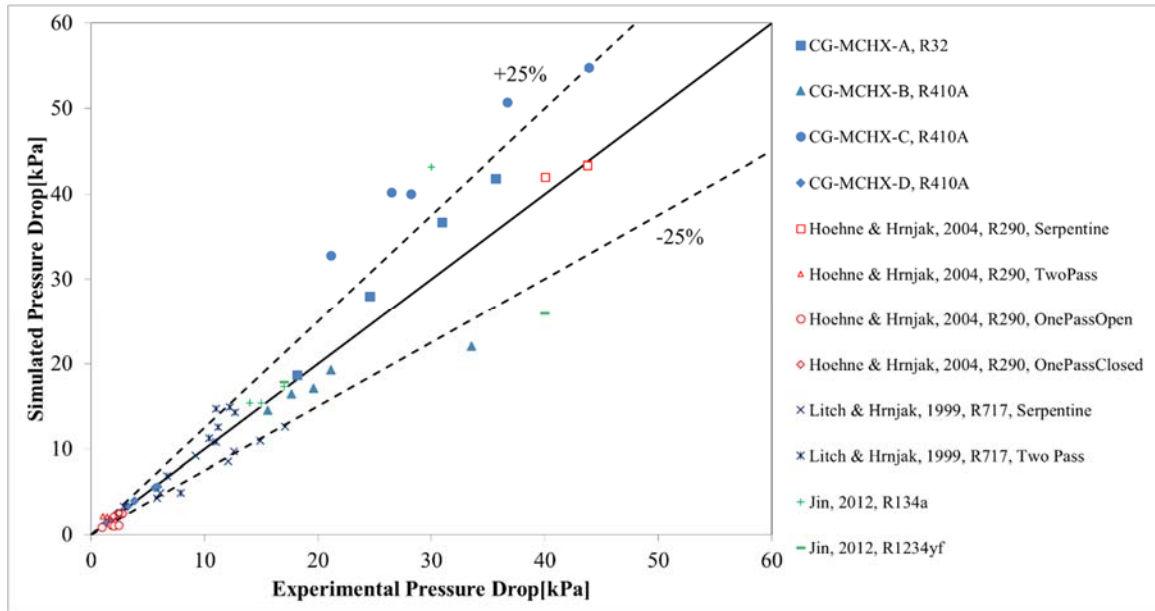


**Figure 2-10 Validation of conventional geometry condensers(b) Pressure drop validation of conventional geometry condensers**

**Figure 2-10 Validation of conventional geometry condensers**

### 2.3.2 Conventional geometry CO<sub>2</sub> gas cooler/condenser data

84 data points of CO<sub>2</sub> gas coolers and trans-critical condenser test data from Zhao *et al* (2001) and Yin *et al.* (2001) are validated in this section. For Zhao's MCHX, the variable geometry feature in the proposed model is applied to simulate the extra fin height at each bank's center. Through literature review, the authors were not able to find any empirical correlation for super-critical CO<sub>2</sub> pressure drop prediction. The experimental pressure drop is only 0.7%-4.4% of the working pressure level. The heat transfer deviation induced by pressure drop is minor in the cases of super-critical and trans-critical CO<sub>2</sub> applications. In the validation, a correction factor of 3.9 on pressure drop calculation is applied to Zhao's data at relatively lower working pressure. A correction factor of 5 is applied on the validation of Yin's data where the reduced pressure ranges from 1.04-1.95. Table 2-4 summarizes of correlations and correction

factors used in this validation. The comparison between experimental data and simulated value is shown in Figure 2-11. In this set of validation, 82 out of 84 simulated data point match the experimental heat load within  $\pm 5\%$ . For pressure drop, as shown in Figure 2-11 (b), the deviations are not one-directional for both data sets. A suitable CO<sub>2</sub> super-critical correlation is desired to accurately predict the pressure drop for such applications.

**Table 2-4 Selected correlations and correction factors for conventional geometry CO<sub>2</sub> gas cooler/condenser validation**

Data source	Heat transfer correlation (Correction factor)			Pressure drop correlation (Correction factor)	
	Air side	Refrigerant side two-phase	Refrigerant side super-critical	Refrigerant side two-phase	Refrigerant side super-critical
Zhao <i>et al.</i> 2001	Chang (1.0)	Shah (1.0)	Liao (1.0)	Friedel (5.0)	Churchill (5.0)
Yin <i>et al.</i> 2001	Chang (1.0)	N/A	Liao (1.0)	N/A	Churchill (3.9)

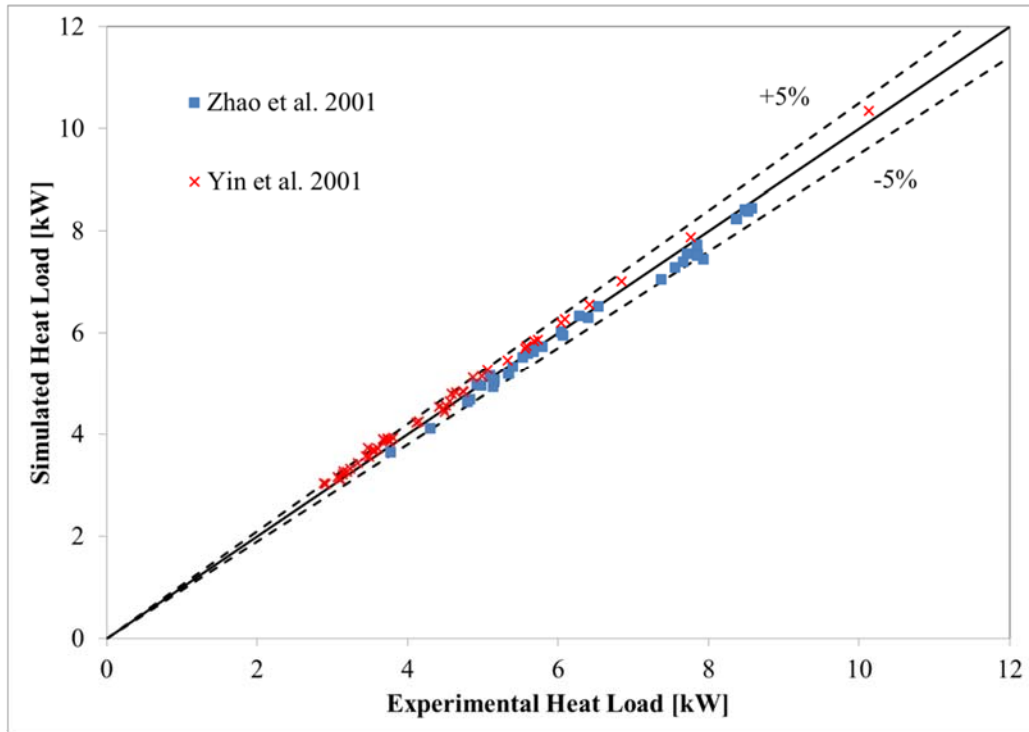


Figure 2-11(a) Heat load validation of conventional geometry CO<sub>2</sub> gas coolers/condensers

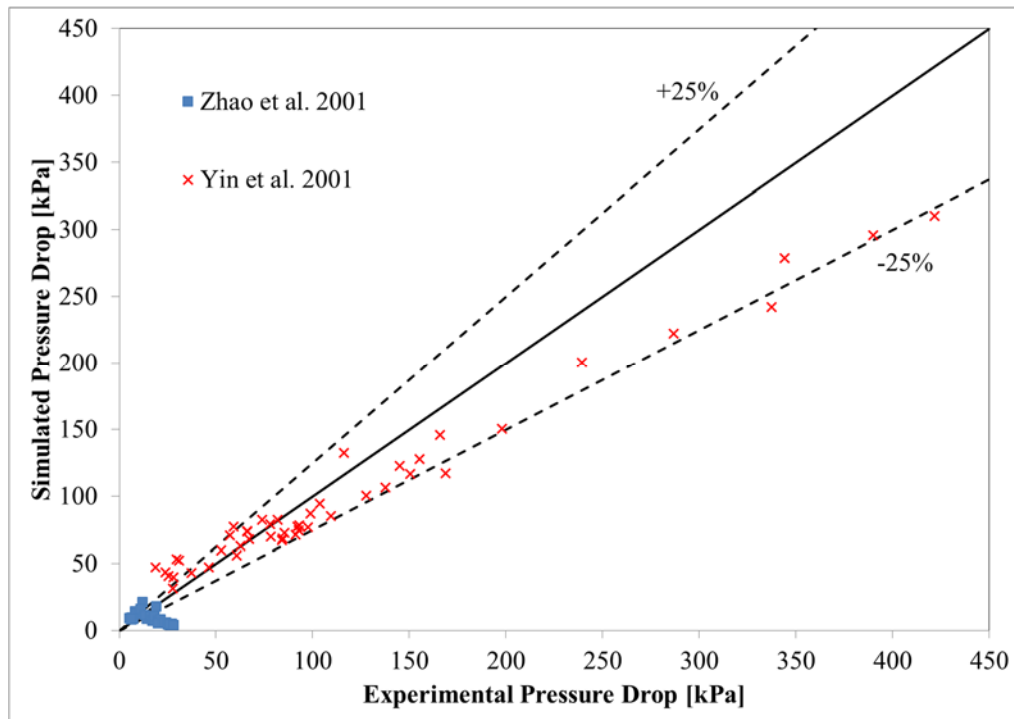


Figure 2-11(b) Pressure drop validation of conventional geometry CO<sub>2</sub> gas coolers/condensers

Figure 2-11 Validation of conventional geometry CO<sub>2</sub> gas coolers/condensers

### 2.3.3 Variable geometry condenser data from industrial partner

This set of validation includes four VG-MCHXs. The basic geometry information is provided in Table 2-5. For each VG-MCHX case, there are two different tubes and two different set of port dimensions. For each tube, the end ports (e) and intermediate ports (i) are modeled based on their respective geometries. The selected correlations and correction factors are tabulated in Table 2-6. The air-side correlations are manufacture provided correlations for the three fin types used in the MCHXs. There are no correction factors required for heat transfer. The pressure drop calculations for VG-MCHX-A is slightly tuned. The comparison between simulated results and experimental data are presented in Figure 12. The average absolute heat load and pressure drop deviations are 2.56% and 12% respectively. Based on the presented validations, the proposed model is capable of accurately predicting VG-MCHX performance.

**Table 2-5 Geometry details of manufacture provided VG-MCHXs**

Heat exchanger	Number of tubes	Number of main section tubes	Fin type	Tube type	Port type
VG-MCHX-A	26	21	Fin-C	Tube-C,D	Port-C (i,e),D (i,e)
VG-MCHX-B	25	21	Fin-C	Tube-E,F	Port-E (i,e),F (i,e)
VG-MCHX-C	25	20	Fin-C	Tube-E,F	Port-E (i,e),F (i,e)
VG-MCHX-D	25	18	Fin-C	Tube-E,F	Port-E (i,e),F (i,e)

**Table 2-6 Selected correlations and correction factors for industrial partner provided condenser data**

MCHX type	Heat transfer correlation (Correction factor)		Pressure drop correlation (Correction factor)
	Air side	Refrigerant side two-phase	Refrigerant side two-phase
VG-MCHX-A	Fin-C correlation (1.0)	Shah (1.0)	Homogeneous (0.68)
VG-MCHX-B	Fin-C correlation (1.0)	Shah (1.0)	Friedel (1.0)
VG-MCHX-C	Fin-C correlation (1.0)	Shah (1.0)	Friedel (1.0)
VG-MCHX-D	Fin-C correlation (1.0)	Shah (1.0)	Friedel (1.0)

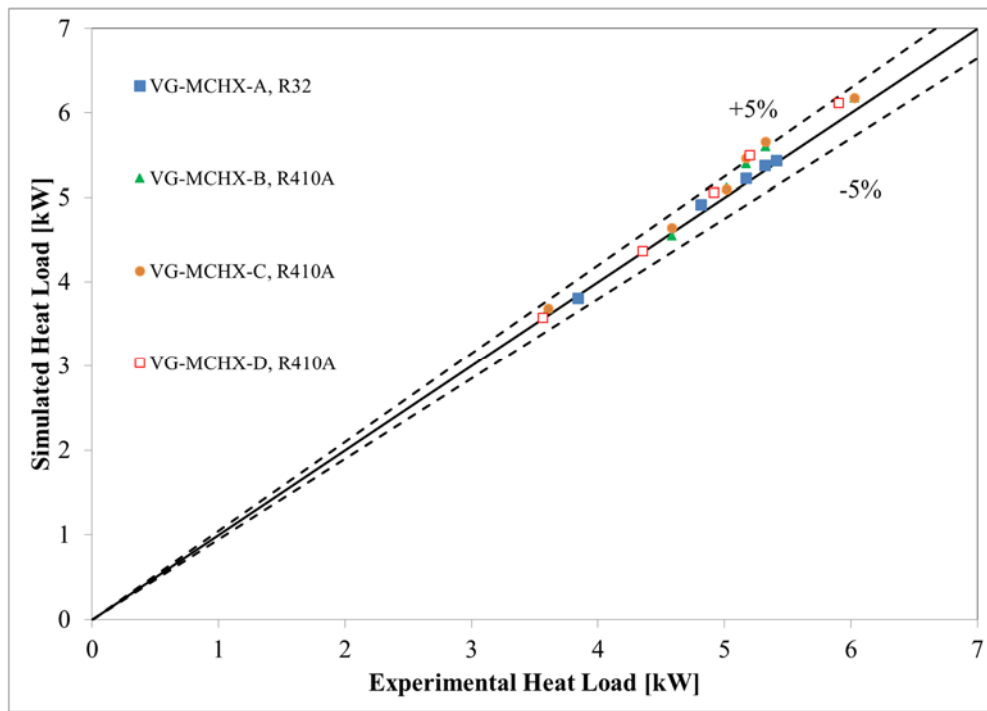


**Figure 2-12(a) Heat load validation of variable geometry condensers**

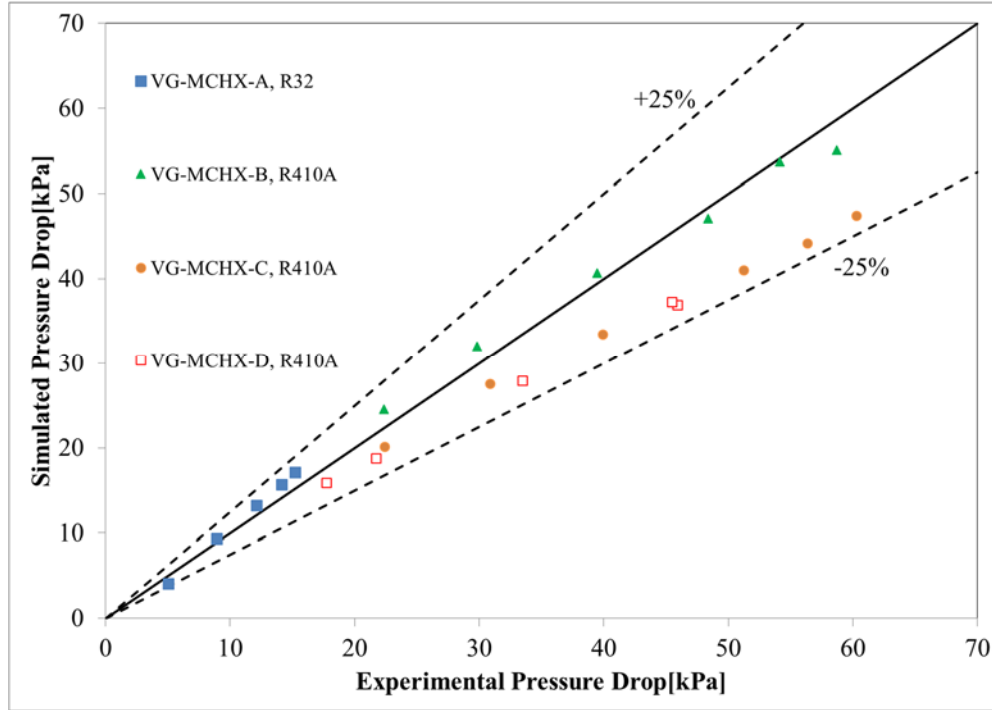


**Figure 2-12(b) Pressure drop validation of variable geometry condensers**

**Figure 2-12 Validation of variable geometry condensers**

### 2.3.4 Validation summary

All the validation results presented in previous sub-sections are based on UA-AMTD method in the proposed model. The same validations were carried out using three-stream effectiveness-NTU method. We also implemented Schwentker’s model to represent the previous microchannel condenser models. We validated Schwentker’s model for all the conventional geometry condensers/gas coolers. The validation carried out using three different approaches is summarized in Table 8. Based on the validation summary, the authors conclude that:

- a) The proposed model is capable of modeling the new generation VG-MCHXs.
- b) Both heat load and pressure drop are well captured using the proposed model.
- c) Using the three-stream UA-AMTD method developed in this paper, the computational cost is only 8.8% of the three-stream effectiveness-NTU method.

**Table 2-7 Validation summary and comparison of three approaches**

MCHX type	Avg. abs. heat load deviation [%]			Avg. abs pressure drop deviation [%]			Avg. calculation time [s]		
	UA-AMTD	Three-Stream NTU	Schwentker <i>et al.</i> (2006)	UA-AMTD	Three-Stream NTU	Schwentker <i>et al.</i> (2006)	UA-AMTD	Three-Stream NTU	Schwentker <i>et al.</i> (2006)
Conventional geometry condensers	2.92%	2.96%	2.45%	21.51%	22.76%	21.49%	4.69	11.65	0.23
Conventional geometry CO <sub>2</sub> gas coolers/condensers	2.51%	2.28%	2.53%	39.64%	39.23%	39.83%	23.04	316.34	4.87
Variable geometry condensers	2.56%	2.38%	N/A	12.04%	11.98%	N/A	5.14	13.11	N/A
All data points	2.70%	2.60%	2.49%	28.09%	28.52%	30.50%	12.60	142.40	2.47

## 2.4 Summary

I developed a new model for variable geometry microchannel air-to-refrigerant condensers and gas coolers. This model has the capability of accounting for variable geometric parameters, such as fin types, fin dimensions, tube geometries, port shapes and the locations of the tubes and fins. The model adopts a port-by-port segmented approach along with sub-divided function that can locate the refrigerant flow phase change point. The three-stream UA-AMTD method is developed in order to account for the variable fins on top and bottom of the tube. The model based the air-side propagation on the location of the tubes and fins on a Cartesian grid. The port-by-port approach allows one to account for the change in air-side heat transfer coefficient in the direction of air flow. I validated the new model against experimental data from seven different sources, for eight different fluids, and eighteen MCHX geometries. The average absolute deviations of heat transfer and pressure drop are 2.7% and 28% respectively. For specific geometries and operating conditions that are out of the valid

ranges of the existing heat transfer and pressure drop correlations, correction factors are applied on the presented validation. Although the primary contribution of this research is the modeling methodology of VG-MCHXs, the authors share the findings on the heat transfer and pressure drop correlations during the validation for the proposed model's usefulness in engineering applications. More investigations are needed, both experimentally and numerically, to improve model's the performance under these specific conditions and geometries. Compared to effectiveness-NTU based method, the developed three-stream UA-AMTD method achieved more than 10X computational speedup without sacrificing accuracy. The design case study showed a potential material saving of more than 12% comparing VG-MCHX and CG-MCHX.

### 3 MICROCHANNEL HEAT EXCHANGER MODELING UNDER DRY, WET AND PARTIALLY WET SURFACE CONDITIONS ACCOUNTING FOR TUBE-TO-TUBE HEAT CONDUCTION

The literature survey suggests that there lacks a general MCHX modeling approach that accounts for tube-to-tube heat conduction under dry, wet and partially wet surface condition. This chapter introduces a comprehensive fin analysis approach to model the heat and mass transfer for the above mentioned three surface conditions within a finite volume. A top level VG-MCHX model was developed along with the proposed fin analysis method to correctly account for the air and refrigerant flow on the heat exchanger level. The model was validated against 65 data points for eight different microchannel condensers and evaporators, including conventional geometry MCHX (CG-MCHX) as well as VG-MCHX.

#### **3.1 Modeling Details**

##### 3.1.1 Basic solving methodology

The proposed model applies a segment-by-segment approach to analyze both the refrigerant side and the air side. The following assumptions are made:

- Steady state model
- Thermally and hydro-dynamically fully developed flow
- The thermo-physical properties and heat transfer coefficients are evaluated based on the inlet of each segment
- Refrigerant is well-mixed in the intermediate header
- Horizontal air flow
- Uniform port inner wall temperature
- No conduction between tube end walls and end ports/segments

- No longitudinal conduction in the air flow direction

The refrigerant side is solved in a sequential order in the direction of refrigerant flow as discussed in Chapter 1. The air-side propagation is conducted iteratively between tube banks. For single bank MCHX, the proposed model does not require air-side iteration as the model solves each air/fin segment in a sequential order. An example of air-side discretization for a VG-MCHX is shown in Figure 3-1. The top Tube-1 has three refrigerant side port/segment whereas the bottom Tube-2 has four refrigerant side port/segment. The proposed model divides the fin into 7 segments in the airflow direction based on the relative locations of the refrigerant side port/segment. This is different than previous models that divide the air and fin into segments perpendicular to the air flow. The proposed model does not require such discretization when applying the proposed air-to-surface heat and mass transfer approach.

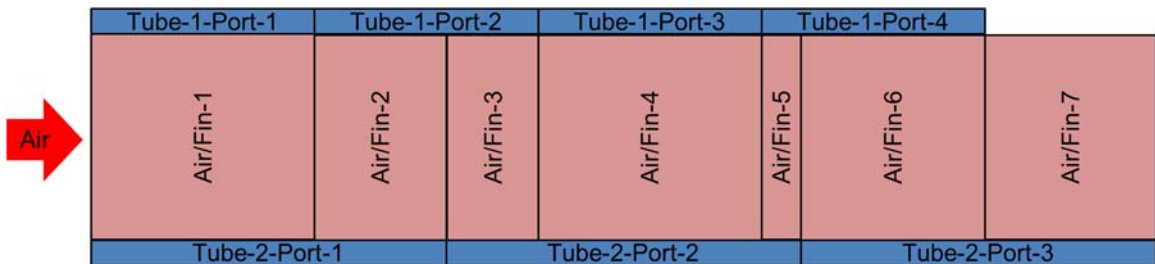


**Figure 3-1 Air side discretization**

The top level solution methodology is presented in Figure 3-2. In order to account for the tube-to-tube conduction, the tube wall temperatures of every port/segment are solved iteratively. A reasonable set of wall temperature guess values is required to speed up the calculation. For the proposed model, the calculated wall temperatures from the three stream model in Chapter 2 are used as the initial guess values.

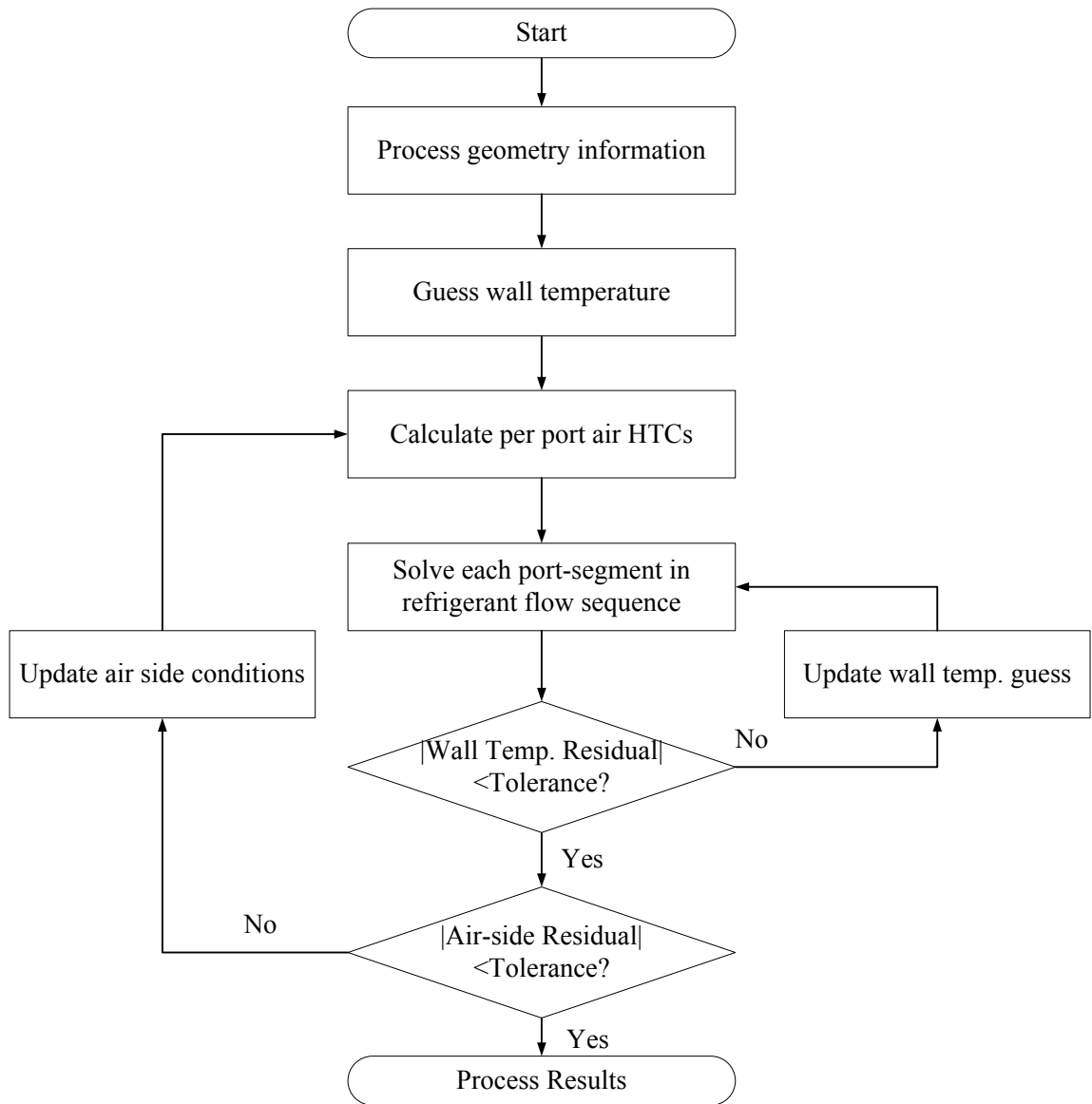


**Figure 3-2 Solution methodology for proposed model**

### 3.1.2 Air-to-surface heat and mass transfer

This section focuses on the analytical approach used to solve one air/fin segment shown in Figure 3-2. The proposed approach solves the air-to-surface heat and mass transfer for the control volume under dry, wet and partially wet conditions. For VG-MCHX, there are two possible fin and tube geometries. Typically, the fin is in between of two tubes (ports). This case is referred to as “prescribed temperature” case. For the

top and bottom tube of the MCHX, as well as the fin extension as indicated by Air/Fin Segment-7 in Figure 2, the proposed model assumes that the fin tip is adiabatic.

### 3.1.2.1 Dry surface condition

According to Asinari *et al.* (2004), the longitudinal conduction in the air flow direction has negligible effect on the total heat flow and temperature distribution. Thus, the model assumes that there is no heat conduction over the fin in the air flow direction. The conduction analysis on the fin surface becomes a one-dimensional problem (tube-to-tube). The dry surface case heat conduction problem has been solved as an empirical heat transfer problem (Incropera *et al.* 2011). Considering MCHX applications, both the adiabatic fin tip case and the prescribed fin tip temperature case need to be accounted for. The adiabatic fin tip assumption is applied to the top and bottom fins and fin extensions arising in variable geometry MCHX. In this case, fin tip is generally assumed to be adiabatic due to the minimal heat transfer area and low temperature difference between the tip surface and air. The energy balance on the fin element can be expressed as:

$$\frac{d^2T}{dx^2} = \frac{\alpha P}{kA_c} [(T - T_{air})] \quad (3-1)$$

Where T is the surface temperature. For simplification of the equation, excess temperature  $\theta$  can be defined:

$$\theta = T - T_{air} \quad (3-2)$$

Equation (3-1) can be re-written as:

$$\frac{d^2\theta}{dx^2} = m^2\theta \quad (3-3)$$

where m is defined in Equation (3-4).

$$m^2 = \alpha P / kA_c \quad (3-4)$$

Equation (3-3) then becomes a second-order differential equation with constant coefficient. The general solution is

$$\theta(x) = C_1 e^{mx} + C_2 e^{-mx} \quad (3-5)$$

For the adiabatic fin tip case shown in Figure 3-3, we have the boundary condition at the port wall surface ( $L=0$ ) and fin tip in Equation (3-6).

$$\begin{aligned} \theta(0) &= \theta_{top} \\ d\theta / dx \big|_{x=L} &= 0 \end{aligned} \quad (3-6)$$

Where  $L$  is the fin height. Hence the temperature distribution over the fin can be obtained.

$$\theta / \theta_{top} = \frac{\cosh m(L-x)}{\cosh mL} \quad (3-7)$$

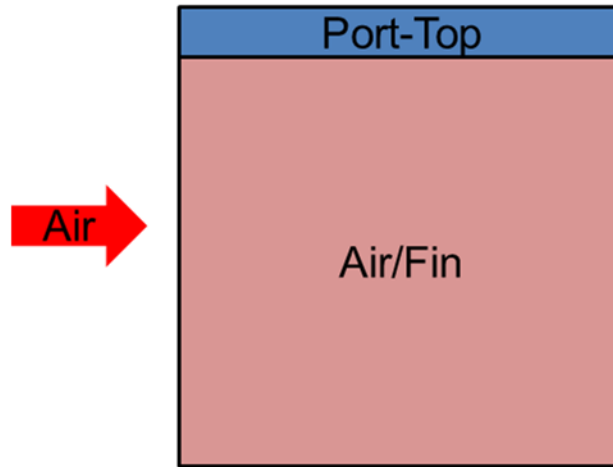


**Figure 3-3 Adiabatic fin tip air/fin segment**

To obtain the heat transfer rate on the fin, apply Fourier's law at the fin base.

$$Q = -kA_c \frac{d\theta}{dx} \bigg|_{x=0} \quad (3-8)$$

Since the temperature distribution over the fin is known, the heat transfer rate can be calculated as

$$Q_{top} = \frac{\alpha P}{m} \theta_{top} \tanh(mL) \quad (3-9)$$

For the case with prescribed temperature at the fin tip as shown in Figure 3-4, the boundary conditions are described in Equation (3-10).

$$\begin{aligned} \theta(0) &= \theta_{top} \\ \theta(L) &= \theta_{bottom} \end{aligned} \quad (3-10)$$

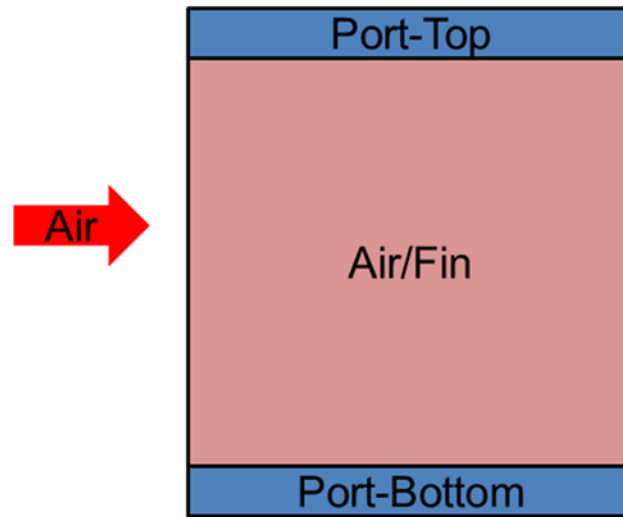


**Figure 3-4 Prescribed temperature air/fin segment**

For this case, the fin temperature distribution is derived as below

$$\theta / \theta_{top} = \frac{(\theta_{bottom} / \theta_{top}) \sinh mx + \sinh m(L-x)}{\sinh mL} \quad (3-11)$$

The heat transfer rate at the top and bottom of the fin surface are

$$Q_{top} = \frac{\alpha P}{m} \theta_{top} \frac{\cosh mL - \theta_{bottom} / \theta_{top}}{\sinh mL} \quad (3-12)$$

$$Q_{bottom} = \frac{\alpha P}{m} \theta_{bottom} \frac{\cosh mL - \theta_{top} / \theta_{bottom}}{\sinh mL} \quad (3-13)$$

### 3.1.2.2 Wet surface condition

McQuiston (1975) derived the fin efficiency formulation for combined heat and mass transfer for the adiabatic fin tip case. In the proposed model, McQuiston's assumption on the relationship between humidity ratio difference and temperature difference is simplified by calculating the ratio based on air inlet condition for a control volume. We derive the heat and mass transfer for prescribed fin tip temperature air/fin segment.

The energy balance on a fin element assuming one-dimensional heat conduction:

$$\frac{d^2T}{dx^2} = \frac{P}{kA_c} [\alpha(T - T_{air}) + \alpha_d h_{fg} (\omega - \omega_{air})] \quad (3-14)$$

Unlike the dry surface condition problem, in Equation (3-14), there are two unknowns: the fin surface temperature and the humidity ratio of saturated air based on surface temperature. Several assumptions are made to simplify this problem. First, the Lewis number is assumed to be unity.

$$Le^{2/3} = 1 = \alpha / (\alpha_d C_{p,air}) \quad (3-15)$$

McQuiston (1975) proposed a linearized relationship between air-to-surface temperature difference and humidity difference.

$$C = \frac{(\omega - \omega_{air})}{(T - T_{air})} = \frac{(\omega_{fin,base} - \omega_{air})}{(T_{fin,base} - T_{air})} \quad (3-16)$$

McQuiston (1975) suggested to use the average C value calculated at heat exchanger inlet and outlet. Here, for the finite-volume, C is assumed to be constant within the segment in order to avoid additional iterations. Applying Equation (3-15) and Equation (3-16), Equation (3-14) becomes:

$$\frac{d^2T}{dx^2} = \left(\frac{\alpha P}{kA_c}\right)\left(1 + C \frac{h_{fg}}{C_{p,air}}\right)(T - T_{air}) \quad (3-17)$$

Here, we define parameter M as:

$$M^2 = \left(\frac{\alpha P}{kA_c}\right)\left(1 + C \frac{h_{fg}}{C_{p,a}}\right) \quad (3-18)$$

Similar to the derivation of temperature distribution for the dry surface condition.

For adiabatic fin tip case

$$\theta / \theta_{top} = \frac{\cosh M(L-x)}{\cosh ML} \quad (3-19)$$

The heat transfer rate can be calculated as

$$Q_{top} = \frac{\alpha P}{M} \left(1 + C \frac{h_{fg}}{C_{p,a}}\right) \theta_{top} \tanh(ML) \quad (3-20)$$

For prescribed temperature case, with above simplifications, the temperature distribution is

$$\theta / \theta_{top} = \frac{(\theta_{bottom} / \theta_{top}) \sinh Mx + \sinh M(L-x)}{\sinh ML} \quad (3-21)$$

The heat transfer rate at the top and bottom of the fin:

$$Q_{top} = \frac{\alpha P}{M} \left(1 + C \frac{h_{fg}}{C_{p,a}}\right) \theta_{top} \frac{\cosh ML - \theta_{bottom} / \theta_{top}}{\sinh ML} \quad (3-22)$$

$$Q_{bottom} = \frac{\alpha P}{M} \left(1 + C \frac{h_{fg}}{C_{p,a}}\right) \theta_{bottom} \frac{\cosh ML - \theta_{top} / \theta_{bottom}}{\sinh ML} \quad (3-23)$$

### 3.1.2.3 Partially wet surface condition

The proposed top level heat exchanger model adapts segment-by-segment (as known as finite volume) approach. Over the fin surface, even on a finite volume basis as shown in Figure 3-1, it is possible that only a portion of the surface is wet. Under

this circumstance, the dry portion and wet portion(s) need to be treated separately. Figure 3-5 shows a typical case of partially wet surface condition with adiabatic fin tip. Near the cold port outer wall, Section-a is wet whereas Section-b is at dry condition. It is known that at the boundary of Section-a and Section-b, the fin temperature is at air dew point temperature. Given the steady state condition, the heat transfer rate from Section-a to Section-b should be equivalent to that from Section-b to Section-a as shown in Equation (3-24). The height of Section-a can then be determined iteratively.

$$Q_{a-b} = -Q_{b-a} \quad (3-24)$$

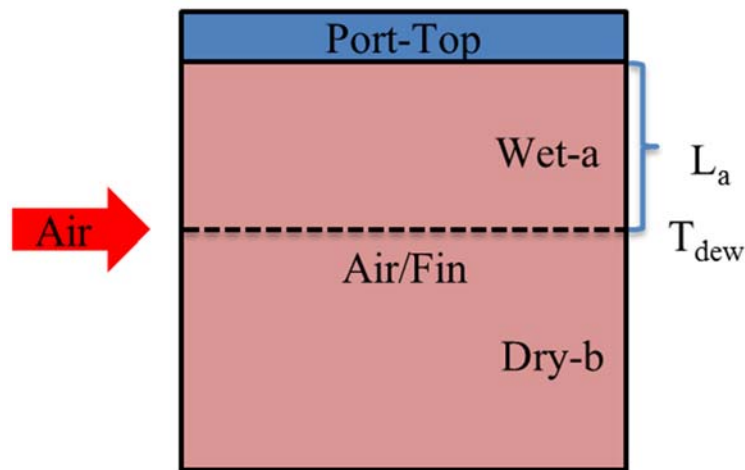


**Figure 3-5 Partially wet adiabatic fin tip air/fin segment**

For the fin surface between two port walls, a typical partially wet case is shown in Figure 3-6. In this case, Section-a and Section-c are under wet condition. Section-b has surface temperature above dew point. Knowing the temperature at the boundaries, the heat transfer rate at these three surfaces can be solved. Given Equation (3-25), the heights of these three fin sections can be obtained using an iterative approach.

$$\begin{aligned} Q_{a-b} &= -Q_{b-a} \\ Q_{b-c} &= -Q_{c-b} \end{aligned} \quad (3-25)$$

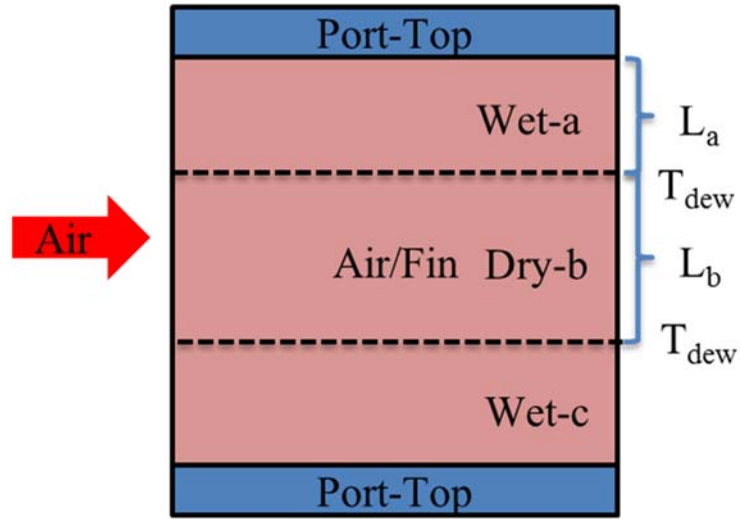


**Figure 3-6 Partially wet prescribed temperature air/fin segment**

### 3.1.3 Governing equations for refrigerant side control volume

The air-to-fin heat and mass transfer equations are given in Section 3.1.2 based on known tube wall temperature(s). As for the refrigerant side, the control volume (port-segment) is shown in Figure 3-7.

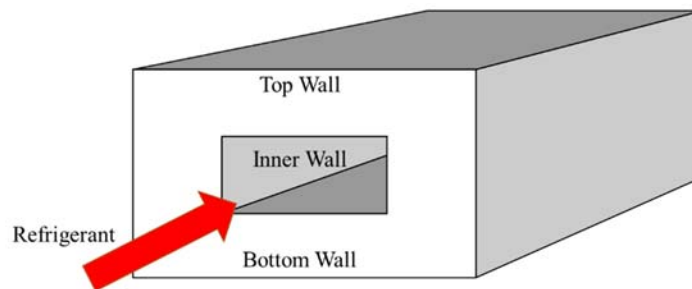


**Figure 3-7 Refrigerant side control volume**

This section provides a step-by-step approach to solve for the heat transfer rate on the refrigerant side and to update tube wall temperatures for the next iteration. Based on energy balance, the refrigerant side heat transfer rate equals to the heat transfer rate from air to fin surface as well as the tube walls. The refrigerant outlet enthalpy can

obtained by Equation (3-26) below. The air-side outlet conditions for each air/fin segment can be obtained based on the heat and mass transfer rate from air to fins and tubes. When the tube wall is attached to more than one air/fin segment (e.g. Tube-2-Port-2 in Figure 3-1), the air/fin segments are solved sequentially in the air flow direction.

$$\begin{aligned} \dot{m}_{ref} (h_{ref,in} - h_{ref,out}) = & \sum Q_{air-fin,top} + \sum Q_{air-tube,top} \\ & + \sum Q_{air-fin,bottom} + \sum Q_{air-tube,bottom} \end{aligned} \quad (3-26)$$

For each port-segment, the right hand side of Equation (3-26) is known with given wall temperatures. The momentum pressure drop on refrigerant side is neglected in the proposed model. Using frictional pressure drop predicted by empirical correlations, the refrigerant side outlet pressure can be calculated. The refrigerant outlet temperature is then calculated using property routines based on enthalpy and pressure. Knowing the refrigerant inlet and outlet temperatures, the proposed model use the arithmetic mean value of these two temperatures to represent refrigerant temperature. The effect of refrigerant saturation temperature drop is crucial for evaporator modeling. Unlike most of previous modeling efforts that assume constant refrigerant temperature at two-phase region, the proposed approach accounts for the two-phase refrigerant temperature variation due to pressure drop.

$$U_{ref} A_{inner} (T_{ref} - T_{wall,inner}) = \dot{m}_{ref} (h_{ref,in} - h_{ref,out}) \quad (3-27)$$

The port inner wall temperature can be calculated from Equation (3-27). Upon obtaining the inner wall temperature, the updated top and bottom wall temperatures can be calculated based on Equation (3-28) and (3-29). Here,  $\Delta x_{top}$  and  $\Delta x_{bot}$  port inner

walls and the tube walls on top and bottom. The inner port wall surface areas facing top and bottom are  $A_{inner,top}$  and  $A_{inner,bot}$ .

$$\frac{kA_{inner,top}}{\Delta x_{top}}(T_{wall,inner} - T_{wall,top}) = \sum Q_{air-fin,top} + \sum Q_{air-tube,top} \quad (3-28)$$

$$\frac{kA_{inner,bot}}{\Delta x_{bot}}(T_{wall,inner} - T_{wall,bot}) = \sum Q_{air-fin,bottom} + \sum Q_{air-tube,bottom} \quad (3-29)$$

### 3.2 Air-to-Fin Heat and Mass Transfer Model Comparison with CFD Simulation

#### 3.2.1 CFD simulation

Since conducting experimental testing on a single fin surface seems infeasible at this moment, CFD simulation is selected in this research as a basis for verification of the proposed model at the finite volume level (i.e., for one Air/Fin segment). CFD simulation can account for the following physics that are of interest in this study: 1) heat and mass transfer from air to surface; 2) heat conduction along the surface; 3) air flow propagation. A three dimensional computational domain for one fin was developed, as shown in Figure 3-8. At the inlet boundary of the computational domain, uniform distribution of velocity, dry bulb temperature and humidity ratio were assumed. The outlet boundary condition was set at a constant pressure (0.0 Pa gauge). The top and bottom tubes are set to constant temperature, whilst the fin was modeled as a solid body coupled to the tube wall so conduction can be evaluated. The lateral boundaries, longitudinal to fluid flow, were set as symmetry faces. The mesh of fluid portion within the heat transfer area has 251 nodes in the x-direction, with a element size growth ratio of 1.025, 251 equidistant nodes in the y-direction and 26 nodes in the z-direction with element size growth ratio of 1.125 shown in Figure 3-8 (b). The fin was meshed with 7 equidistant nodes in the z-direction.

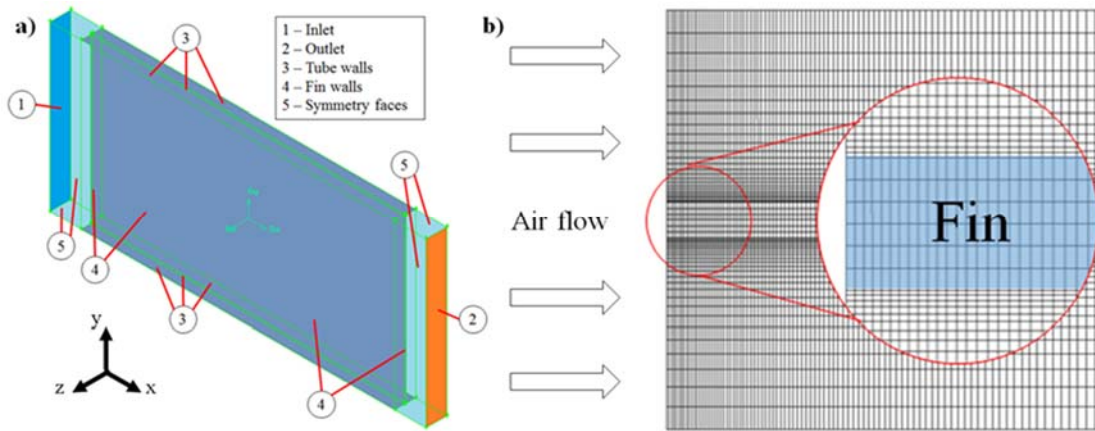


**Figure 3-8 CFD Computational domain a) Boundaries; b) Mesh view of top tube**

The turbulent  $k$ - $\epsilon$  realizable and laminar models were both investigated. For the dry fin case a steady state model was used, whereas for the wet fin case a transient condition was imposed and simulated until steady state. For the latter case a time step of 0.0001s and five iterations for each time step were found to be reasonable when using at least second order discretization schemes.

For post-processing purposes the local temperatures within the fin and average air properties in the planes transverse to fluid flow were retrieved from CFD results, according to the number of segments desired for comparison with the model presented in this paper.

Since all temperatures are known, the UA-LMTD method (Incropera *et al.*, 2011) can be used to determine the local sensible heat transfer coefficients for each segment. Additionally fin effectiveness does not need to be evaluated since an average wall temperature is used. Although the fin is modeled as a solid body, the Biot number for the fin is of the order of  $10^{-5}$ , therefore no temperature gradient in the  $z$ -direction is considered. The average wall temperature can be weighted by heat transfer area.

Additionally, neglecting the conduction resistance, the air side heat transfer coefficient is determined using the equations below.

$$\dot{Q}_i = \dot{m}_{air} \cdot c_{p,air} \cdot (\bar{T}_{air,i+1} - \bar{T}_{air,i}) \quad (3-30)$$

$$\dot{Q}_i = \alpha_{air,i} \cdot A_o \frac{(\bar{T}_{wall,i} - \bar{T}_{air,i}) - (\bar{T}_{wall,i} - \bar{T}_{air,i+1})}{\ln(\bar{T}_{wall,i} - \bar{T}_{air,i}) / (\bar{T}_{wall,i} - \bar{T}_{air,i+1})} \quad (3-31)$$

Where,

$$\bar{T}_{wall,i} = \frac{A_{fin} \cdot \bar{T}_{fin,i} + A_{tube} \cdot \bar{T}_{tube,i}}{A_{fin} + A_{tube}} \quad (3-32)$$

For the wet fin case, convective and diffusive mass transfer also need to be accounted for. A User-Defined-Function (UDF) based on Saraireh (2012) was implemented to evaluate the water flux based on humid air dew point temperature and water concentration gradient at the liquid-gas interface.

The CFD uncertainty analysis was carried out by employing the Grid Convergence Index (GCI) method (Roach, 1997). The uncertainty quantification was based on a constant mesh refinement ratio of 1.3, a limited observed order of accuracy between 0.5 and 2.0 (Oberkampf and Roy, 2010) and a factor of safety of 3, recommended by Roach (1997). The average air-side heat transfer coefficient presented an uncertainty of 0.20%, whereas the air-side pressure drop the uncertainty was 0.72%.

### 3.2.2 Dry fin surface comparison

A typical fin geometry is selected for the verification study. The dimensions are 17 mm depth, 8.89 mm height, 0.1 mm thickness and 1.14 mm spacing. All the simulations conducted using the proposed fin model is based on a 50 by 50 grid. It should be noted that the air-to-tube heat transfer is considered in both the proposed

model and the CFD simulation. Two wall temperature scenarios are modeled: 1) same constant wall temperatures on top and bottom of fin, 2) different wall temperatures on top and bottom of fin.

In the comparison study for dry fin case, we applied the model to a condenser application. The air inlet temperature is 308.15 [K]. In the equivalent constant wall temperature case, the top wall and bottom wall are kept constant at 350.15 [K]. Figure 3-9 shows the comparison of fin temperature distributions for both the proposed fin model and the CFD results. It is observed that the proposed model under predicts the fin temperature in the entrance region. Figure 3-10 represents the air temperature change from the air inlet (segment-0) to air outlet (segment-50). The capacities calculated by the two methods differ by 4.13%. For typical heat exchanger level capacity validation against experimental data, below 5% is considered good agreement.

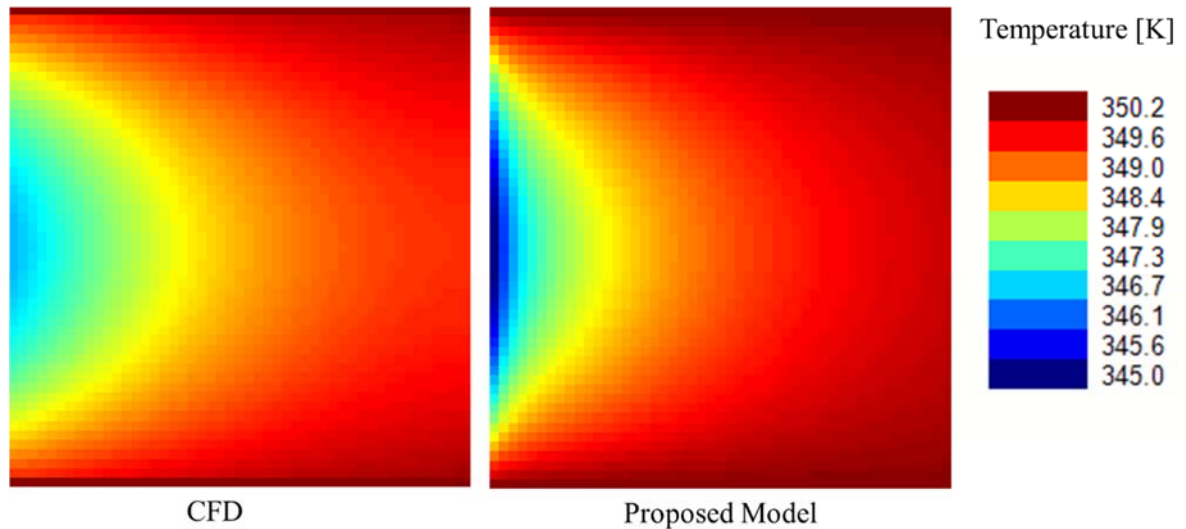


**Figure 3-9 Fin temperature distribution: top wall 350.15 [K], bottom wall 350.15 [K]**

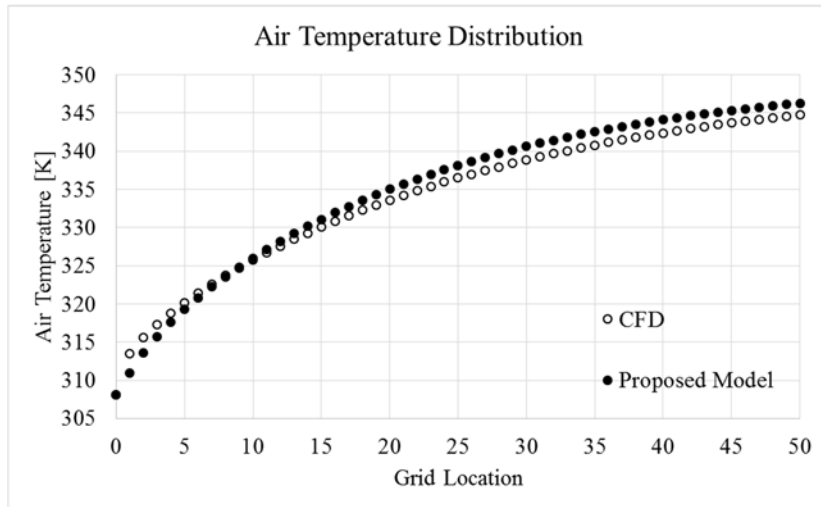


**Figure 3-10 Air temperature distribution: top wall 350.15 [K], bottom wall 350.15 [K]**

The comparison is then performed in the case where the top wall temperature is 340.15 [K] and the bottom wall temperature is 350.15 [K]. Figure 3-11 shows the fin surface temperature distribution. The wall temperatures predicted by the proposed model and the CFD simulation match very well. Figure 3-12 shows the comparison of air temperature distribution. The deviation in capacity prediction is 4.13%. The deviation is consistent with previous case study because the two case studies applied the same type of boundary conditions, using difference values.

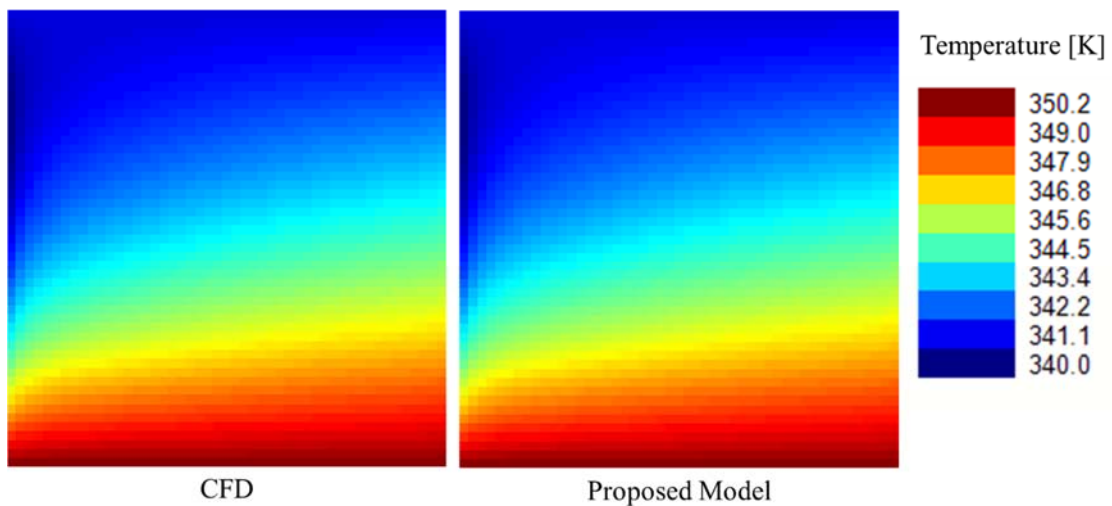


**Figure 3-11 Fin temperature distribution: top wall 340.15 [K], bottom wall 350.15 [K]**

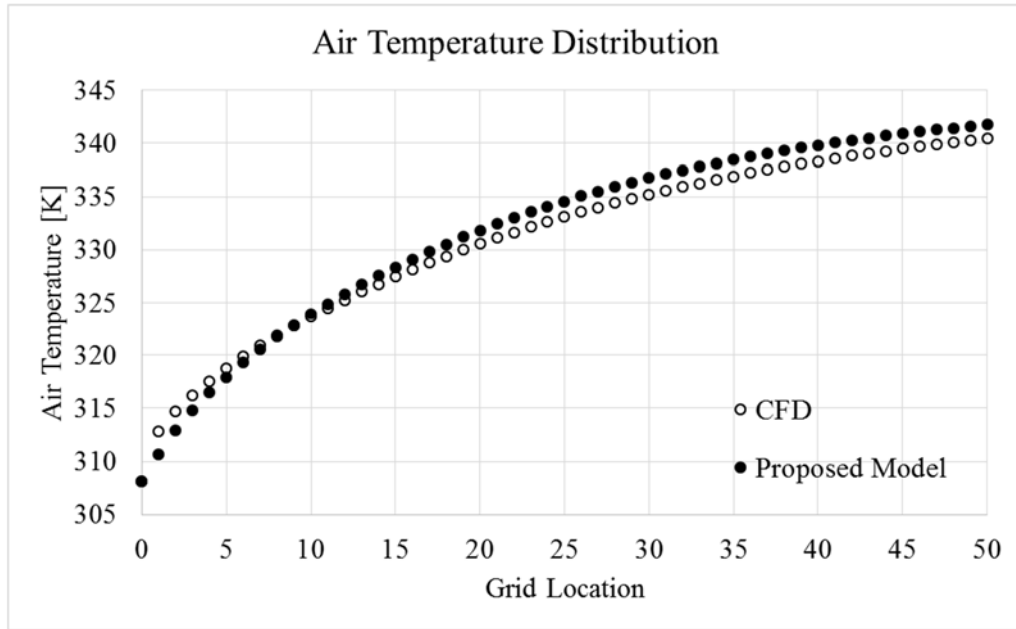


**Figure 3-12 Air temperature distribution: top wall 340.15 [K], bottom wall 350.15 [K]**

### 3.2.3 Wet fin surface comparison

The wet fin surface verification is conducted using the same fin geometry with air inlet temperature of 299.85 [K] and a relative humidity of 50.65%. Figure 3-13 shows the comparison of fin temperature distributions for the case where both wall temperatures are held constant at 278.15 [K]. Figure 3-14 represents the temperature and humidity ratio change from the air inlet to air outlet (segment 50). Due to different assumptions between CFD simulation and the proposed model in the relationship between temperature difference and humidity ratio difference between air and tube wall, also the difference in predicted inlet region fin surface temperature, the trend of humidity ratio change differs slightly. However, the two curves eventually converge at the same level of outlet humidity ratio because of the good agreement of fin surface temperature prediction in the majority of the fin surface. The capacities calculated by

the two different approaches shows a 3.39% deviation. The difference in sensible heat ratio between the two methods is 0.0074.

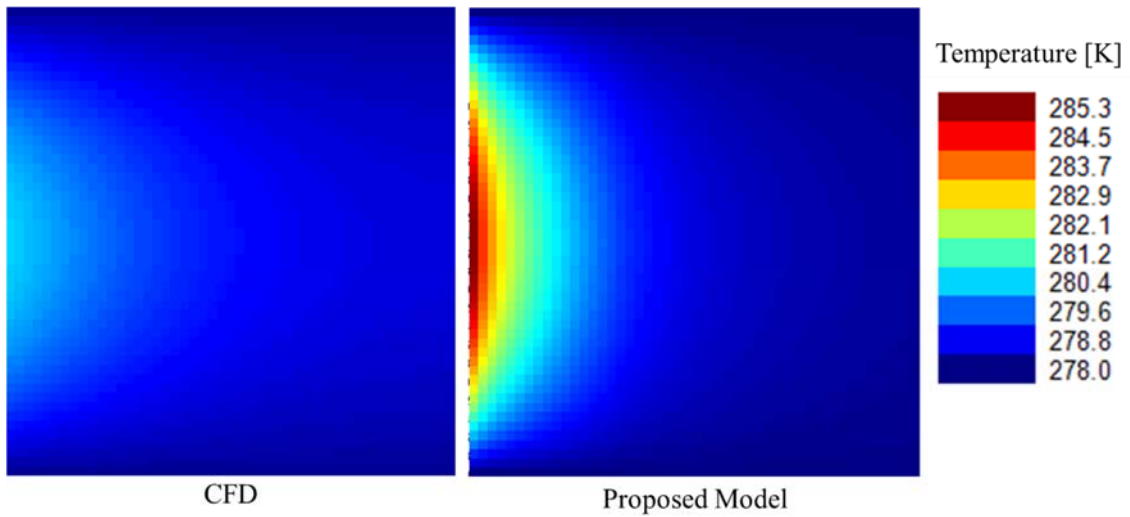


Figure 3-13 Fin temperature distribution: top wall 278.15 [K], bottom wall 278.15 [K]

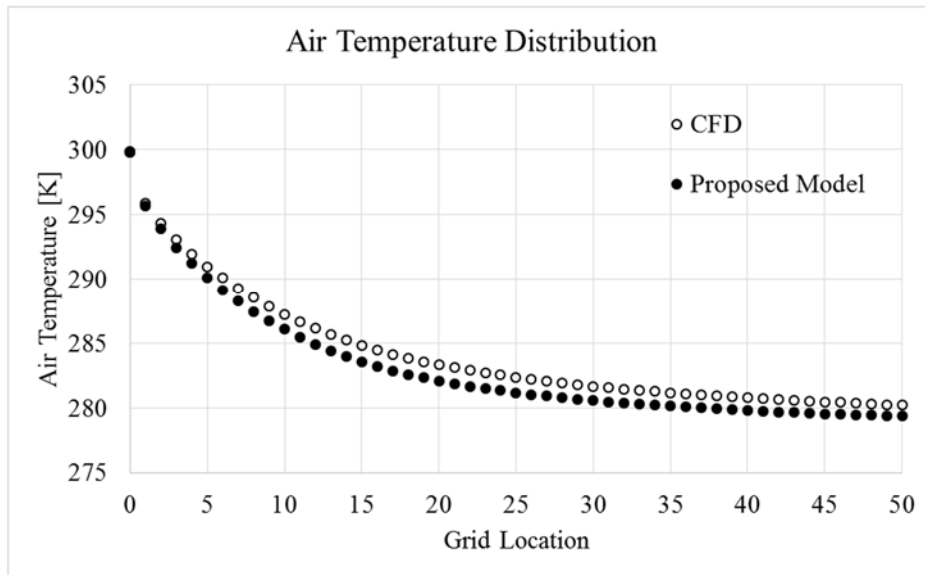
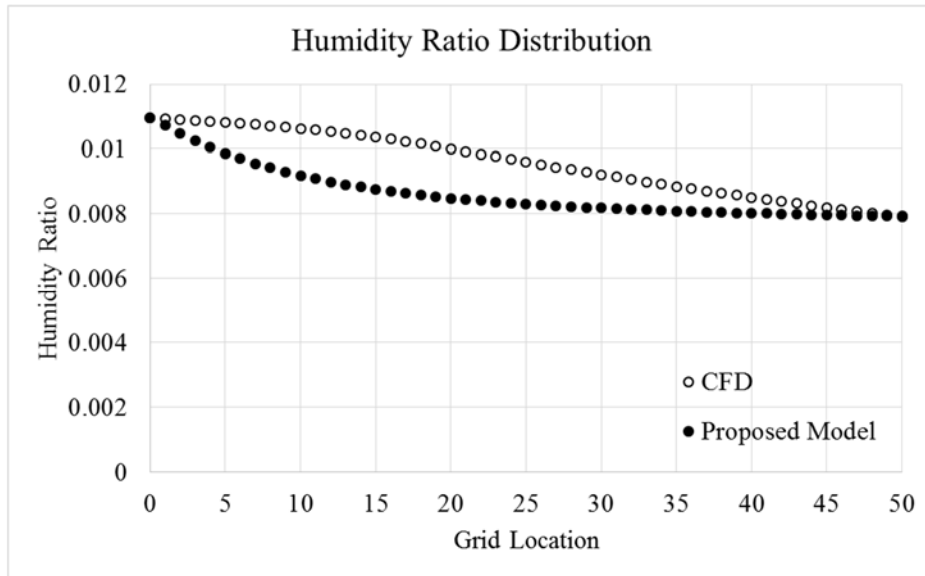


Figure 3-14 (a) Air temperature distribution: top wall 278.15 [K], bottom wall 278.15 [K]



**Figure 3-14 (b) Air humidity ratio distribution: top wall 278.15 [K], bottom wall 278.15 [K]**

**Figure 3-14 Air temperature and humidity ratio distribution: top wall 278.15 [K], bottom wall 278.15 [K]**

The comparison is also carried out by applying different wall temperatures on top and bottom of the fin. This comparison yields deviation of 4.16% in capacity and 0.46% in sensible heat ratio. Figure 3-15 and Figure 3-16 show the fin temperature, air temperature and air humidity ratio distribution comparisons.

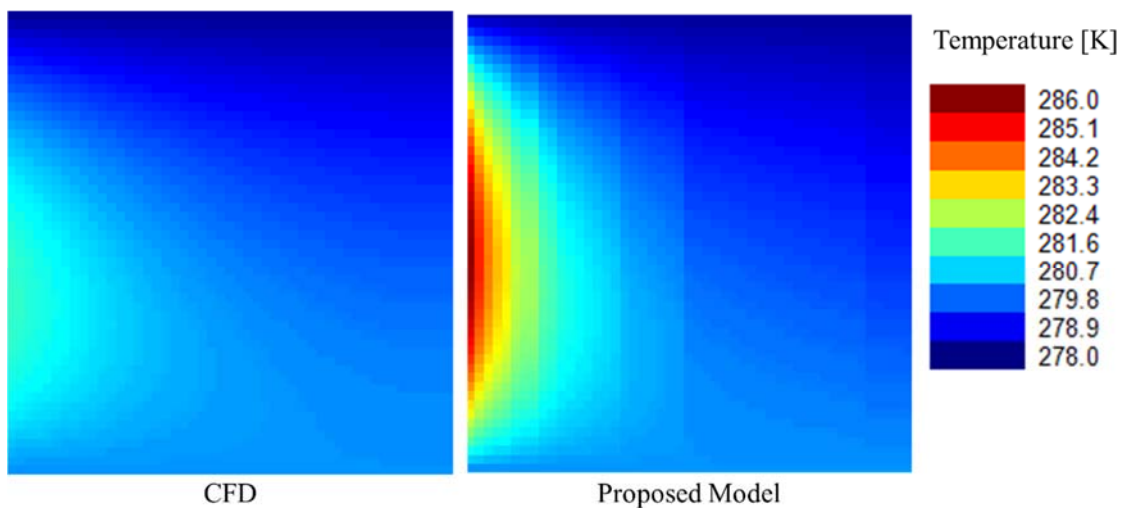


**Figure 3-15 Fin temperature distribution: top wall 278.15 [K], bottom wall 280.15 [K]**

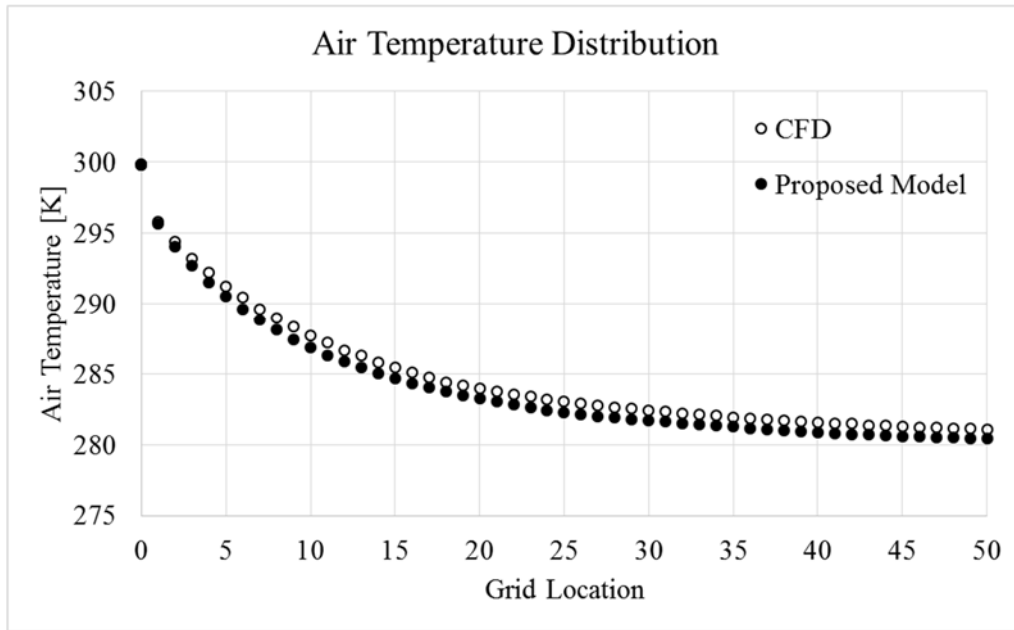


Figure 3-16 (a) Air temperature distribution: top wall 278.15 [K], bottom wall 280.15 [K]

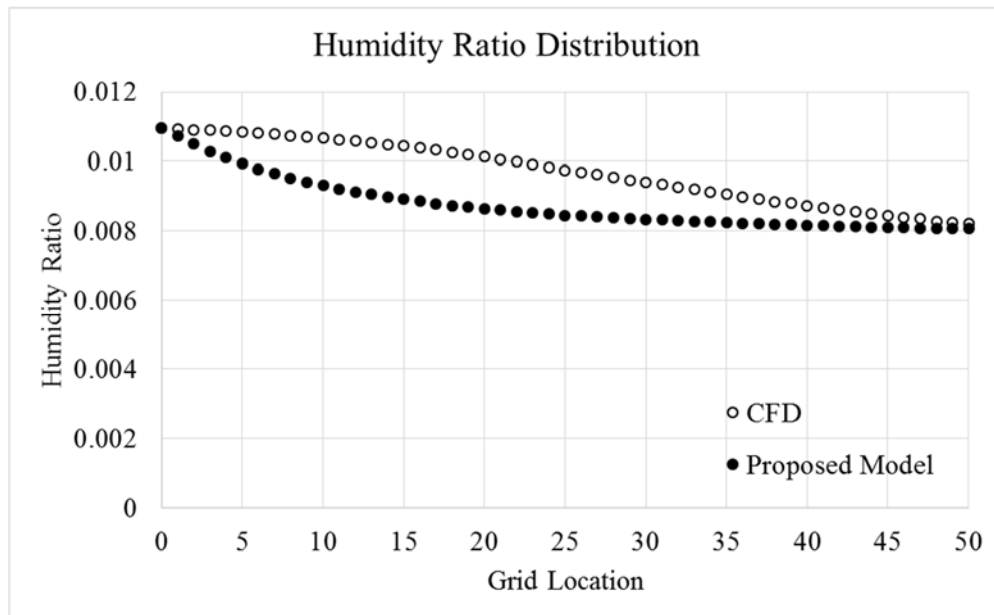


Figure 3-16 (b) Air humidity ratio distribution: top wall 278.15 [K], bottom wall 280.15 [K]  
 Figure 3-16 Air temperature and humidity ratio distribution: top wall 278.15 [K], bottom wall 280.15 [K]

To summarize the model comparison for both dry surface and wet surface, the fin surface temperature comparison shows good match. The deviation between the two

models mainly comes from the entrance region of the fin. The deviation in capacity predicted by the proposed model and the CFD simulation ranges from 3 to 4%. The sensible heat ratios predicted by the two models agree within 1%.

### 3.3 Model Validation

The model is validated against experimental data for both condenser and evaporator applications using R410A and R32. Four different CG-MCHXs (A, B, C, D) and four different VG-MCHXs (A, B, C, D) are validated. In total, 65 data points are validated, including 45 condenser data points and 20 evaporator data points. The details of the tested heat exchangers are presented in Table 2-2 and Table 2-5 in previous chapter. A summary of the test data is tabulated in Table 3-1. The NIST REFPROP 9.1 (Lemmon *et al.*, 2013) along with a speed up algorithm (Aute and Radermacher, 2014) is used to calculate thermo-physical properties of refrigerants.

**Table 3-1 Summary of experimental data**

Application	Condenser	Evaporator
Refrigerant	R32, R410A	R32, R410A
Refrigerant mass flux [kg/m <sup>2</sup> s]	23-1023	27-634
Refrigerant reduced pressure	0.51-0.61	0.15-0.19
Air inlet dry bulb point temperature [°C]	35	7-12
Air inlet dew point temperature [°C]	19.5	4.9-8.3
Air frontal velocity [m/s]	1-2	1-2

#### 3.3.1 Validation results

Eight different microchannel condensers are validated. The correlations and correction factors used in this set of validation can be found in Table 2-3 and Table 2-6. Without any correction factors on heat transfer correlations, the absolute average capacity prediction errors are 3.1% and 1.75% respectively for CG-MCHXs and VG-MCHXs, and are shown in Figure 3-17 (a) and Figure 3-18 (a). The pressure drop

deviations are 16.71% and 11.14% for the two types of geometries tested, as presented in Figure 3-17 (b) and Figure 3-18 (b).

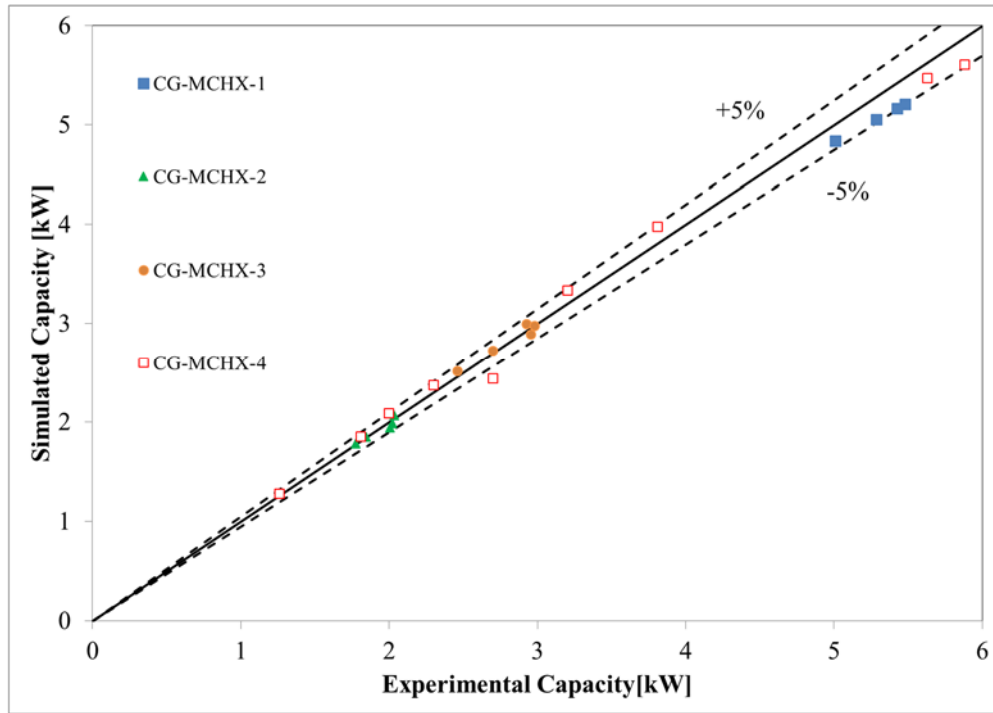


Figure 3-17 (a) Capacity validation of conventional geometry condensers

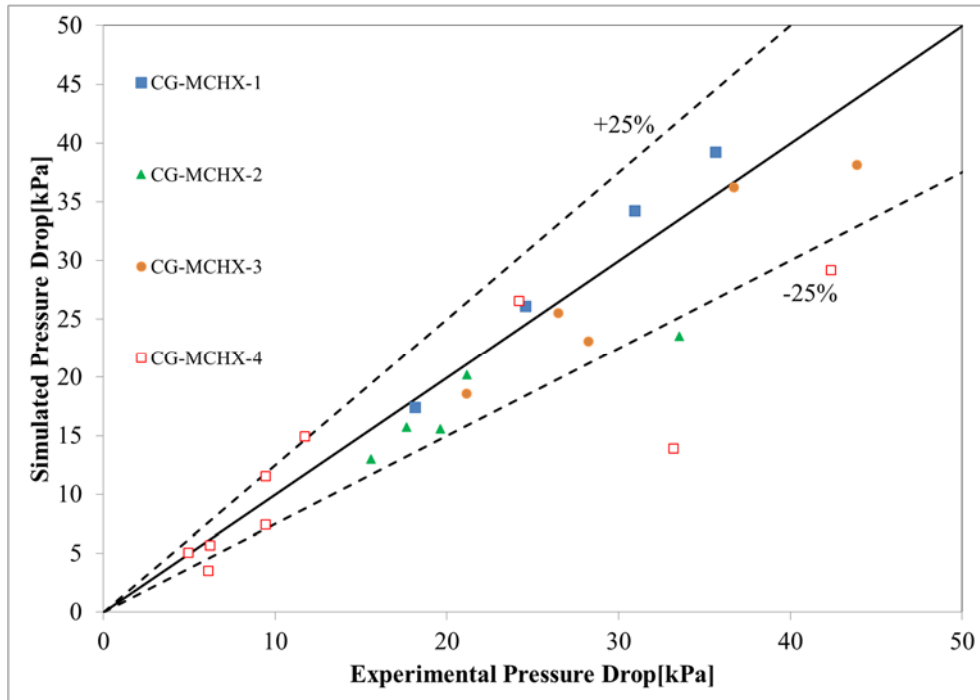


Figure 3-17 (b) Pressure drop validation of conventional geometry condensers

Figure 3-17 Validation of conventional geometry condensers

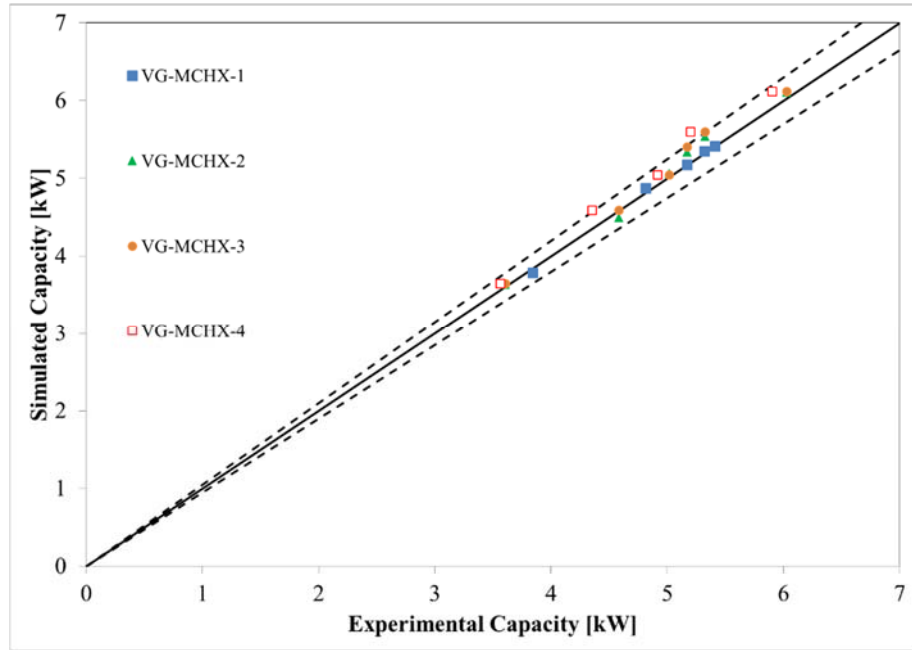


Figure 3-18 (a) Capacity validation of variable geometry condensers

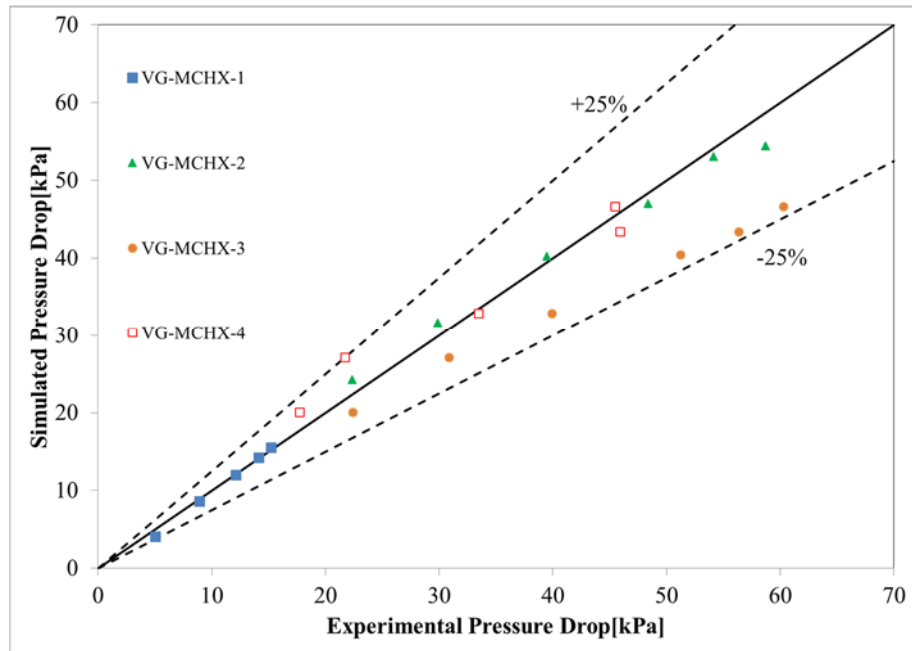


Figure 3-18 (b) Pressure drop validation of variable geometry condensers

Figure 3-18 Validation of variable geometry condensers

CG-MCHX-A and all four different VG-MCHXs are tested under cooling mode. For this set of test data, no correction factor is required on heat transfer correlations. Only CG-MCHX-A data require pressure drop correlation tuning to match the experimental values. The selected correlations and corresponding correction factors can be found in Table 3-2. Except the pressure drop calculation for CG-MCHX-A, no other correction factor on heat transfer and pressure drop is required in this validation set. The comparison of simulated capacity, refrigerant pressure drop and sensible heat ratio against experimental data are plotted in Figure 3-19. The average absolute deviation of capacity is 2.92%, that of pressure drop is 11.66% and that of sensible heat ratio is 0.018. The low sensible heat ratio deviation indicates that the proposed model has excellent prediction capability for combined heat and mass transfer phenomenon.

**Table 3-2 Selected correlations and correction factors for conventional and variable geometry evaporator data**

MCHX type	Heat transfer correlation (Correction factor)		Pressure drop correlation (Correction factor)
	Air side	Refrigerant side two-phase	Refrigerant side two- phase
CG-MCHX-A	Fin-A correlation (1.0)	Kandlikar &Steinke (1.0)	Homogeneous (0.2)
VG-MCHX-A	Fin-C correlation (1.0)	Kandlikar &Steinke (1.0)	Homogeneous (1.0)
VG-MCHX-B	Fin-C correlation (1.0)	Kandlikar &Steinke (1.0)	Friedel (1.0)
VG-MCHX-C	Fin-C correlation (1.0)	Kandlikar &Steinke (1.0)	Friedel (1.0)
VG-MCHX-D	Fin-C correlation (1.0)	Kandlikar &Steinke (1.0)	Friedel (1.0)

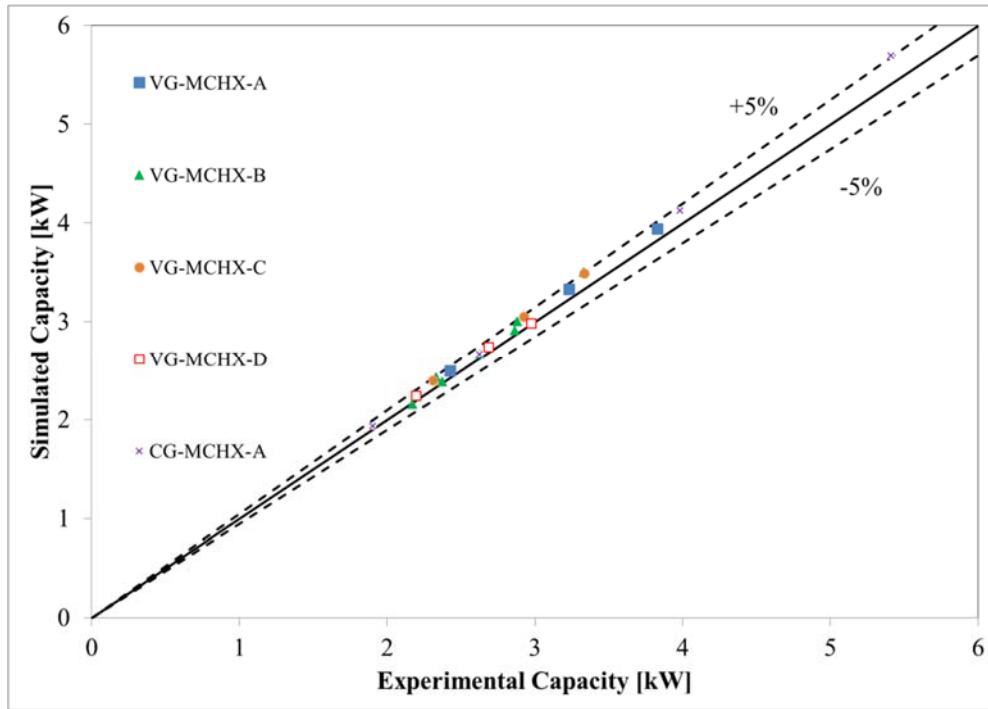


Figure 3-19 (a) Capacity validation of microchannel evaporators

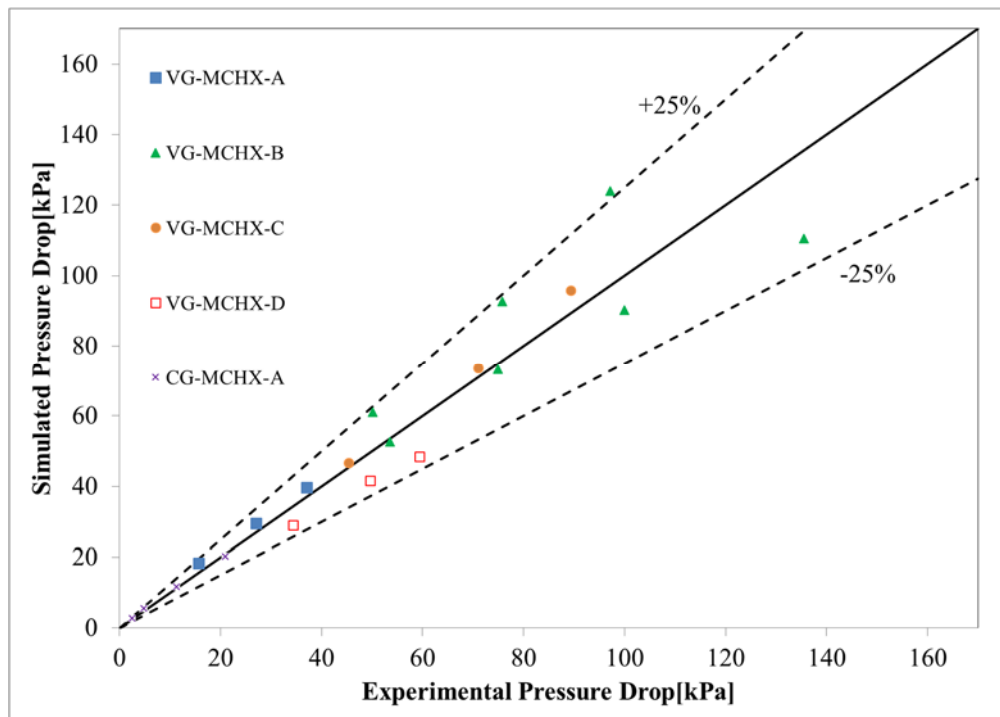
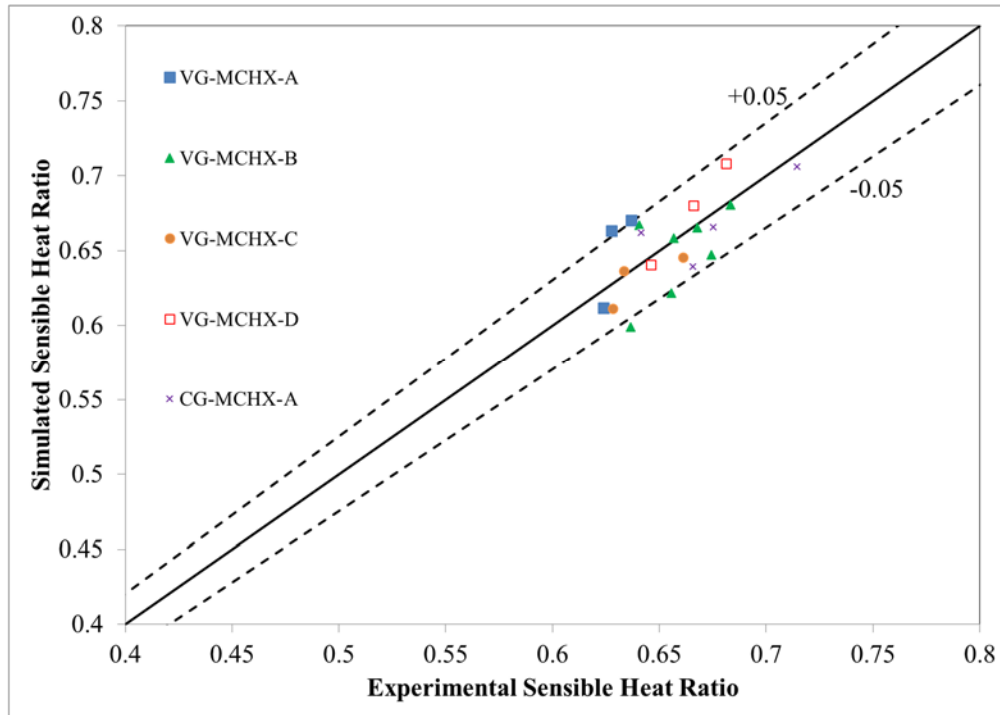


Figure 3-19 (b) Pressure drop validation of microchannel evaporators



**Figure 3-19 (c) Sensible heat ratio validation of microchannel evaporators**

**Figure 3-19 Validation of microchannel evaporators**

### 3.3.2 Model comparison: effect of fin conduction

In Chapter 2, I proposed a computationally fast three-stream model for variable geometry heat exchangers. In the three-stream model, each port-segment shares half of the fin at top and bottom of the tube. For each fin, the surface is divided into half to accommodate the above mentioned model discretization. The three-stream model assumes that the fin center is adiabatic such that each port-segment can be solved individually without having to know the neighboring port-segments' wall temperatures. McQuiston (1975) method for heat and mass transfer is implemented in the three-stream model assuming fin tip is adiabatic.

The comparison of validation result for three-stream model and the conduction model is presented in Table 3-3. For conventional geometry condensers, due to the geometric uniformity, the temperature difference between adjacent tube walls is very small. The two models validated here obtained consistent results. For variable geometry condensers, the wall temperature variation between difference microchannel tubes becomes significant, especially in the region between two refrigerant flow passes. The newly proposed model achieved better prediction by accounting for such phenomena. The sensible heat ratio prediction is improved while using the proposed model for evaporator designs. However, the proposed model requires solving the wall temperatures iteratively. Thus, the proposed model's computational cost increases by the factor of 3-16 compared to the three-stream model. The factor is higher especially for the cases where large wall temperature differences exist (e.g. variable geometry condenser and evaporator). Based on the comparison, it is suggested to apply three-stream model for preliminary heat exchanger optimization and parametric analysis in

the heat exchanger design process. The conduction model should be used for evaporator designs and to calibrate the performance prediction of final condenser designs.

**Table 3-3 Validation summary and comparison of fin conduction assumptions**

MCHX type	Avg. abs. capacity deviation [%]		Avg. abs pressure drop deviation [%]		Avg. abs. sensible heat ratio deviation		Relative avg. calculation time	
	Three-stream model	Conduction model	Three-stream model	Conduction model	Three-stream model	Conduction model	Three-stream model	Conduction model
Conventional geometry condensers	3.09%	3.10%	16.93%	16.71%	N/A	N/A	1	3.17
Variable geometry condensers	2.56%	1.75%	12.04%	11.14%	N/A	N/A	1	14.95
Variable geometry evaporators	2.92%	2.92%	10.40%	11.66%	0.022	0.018	1	15.78

### 3.4 Summary

This chapter presented a new air to surface heat and mass transfer solution for microchannel heat exchanger fins under dry, wet and partially wet conditions. A new variable geometry condenser and evaporator model was developed using the proposed comprehensive fin analysis approach. The results for single fin analysis from the proposed model were verified against those from CFD simulations and the comparison showed good agreement. The heat exchanger model was validated against experimental data for eight different evaporators and condensers comprising of both conventional and variable geometry designs. The validation showed good agreement with measured data, with an average absolute capacity deviation of 2.44% for condensers and 2.92 for evaporators. For the evaporator cases, the sensible heat ratio (0.018 average absolute deviation). The proposed model exhibits improved prediction accuracy compared to

previously proposed models. It should be noted that the model is also computationally more expensive due to the additional iterations involved in solving for the tube wall temperatures. The proposed model can be used to evaluate variable geometry microchannel heat exchangers which offer tremendous potential in terms of cost versus performance tradeoff for a given application. This model will help engineers to develop more sophisticated microchannel heat exchangers ultimately resulting in improved systems efficiency and lower cost.

## 4 A COMPUTATIONAL FLUID DYNAMICS AND EFFECTIVENESS-NTU BASED CO-SIMULATION APPROACH FOR FLOW MAL-DISTRIBUTION ANALYSIS IN MICROCHANNEL HEAT EXCHANGER HEADERS

The objective of this research is to develop a co-simulation approach that provides accurate prediction of flow distribution in header along with the capability of modeling the microchannel tubes in a fast and reliable manner. The mal-distribution effects were investigated for both single-phase and two-phase working fluids within the heat exchanger, under both zero gravity and standard gravity, facing uniform airflow and uneven airflow. The modeling studies focuses on heat exchanger with single-phase flow in inlet headers. Finally, the co-simulation model was validated against experimental data. It should be noted that the proposed approach is not limited to single-phase header simulation. Coupling with a proper two-phase CFD solver would allow such approach to be applied to MCHXs with two-phase flow in headers.

In the remainder of the paper, the details of the effectiveness-NTU based tube model and the CFD header model are described in Section 4.1 and 4.2. In Section 4.3, the co-simulation methodology is explained. A case study on a simplified ten-tube MCHX is presented in Section 4.4. The ten-tube case study investigated the impact of different fluid, gravity effect and air flow distribution influence on MCHX. Then, the model is validated against experimental data of an R134a automotive condenser (Eisele, 2012). The simulated heat load and pressure drop are compared to the experimental results in Section 0.

### **4.1 Effectiveness-NTU Based Segmented Microchannel Tube Model**

The segment-by-segment model is capable of simulating both single-phase and two-phase flow. Under dry surface condition, the effectiveness-NTU approach (Kays

and London, 1984) is applied to solve the heat transfer between air and refrigerant. The dehumidification process is modeled using enthalpy potential method McQuiston (1994). Segment sub-division method (Jiang *et al.*, 2006) is implemented to achieve better accuracy in the segments where refrigerant phase change occurs.

An iterative approach is adopted in the model to track the flow distribution by checking the pressure residuals among tubes that belongs to the same headers and all outlet header pressure residuals. In the proposed co-simulation approach, the intermediate headers and outlet headers are not simulated by CFD header model but integrated into the segmented tube model. This was done mainly to reduce the computational costs and the proposed approach can be easily modified to include those headers. It is assumed that each tube outlet within the same header should have the same pressure. In addition, all the outlet headers should have equal pressure level. The segmented tube model provides a functionality to build pressure drop approximations for each tube. Such feature avoids the discontinuity issue of pressure drop correlations. In the meantime, applying such method expedites and ensures solver convergence.

The top level single-pass MCHX schematic is presented in Figure 4-1. Total inlet refrigerant mass flow rate was known. Mass flow distribution was assumed to be uniform in the initial guess. Then the nonlinear equation solver would solve for mass flow distribution iteratively based on the outlet pressure residuals.

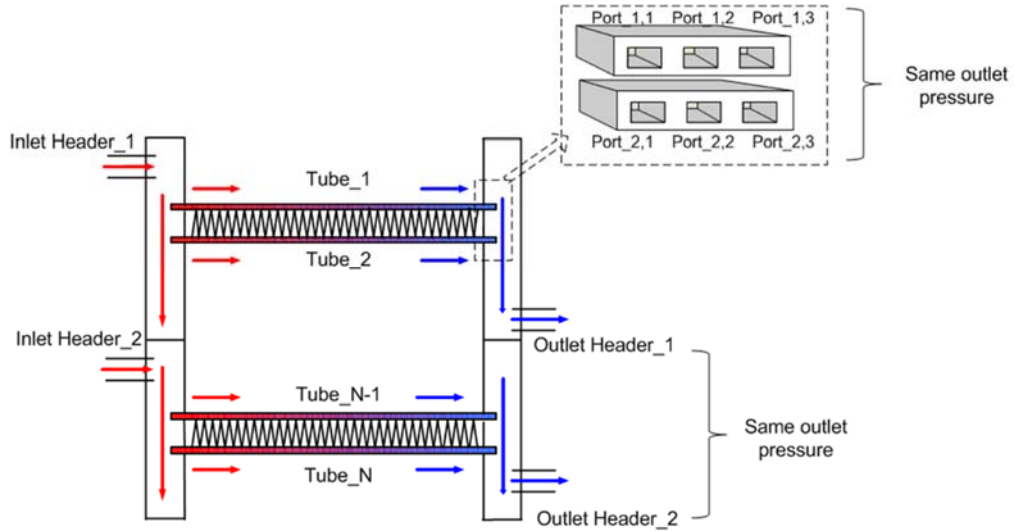


**Figure 4-1 MCHX top level illustration and tube level view**

The flow maldistribution within each tube, between the ports are solved at the tube level calculation. The residual of each port pair is calculated using the following equation.

$$Res_{PortPair} = \frac{|P_{1stPort,out} - P_{2ndPort,out}|}{\Delta P_{Port,scale}} \quad (4-1)$$

Here the scaled port pressure drop is taken from the pressure drop in the first port on air flow direction. It should be noted that the tube level and port level flow distribution are solved separately and iteratively.

The junction tube matrix is dynamically generated based on the header position and the pass configuration. All tube pairs are tracked based on the junction-tube matrix, and then each tube pair's residual is calculated using the following equation:

$$Res_{TubePair} = \frac{|P_{1stTube,out} - P_{2ndTube,out}|}{\Delta P_{Tube,scale}} \quad (4-2)$$

Where  $\Delta P_{Tube,scale}$  is defined as the average pressure drop between refrigerant inlet tubes and outlet tubes.

For the cases of multiple outlet headers, each outlet header pair's residual is calculated based on the following equation:

$$Res_{HeaderPair} = \frac{|P_{1stHeader} - P_{2ndHeader}|}{\Delta P_{Tube, scale}} \quad (4-3)$$

The overall hydraulic residual is calculated based on the following equation:

$$Res_{Hydraulic} = \frac{\sqrt{\sum Res_{HeaderPair}^2 + \sum Res_{TubePair}^2}}{N_{HeaderPair} + N_{TubePair}} \quad (4-4)$$

Most of the pressure drop correlations use separate equations for different ranges of the Reynolds number. During numerical simulations, it was observed that using separate equations often causes discontinuity in the pressure drop calculation in the model. An approximation technique was used here to reduce the calculation time and enhance the robustness of the nonlinear solver. In the initial run, after the refrigerant side pressure drop is calculated, the tube level solver creates a parabolic curve fit to find the relationship between each segment's pressure drop and the mass flow rate. The approximated curve fit equation is defined as:

$$\Delta P = C m^2 \quad (4-5)$$

Once the approximation coefficient C has been determined, this equation is then used in the following iterations in order to predict the refrigerant pressure drop and in deciding the refrigerant mass flow distribution.

Two solvers were established in this model: the energy solver and the hydraulic solver. The energy solver conducts a tube by tube calculation from inlet of MCHX to the outlet. Both solvers included the friction, expansion and contraction pressure drop calculation in the connecting tubes, headers and tubes. The heat transfer between air

and refrigerant in each segment would only be calculated in the energy solver. All the inlet and outlet conditions in each segment would be stored. The hydraulic solver is dedicated to predict the refrigerant mass flow distribution. Figure 4-2 presents the flow chart of the top level solver.

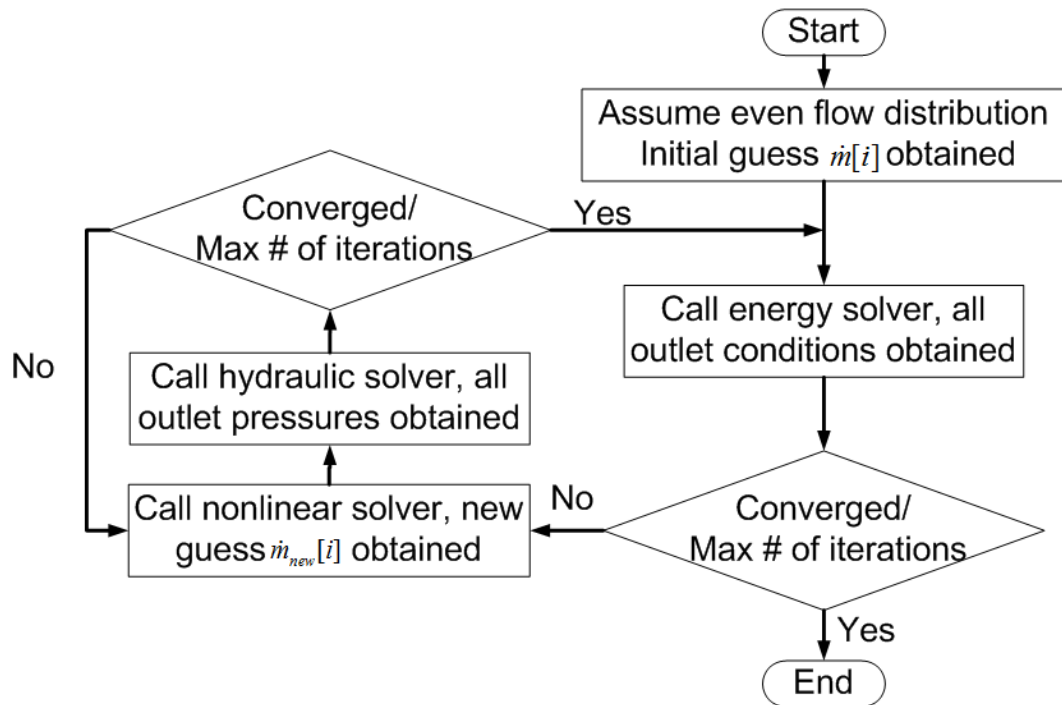


**Figure 4-2 Refrigerant flow distribution top level solver flow chart**

It is worthwhile to mention that the proposed model is capable of handling MCHX with multiple passes and banks for condensers and evaporators. The built-in nonlinear equation solver along with the pressure drop approximation technique provides a robust and fast solution of simulating the refrigerant-side maldistribution. Segment by segment approach offers accurate calculation of both heat transfer and pressure drop with implemented empirical correlations. The correlations can be replaced with more suitable correlations (e.g., based on flow regime or a particular refrigerant) from the literature or those based on manufacturer data. Last but not the

least; two-dimensional air-side maldistribution can be accounted based on the air flow rate profile.

#### **4.2 CFD Header Modeling Details**

The MCHX inlet header is simulated with a commercial CFD code, Fluent (2006). In Fluent (2006), the governing conservation equations for the mass and momentum are solved using the finite volume method and non-staggered grid discretization. The coupled steady-state incompressible Navier-Stokes equations are solved using the SIMPLE scheme and a standard  $k - \epsilon$  model for the turbulence.

In the proposed approach, only the inlet header is simulated using CFD code which is different from previous studies where the header models with an artificial pressure jump condition in the computational domain to represent the tubes (Saleh *et al.*, 2012). The geometries of both inlet header models simulated in current study consist of a connecting inlet tube, a header and a certain length of the microchannels. The entering length of microchannels is modeled to make sure the flow at the outlet of the header model is fully developed. Taking the inlet state and velocity profile of all the microchannel tubes from the heat exchanger model, the inlet header CFD model essentially calculates pressure profile at the header outlet (or port inlet) as an input for the segmented MCHX tube model.

#### **4.3 CFD Header Model and Effectiveness-NTU Based Heat Exchanger Model Co-Simulation Methodology**

In co-simulation approach, the heat exchanger model is responsible for solving the energy and hydraulic equations for tubes and iterating the mass flow distribution to convergence. The CFD model is responsible for solving the pressure inlet profile of

each microchannel tube. Figure 4-3 presents the CFD header and effectiveness-NTU based segmented MCHX model co-simulation concept.

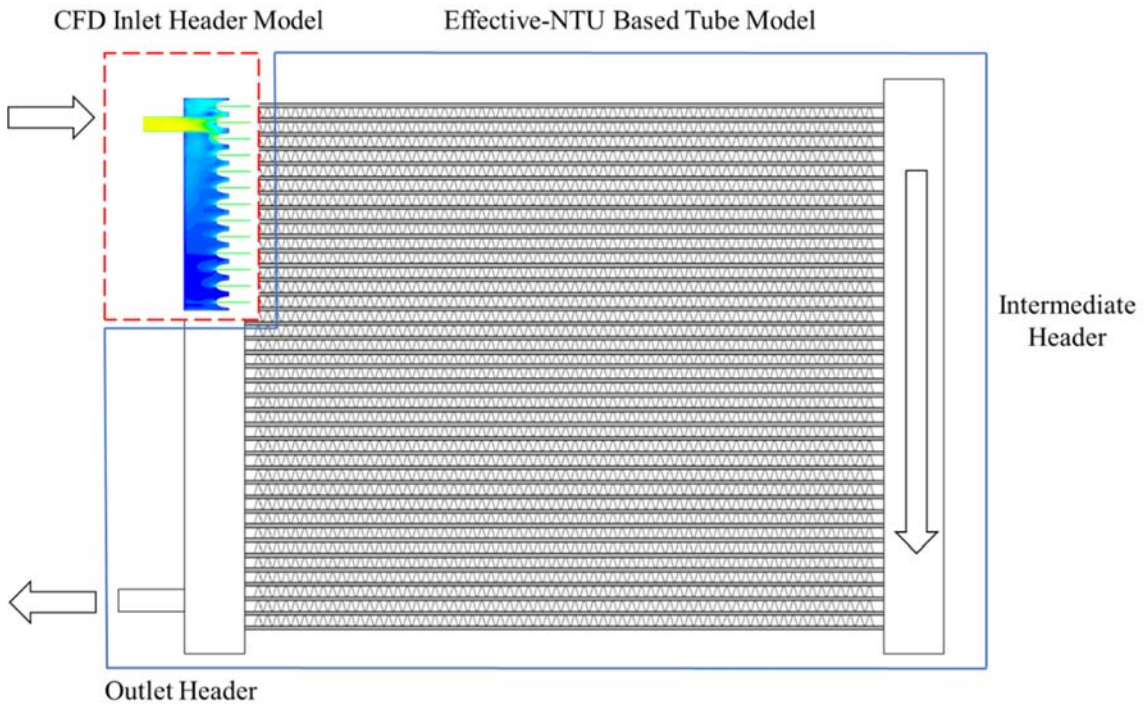


**Figure 4-3 MCHX face view and co-simulation concept illustration**

The solving methodology of the co-simulation approach is illustrated in Figure 4-4. The simulation starts with the assumption of even mass flow distribution in all microchannel tubes. This velocity distribution profile is passed to the CFD header model as the boundary condition. As the CFD model converges, the resulting tube pressure inlet profile is then obtained by the heat exchanger model. The heat exchanger model solves the velocity distribution iteratively using a non-linear (NL) equation solver under current pressure inlet profile resulting from the CFD simulation. Then, the most recent mass flow rate distribution is transferred to CFD for next iteration. After each CFD run, the heat exchanger performs a full simulation solving both energy and hydraulic equations. In other words, it computes the air-to-refrigerant heat transfer, air-

side pressure drop, refrigerant phase change and refrigerant side pressure drop. The solution converges if the outlet pressure residual is smaller than the tolerance under current mass flow distribution and CFD pressure inlet profile. If the convergence criterion is not satisfied, next iteration begins with a heat exchanger model run trying to locate a new mass flow distribution using the updated pressure inlets.

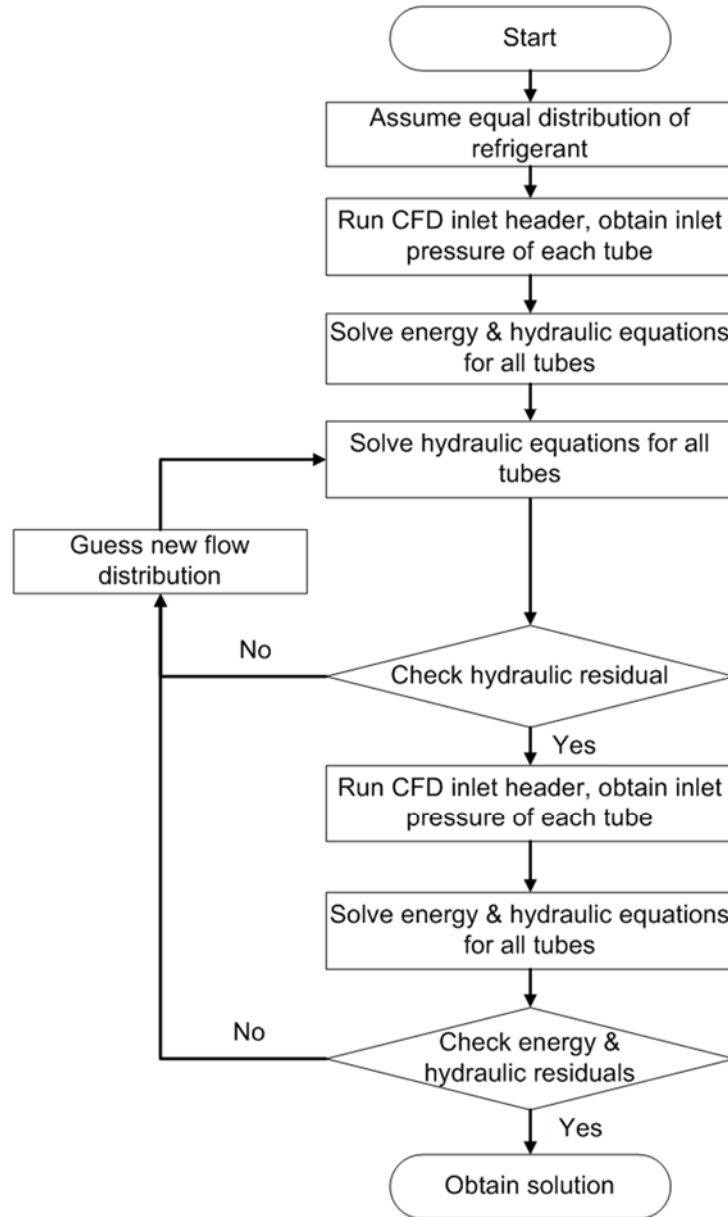


**Figure 4-4 Proposed co-simulation solving methodology**

The interface between Fluent (2006) and the effectiveness-based heat exchanger model is based on a methodology termed as Parallel Parameterized CFD (PPCFD). The PPCFD methodology and its applications are described in Abdelaziz *et al.* (2006) and Saleh *et al.* (2012). This tool automatically generates Gambit (2011) and Fluent (2006)scripts files, executes the CFD simulations and then post-processes the results. This PPCFD tool is slightly modified in the present simulation to set the flow boundary condition in CFD runs and obtain the resulting pressure profiles in between the CFD header model and heat exchanger model. It should be noted that the mesh remains the same throughout the co-simulation presented in this paper. Although both the co-simulation method and CFD header model are iterative in nature, the simulation is very robust in all the case studies and validation cases presented in this paper. The solver can be coupled with any NL equation solver. The Broyden (1965) method is used in the present work.

#### **4.4 Ten-Tube Microchannel Heat Exchanger Case Study**

##### **4.4.1 Heat exchanger modeling details**

In order to demonstrate the capability of the co-simulation approach, a simple fictitious ten-tube MCHX is modeled to investigate gravity effects and impact of air side mal-distribution on its performance. Two working fluids (Water and R134a) were investigated. For each fluid, three cases are simulated: zero-gravity with uniform airflow; standard gravity with uniform airflow; standard gravity with non-uniform airflow. Except for the number of tubes, all other geometric parameters are based on commonly used MCHX applications, in order to keep them realistic. The fluids in CFD modeled inlet headers are single-phase flows in all cases. The geometry details are as presented in Table 4-1. The refrigerant thermo-physical properties were calculated

using NIST REFPROP 8.0 (2007). The uneven airflow cases use a proportional airflow distribution profile input. The air flow rate is the highest at the top tube, and then decreases from top to bottom. The air velocity ranges from 0.46 to 3.5 m/s. The correlations selected are listed in Table 4-2.

**Table 4-1 Case study MCHX geometry parameters**

<b>Parameter</b>	<b>Value</b>
Number of tubes	10
Tube length (mm)	180
Tube height (mm)	2
Tube width (mm)	30
Port height (mm)	1
Port width (mm)	1
Ports per tube	13
Vertical Spacing (mm)	30
Header diameter(mm)	40
Inlet connecting tube diameter (mm)	20
Water inlet pressure (kPa)	350
Water inlet temperature (K)	323
Water mass flow rate (g/s)	100
R134a inlet pressure (kPa)	1470
R134a inlet temperature (K)	357
R134a mass flow rate (g/s)	21

**Table 4-2 Summary of selected heat transfer and pressure drop correlations**

<b>Heat transfer coefficient</b>	
Air-side	Chang & Wang (1997)
Two-phase region	Shah (1979)
Single-phase region	Gnielinski (1976)
<b>Frictional pressure drop</b>	
Two-phase region	Homogeneous (Thome, 2006)
Single-phase region	Churchill (1977)
<b>Contraction pressure drop</b>	
Two-phase region	Schmidt & Friedel (1997)
Single-phase region	Shah & Sekulic (2003)
<b>Expansion pressure drop</b>	
Two-phase region	Chisholm (1983)
Single-phase region	Shah & Sekulic (2003)

#### 4.4.2 CFD header model

A simplified schematic for the MCHX header model is shown in Figure 4-5. The domain is assumed symmetric at the center of the y-coordinate. Specifics of the model dimensions are listed in Table 4-1.

Considerable care in meshing of the MCHX model was required due to the large difference in the length scale of the geometries and to maintain mesh quality with minimal skewness. The size of the mesh is around 1.6 million cells and is later adapted to up to around 2 million cells with the Fluent (2006) adaptive meshing technique based on the pressure and velocity curvatures. The grid used in the simulation is an unstructured grid consisting of tetrahedral and hexahedral elements. Along with the grid independence study, careful inspection of flow and mesh near the entrance to the microchannel ports was performed to ensure that enough cells were used. For single-phase fluid, the density is assumed to be constant within the CFD header model.

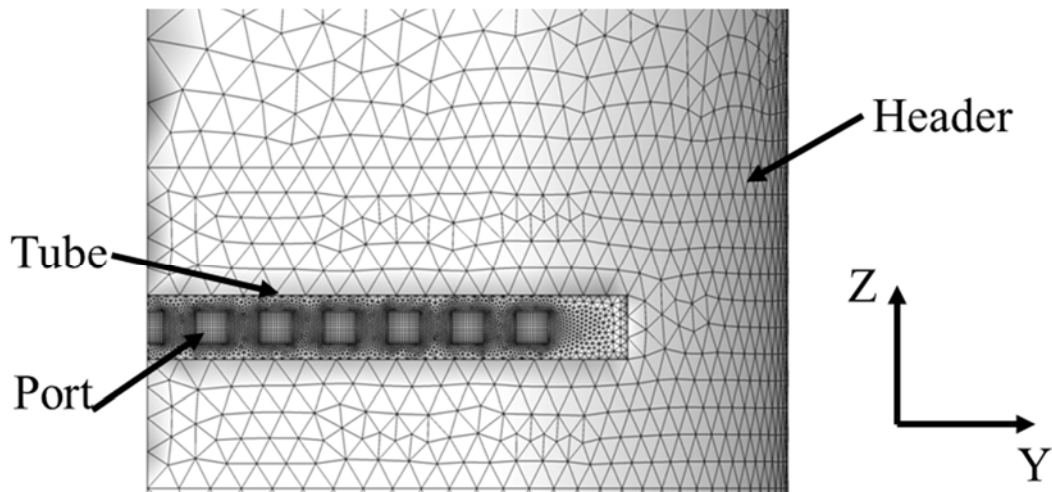
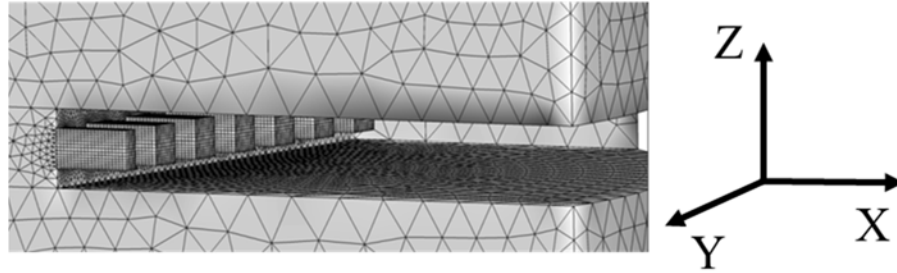
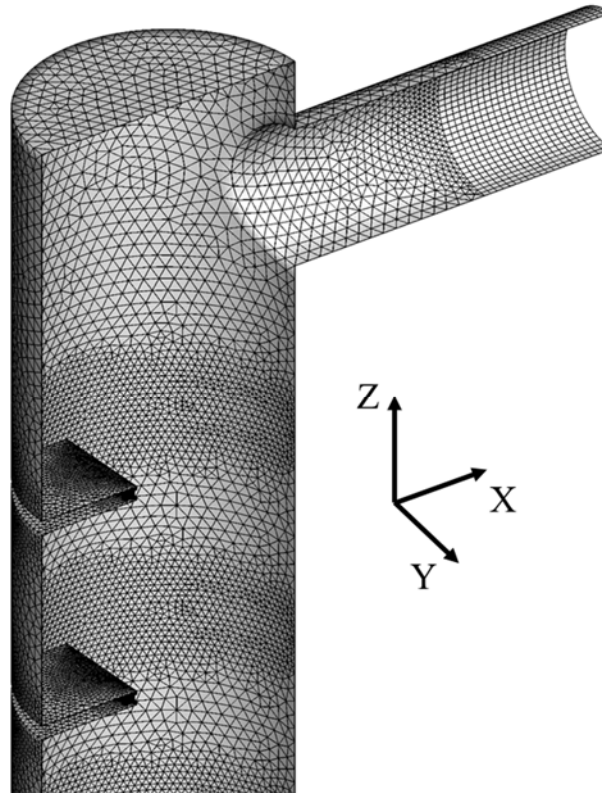


Figure 4-5 (a) Inlet header mesh at tube cross-section (symmetric at  $Y=0$ )



**Figure 4-5 (b) Close view of tube inlet mesh**



**Figure 4-5(c) Meshing details at top portion of the header**

**Figure 4-5 Ten-tube MCHX inlet header mesh**

#### 4.4.3 Results and discussions

The pressure contours, velocity contours and flow distribution histograms for the hot water coil are plotted in Figure 4-6 and those for the R134a condenser are plotted Figure 4-7. Pressure contours and velocity magnitude contours are taken on a sliced plane at the center of a middle port. The mass flow distribution is presented in the form of percentage of overall mass flow. The fluid flow behavior can be visualized from the

velocity contours and the percentage flow distribution provides numerical comparison of the flow distribution. The population standard deviation (STD) is calculated based on all the percentage values instead of the actual mass flow rate.

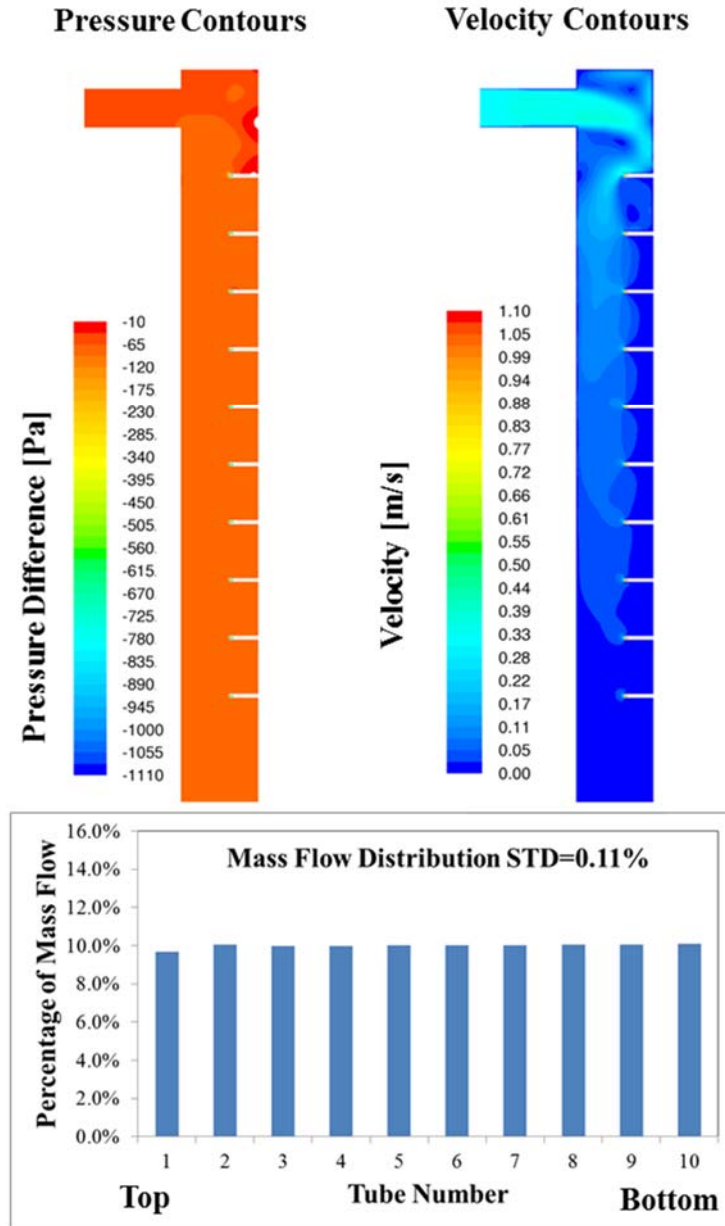


Figure 4-6 (a) Ten-tube hot water MCHX at zero-gravity, uniform air flow

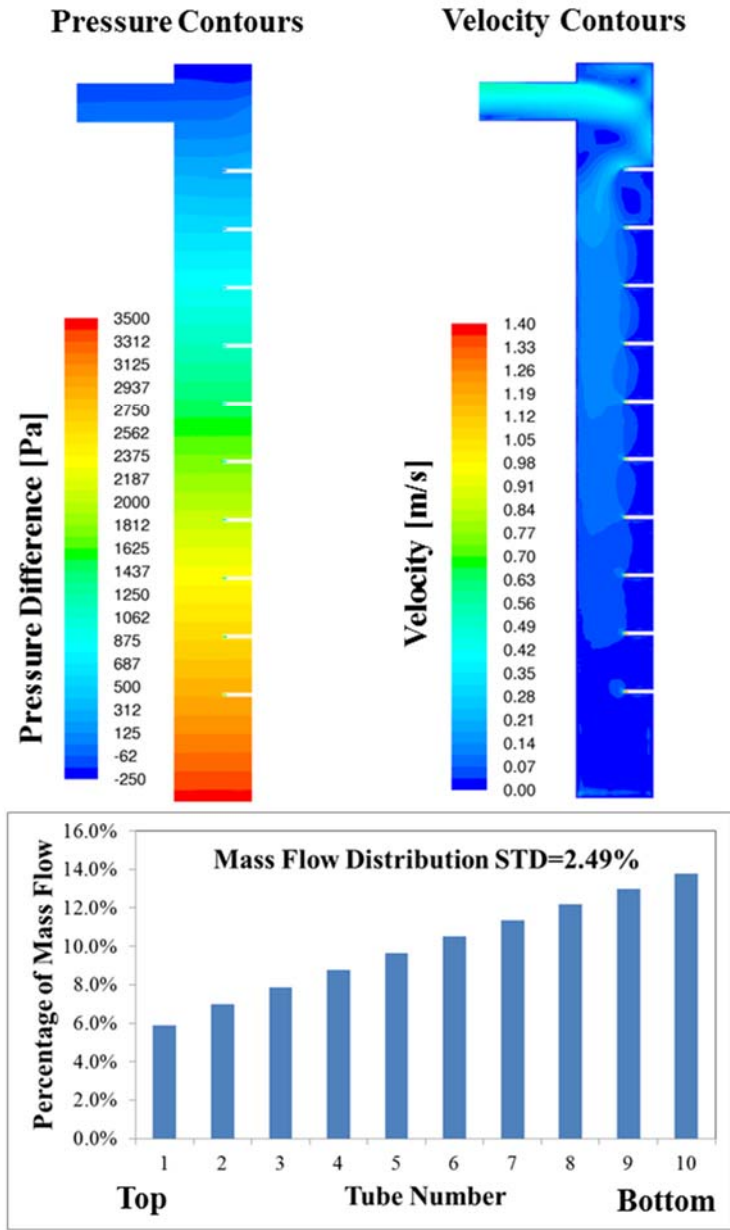


Figure 4-6 (b) Ten-tube hot water MCHX at standard gravity, uniform air flow

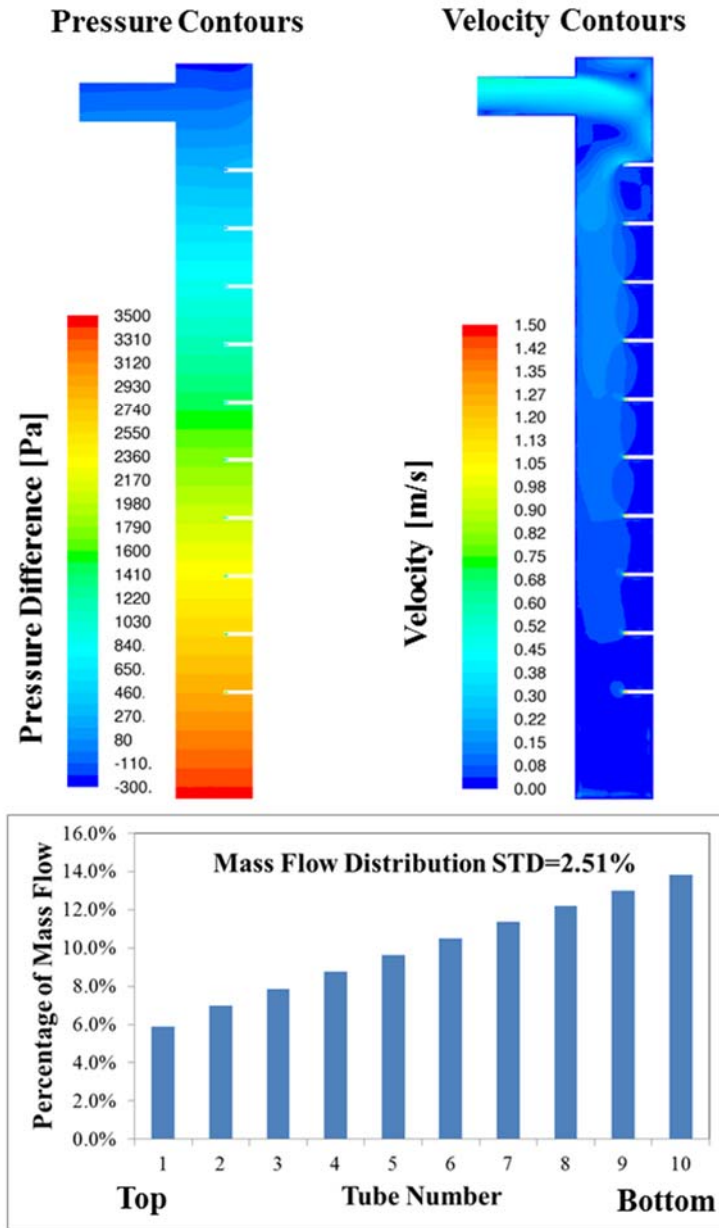


Figure 4-6 (c) Ten-tube hot water MCHX at standard gravity, uneven air flow

Figure 4-6 Pressure contours, velocity magnitude contours and mass flow distributions of the ten-tube hot water MCHX case studies

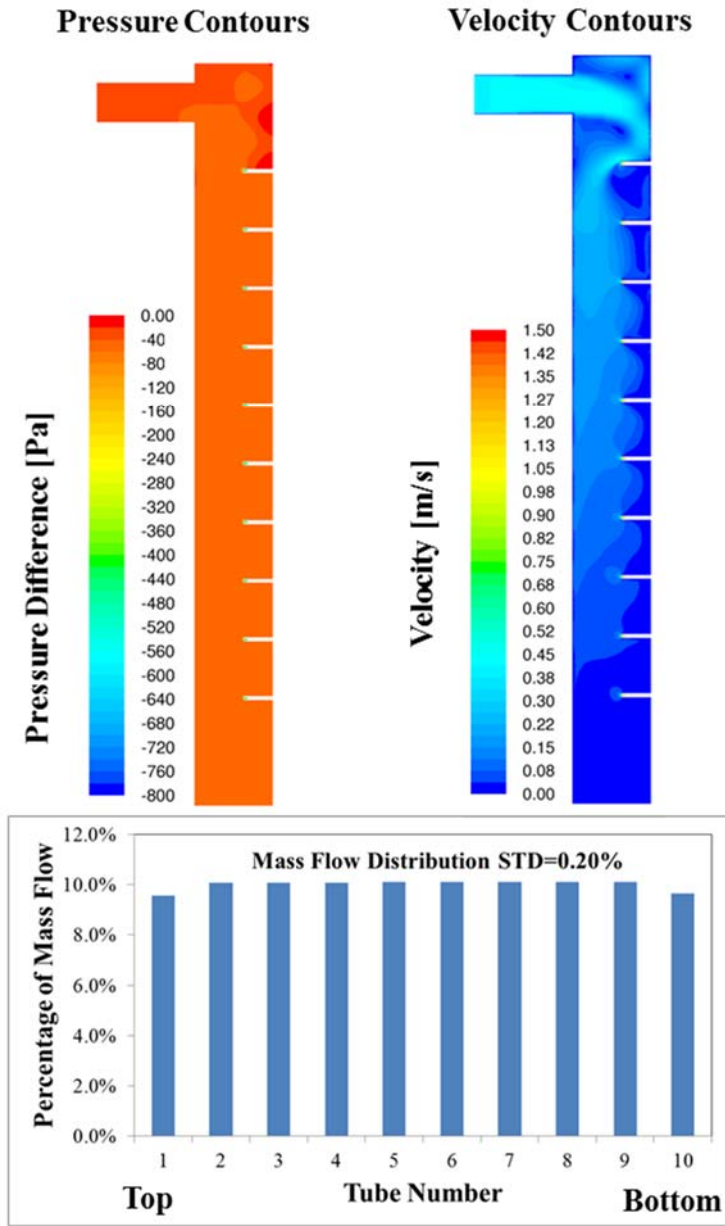


Figure 4-7 (a) Ten-tube R134a microchannel condenser at zero-gravity, uniform air flow

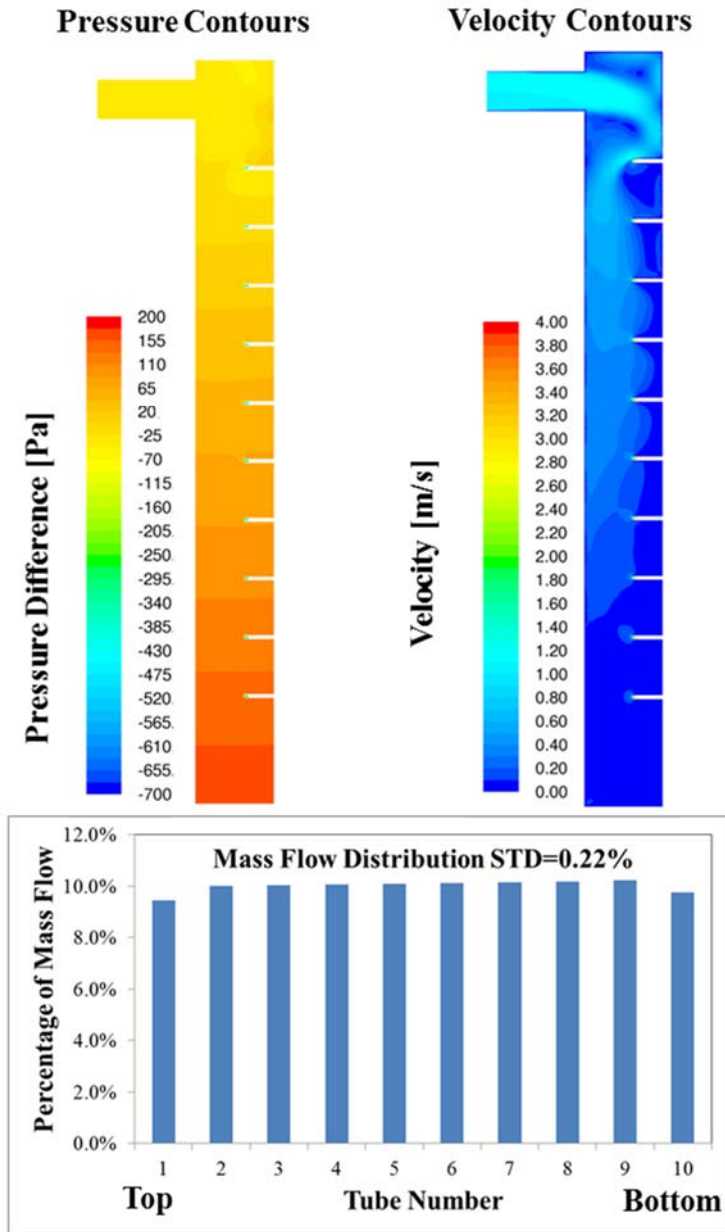
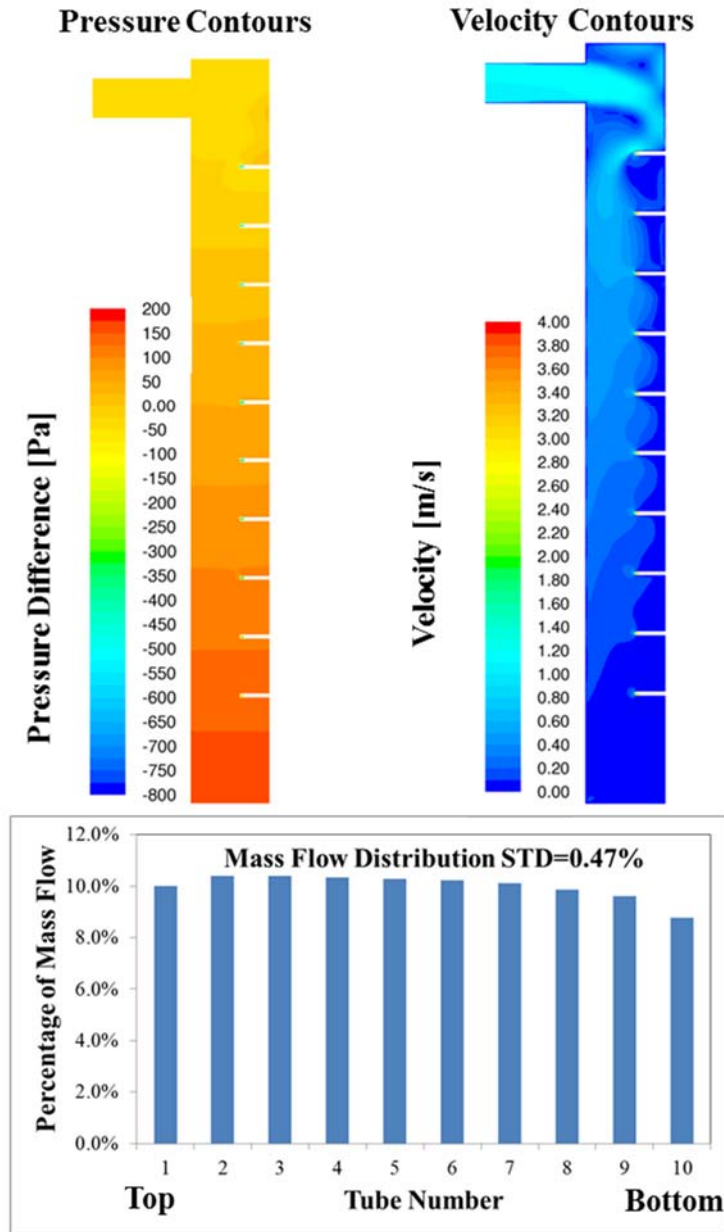


Figure 4-7 (b) Ten-tube R134a microchannel condenser at standard gravity, uniform air flow



**Figure 4-7(c) Ten-tube R134a microchannel condenser at standard gravity, uneven air flow**

**Figure 4-7 Pressure contours, velocity magnitude contours and mass flow distributions of the ten-tube R134a microchannel condenser case studies**

For the single-phase hot water coil, the results indicate that gravity has significant effect on the flow distribution in the inlet header. It can be clearly seen from Figure 3(b) that more mass flow tends to distribute into the bottom tubes. This is mainly due to the high density of liquid flow. As for the air side mal-distribution issue, the

properties of water only suffer minor changes due to heat transfer differences. Thus, the mass flow distributions in the uniform airflow and non-uniform airflow cases result in very small numerical difference.

The flow distribution in the R134a condenser inlet header filled with vapor is not sensitive to gravity due to the low density of vapor. The refrigerant enters each channel in gas phase. Tubes imposed with higher heat flux tend to condense faster therefore have more liquid flow into the channels. Liquid flow has less pressure drop per unit mass flux per unit length, which explains why the tubes facing more airflow has more refrigerant to maintain a certain density distribution. This also clarifies why the top tube and bottom tube with less face area has lower mass flow rates. Similar to many of the previous experimental investigations and numerical results, performance degradation is found when uneven airflow occurs. The uniform airflow condenser yields to capacity of 3.9 kW while the non-uniform airflow case only produces around 3.6 kW heat load (7.7% decrease). The case studies are conducted with single Intel Xeon E5335 2.00GHz processor and 18 GB RAM. The simplest case (zero gravity, uniform air flow) only requires 6 iterations within 5 hours to converge. The R134a case with non-uniform air flow took 760 iterations between CFD header model and the effectiveness-based tube model which cost 25 hours.

## **4.5 Validation Against Experimental Data**

### **4.5.1 Heat exchanger modeling details**

The proposed model was validated against the experimental data for an R134a automotive condenser (Eisele, 2012). The geometry of the condenser and test conditions are summarized in Table 4-3. All the empirical correlations used in the validation are tabulated in Table 4-2. It should be noted that a correction factor of 1.4

was applied on the air side heat transfer coefficient for all the validation cases. No correction factor was required for other correlations. Five experimental data points were simulated and compared during validation. The experimental air side and refrigerant side energy balances of these points are within 3 percent. The uncertainty information is shown in the validation plots as error bars.

**Table 4-3 R134a automotive MCHX specifications**

<b>Parameter</b>	<b>Value</b>
Number of tubes	35
Tube length (mm)	660
Tube height (mm)	2
Tube width (mm)	17
Port height (mm)	0.77
Port width (mm)	1.24
Ports per tube	10
Vertical Spacing (mm)	10.89
Fin type	Louver
Fin thickness(mm)	0.08
Fins per inch	17
Inlet header height (mm)	142.35
Inlet header width (mm)	20
Inlet header depth (mm)	12
Inlet connecting tube diameter (mm)	10.35
R134a inlet pressure (kPa)	980-1867
R134a inlet temperature (K)	338-367
R134a mass flow rate (g/s)	19.2-29.7
Air volume flow rate (m <sup>3</sup> /s)	0.35-0.71
Air inlet temperature (K)	297.5-318.4
Air inlet RH (%)	20-50

#### 4.5.2 CFD header model

After the experimental test was completed, the tested heat exchanger inlet header was physically cut open to obtain geometry details, as shown in Figure 4-8. The detailed geometry information listed in Table 4-3 is measured from the actual header. Figure 4-9 presents different views of the mesh for the validation of the automotive R134a condenser. Figure 4-9 (a) shows the pressure contour of the sliced plane at the

center of a middle port. All results of pressure and velocity magnitude contours are located at this plane. Careful meshing was performed based on a grid independence study. The total number of cells ranged from 7 to 8 million cells depending on the level of grid refinement.



**Figure 4-8 Cross-section view of R134a automotive condenser inlet header**

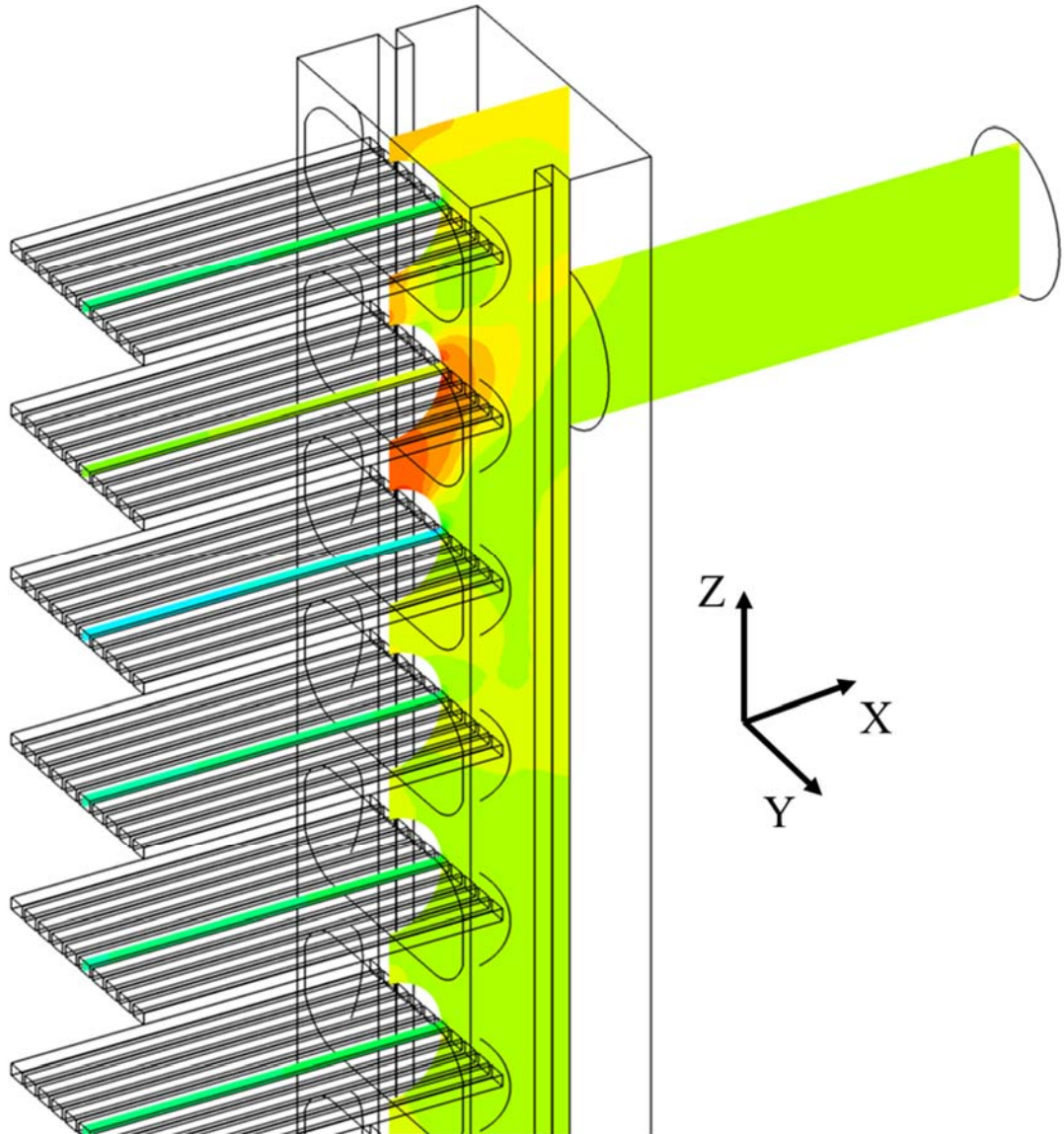


**Figure 4-9 (a) Sliced plane at the center of middle port**

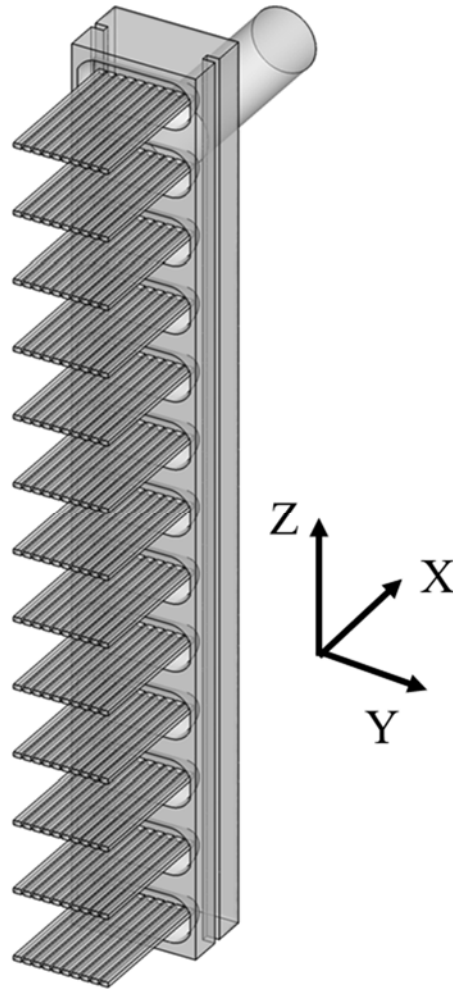


**Figure 4-9 (b) Perspective view of header mesh**

**Figure 4-9 R134a automotive microchannel condenser inlet header mesh**

#### 4.5.3 Results and discussions

Figure 4-10(a) indicates that the co-simulation approach predicts the heat exchanger capacity very well, within 1 percent, which falls within the experimental uncertainty. The predicted errors in pressure drop, as shown in Figure 4-10 (b) are within  $\pm 32$  kPa, which are relatively small compared to the working pressure level (900-1800 kPa). The pressure difference has minor effect on the prediction of the

condenser capacity. The pressure drop validation can be improved further by using more suitable pressure drop correlations and applying CFD simulation to intermediate and outlet headers. Figure 4-10 (c) presents the absolute deviation of air outlet temperature. The simulation yields to deviations within  $\pm 0.6$  K. The simulation of validation cases converged within 5 iterations considering the air velocity is assumed to be uniform.

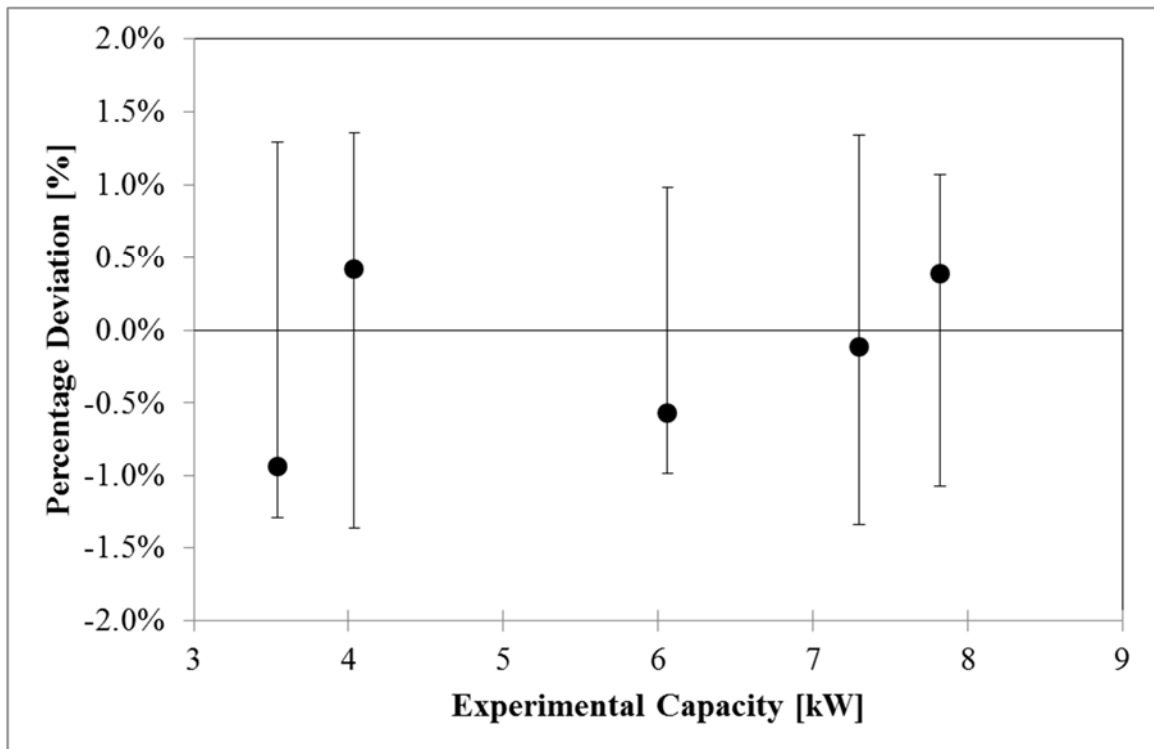


Figure 4-10 (a) Capacity relative errors

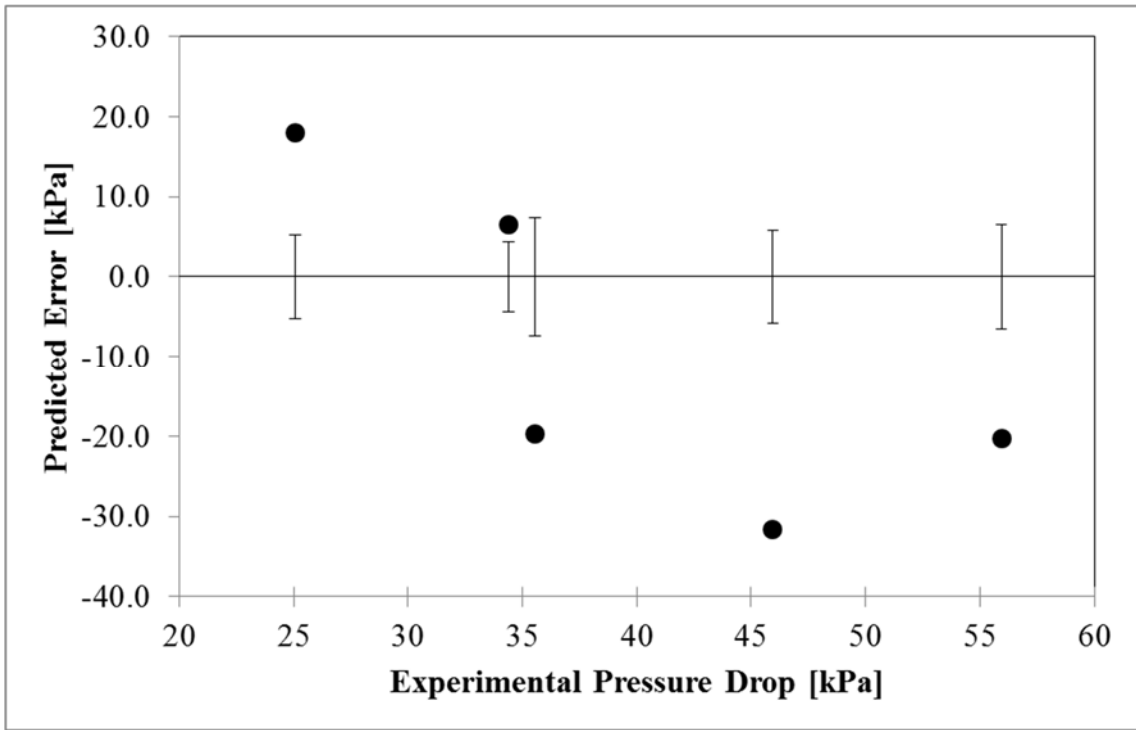


Figure 4-10 (b) Pressure drop absolute deviations

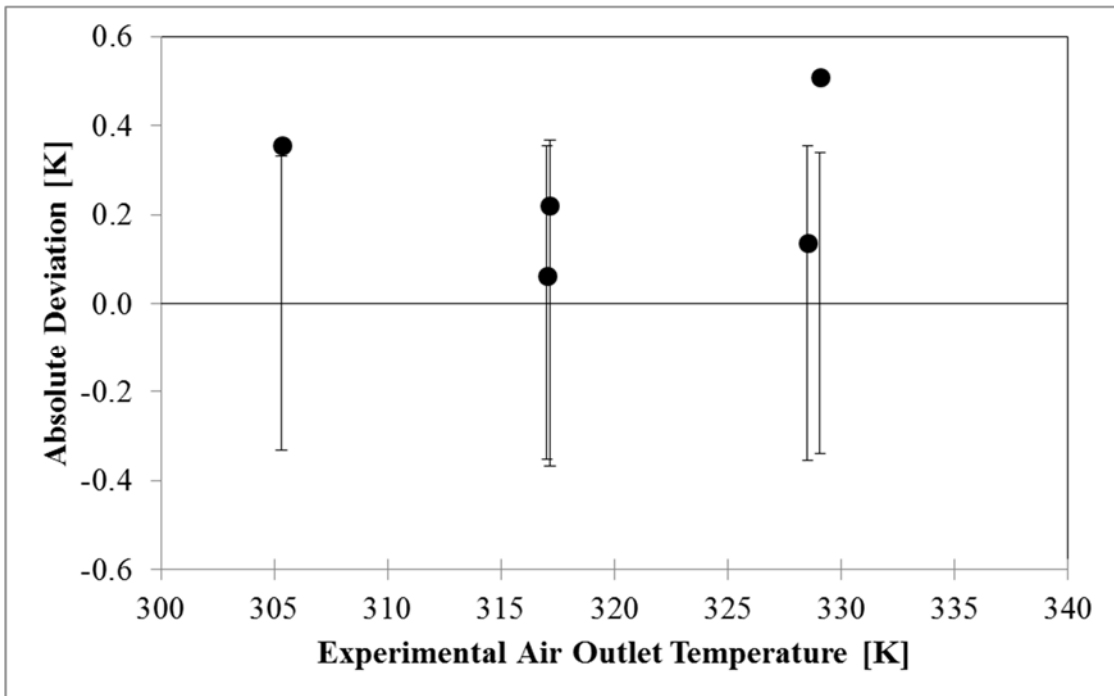


Figure 4-10 (c) Air outlet temperature absolute deviations

Figure 4-10 Comparison between experimental data and simulated results

Figure 4-11 shows the pressure contours, velocity magnitude contours and mass flow distributions of one the five data points used in validation. The flow behavior in these five cases is very similar. Since the refrigerant is single-phase vapor in the inlet header and air side mal-distribution issues on condenser tubes were not considered, the standard deviations of mass flow in these cases are relatively small. The incoming flow from the inlet connecting tube directly hits the second tube. That explains the local pressure rise observed at Tube 2 inlet for all the cases. Tube 2 also has the highest flow rate among all inlet tubes. From Tube 3 to Tube 13, due to the gravity effect, the mass flow rate is slightly increasing from upper tubes to lower tubes.

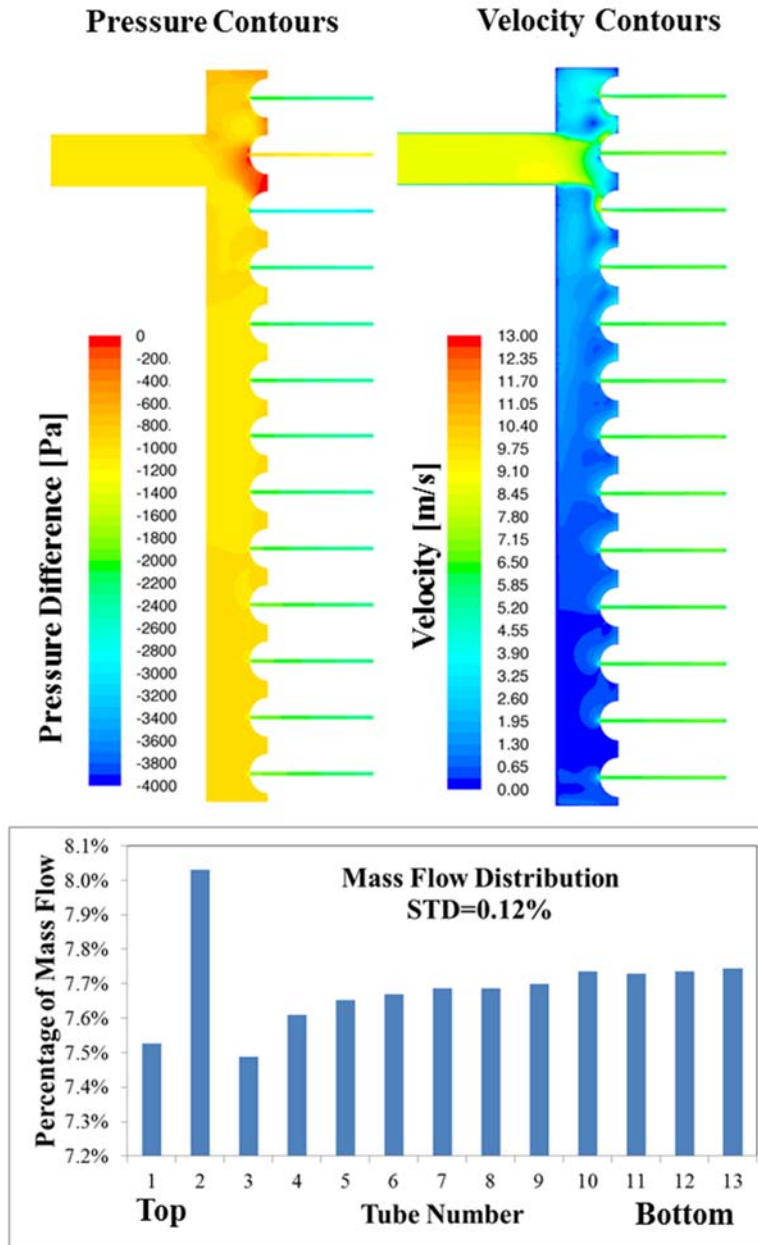


Figure 4-11 Pressure contours, velocity magnitude contours and mass flow distributions of the R134a automotive microchannel condenser validation case (Refrigerant inlet pressure= 979 [kPa], inlet temperature=338 [K], mass flow rate=29.5 [g/s])

## 4.6 Summary

A new numerical co-simulation approach for the performance evaluation of MCHXs was developed and validated against experimental data. The proposed approach combines a CFD-based header simulation model with a fast and robust effectiveness-NTU based segmented heat exchanger model. The PPCFD (Abdelaziz *et al.*, 2010) methodology is implemented to serve as an interface between the two models for co-simulation. It is used to set up boundary conditions in the CFD model and also to post-process the results from the CFD tool. The effectiveness-NTU based segmented MCHX tube model employs an NL solver which provides an efficient iteration scheme to locate the mass flow distribution. Case studies using both single-phase fluid and two-phase fluid were carried out. The case studies identified the significance of gravity effect on the liquid distribution in a vertical header and the negative effect of uneven airflow over heat exchangers with two-phase refrigerant flow. The model was validated against the experimental data for an R134a automotive condenser. The deviation of heat load was within one percent. The pressure drop prediction can be further improved using correlations that are more appropriate. The proposed co-simulation approach achieved stable convergence for all the case study and validation cases. The number of iteration required between CFD code and effectiveness-based tube model ranges from 4 to 760. The case study presented in this paper focused on a microchannel condenser with inlet header filled with R134a vapor (single phase flow). The approach can be further extended to simulate evaporator inlet header filled with two-phase flow as well as to include intermediate and outlet headers. The applicability of the proposed approach to two-phase flow simulation in headers is limited by the two-phase flow simulation capabilities of available CFD codes. The proposed approach can be used to

design better microchannel headers and tubes to keep the detrimental impacts of flow mal-distribution to a minimum and improve system performance.

## 5 AIR FLOW DISTRIBUTION AND DESIGN OPTIMIZATION OF VARIABLE GEOMETRY MICROCHANNEL HEAT EXCHANGERS

MCHXs are favored in HVAC&R applications due to their compactness, high heat transfer efficiency and potential for refrigerant charge reduction. Conventional geometry MCHXs (CG-MCHX) designs are restricted to have uniform geometry such that only one tube type, one fin type and one microchannel port type exist in one heat exchanger. The new VG-MCHX designs aim at achieving the best performance or the most suitable design with lowest material cost. There are several geometric parameters that can be varied within a VG-MCHX, such as tube width, tube height, fin type, fin height, fin density, port type and port dimensions.

In Chapter 2, several potential VG- MCHX applications have been summarized based on literature review and general knowledge of MCHX designs. The VG-MCHX modeling tool proposed in Chapter 2 has been validated against experimental data points for condensers, gas coolers and evaporators. The validation includes eight different fluids, and eighteen MCHX geometries, including four different variable geometry microchannel condensers. The objective of this paper is to evaluate and optimize an automotive condenser and a CO<sub>2</sub> gas cooler using variable geometry concept. A Multi-objective Genetic Algorithm (MOGA) available in the Thermal Systems Integration and Optimization Platform (Aute and Radermacher, 2014) is used as the optimizer in the presented study.

### **5.1 Automotive Condenser Optimization**

Eisele (2012) conducted an experimental study of an automotive secondary loop air conditioning system. The microchannel condenser used in this study was cut open to measure the port dimensions for validation purposes. This condenser design is taken as

the baseline for the optimization study. The refrigerants selected in this study are R134a and R290 (propane). Twenty-five experimental data points are validated using the three-stream model described in Chapter 2 model prior to the optimization study. The correlations chosen for heat transfer and pressure drop calculations are presented in Table 5-1. The comparison between measured capacity and simulated capacity is shown in Figure 5-1.

**Table 5-1 Summary of selected heat transfer and pressure drop correlations**

<b>Heat transfer coefficient</b>	
Air-side	Chang & Wang (1997)
Two-phase region	Shah (1979)
Single-phase region	Gnielinski (1976)
<b>Frictional pressure drop</b>	
Air-side	Chang & Wang (1997)
Two-phase region	Homogeneous (Thome, 2006)
Single-phase region	Churchill (1977)

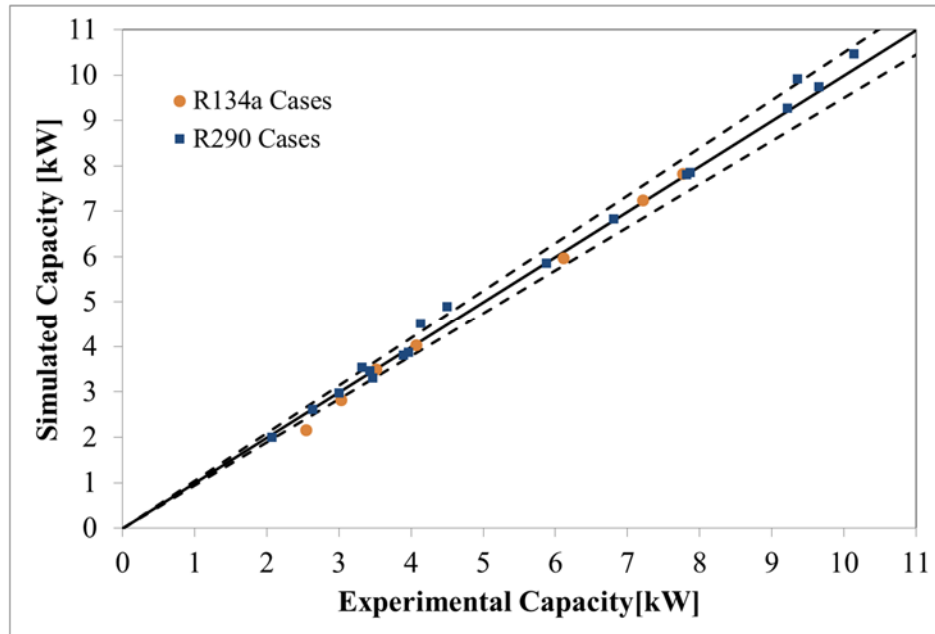
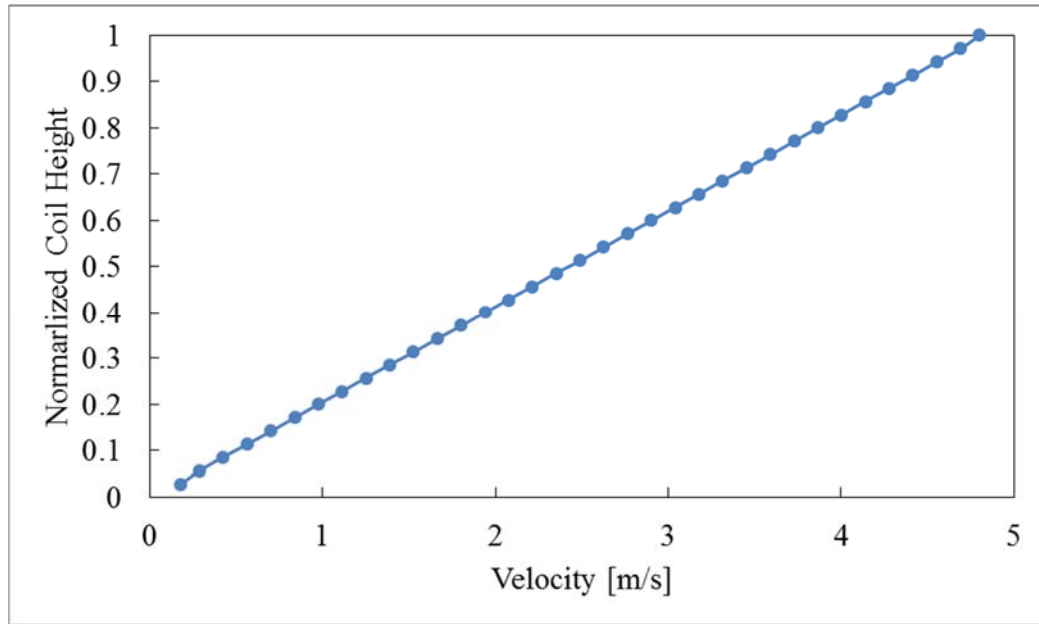


Figure 5-1 Model validation for a conventional geometry automotive condenser

#### 5.1.1 R134a condenser optimization

As the model is validated against experimental data, one of the R134a validated data point is selected to conduct the optimization study. Two different scenarios of air flow distribution are considered, uniform air flow and non-uniform air flow. A top-bottom velocity distribution profile is used where the top tubes of the MCHX have the highest air velocity and the bottom tube has the lowest air velocity. The distribution profile is presented in Figure 5-2.



**Figure 5-2 Top-bottom velocity distribution profile**

The optimization problem formulation is shown in Equation (5-1). The objectives are to minimize material mass and to maximize capacity. There are constraints on the capacity, refrigerant side pressure drop, material mass and heat exchanger envelope volume. The baseline MCHX's material mass is 2.17 [kg] with envelope volume of 4170 [cm<sup>3</sup>]. Under uniform air flow condition, the heat exchanger's capacity is 2446 [W] with refrigerant pressure drop of 8.89 [kPa]. Under non-uniform air flow, the heat exchanger's capacity is 2441 [W] and the refrigerant pressure drop is 7.57 [kPa].

Objectives:

Minimize:Material mass

Maximize:Capacity

Subject to:

Capacity > 2450 [W]

Refrigerant pressure drop < 9 [kPa]

Material mass < 2.3 [kg]

Envelope volume < 4200 [cm<sup>3</sup>]

(5-1)

The baseline R134a condenser geometry parameters and the range of design variables used in the optimization are presented in Table 5-2. Noted that the pass configuration in the current optimization problem is considered as a discrete variable. There are 16 different pass configurations studied.

**Table 5-2 Design variables of R134a microchannel condenser**

	<b>Baseline</b>	<b>Lower Limit</b>	<b>Upper Limit</b>
Vertical Spacing [mm]	10.89	6	20
Fins Per Inch	17	12	27
Port Count	10	5	20
Port Height [mm]	1.24	0.3	2
Port Width [mm]	0.77	0.3	2

Using the baseline design, we first conducted a design optimization with the conventional geometry concept. Such that, we can explore the best conventional designs. Each tube and fin can be different within a VG-MCHX. The microchannel port design can be varied as well. In the presented study, we limited the flexibility on a per-pass basis such that the geometry of tube, fin and port are the same within the same pass. In another words, this 4 pass MCHX can have 4 different tubes, fins and ports. Figure 5-3 shows the comparison between baseline, conventional geometry optimum solutions and the variable geometry solutions. Different design concepts are represented by different symbols. The shading of the symbols indicates the relative face areas between the designs. The size of the symbols represents the relative envelope volumes.

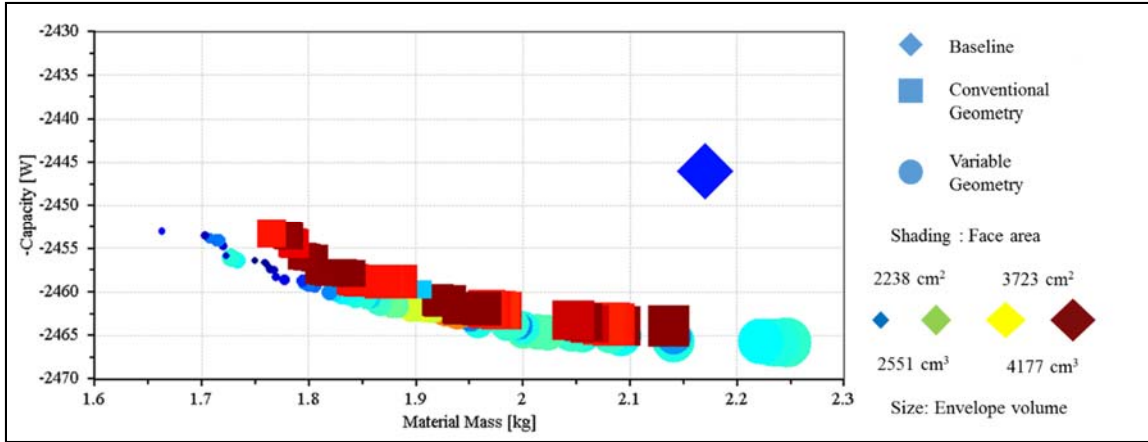


**Figure 5-3 Optimization results of R134a condenser under uniform air flow**

As shown in Figure 5, in terms of material mass, the variable geometry designs always use 5-10% less material mass as compared to the conventional geometry designs with the same capacity. As indicated by the shading of the symbols, the face area of the variable geometry designs can be up to 40% less than the optimum designs of conventional MCHX. Compared to baseline design, the maximum material mass and envelope volume savings found in the variable geometry designs are 24% and 38% respectively. In most heat exchanger optimization studies, the design objectives are improved, however, there are tradeoffs in other aspects as well. The comparison between a variable geometry optimized design and the baseline design is shown in Table 5-3. It can be seen that, for the same capacity, the optimized design has significant reduction in the material mass, envelope volume and face area. The air-side pressure drop is reported as the worst case scenario pressure drop (i.e. the pressure drop at the highest flow resistance section within the VG-MCHX). The air-side pressure drop of variable geometry design, however, suffers a 24% increase.

**Table 5-3 Comparison of baseline and optimized R134a variable geometry condenser design**

	<b>Baseline</b>	<b>Optimized Design</b>
Capacity [W]	2446	2453 (+0.3%)
Refrigerant pressure drop [kPa]	8.9	8.5 (-5%)
Air side pressure drop [Pa]	14	17.32 (+24%)
Material mass [kg]	2.17	1.66 (-24%)
Envelope volume [cm <sup>3</sup> ]	4177	2713 (-35%)
Face Area [cm <sup>2</sup> ]	2457	2110 (-14%)

Figure 5-4 shows the optimization results for R134a condenser designs under non-uniform air flow. It can be seen that, under non-uniform air flow, the variable geometry design optimum solutions pushed the Pareto set much further as compared to the conventional designs. This is because the variable geometry design can offset the effect of air flow maldistribution by having different geometries in different passes. As compared to the baseline case, the variable geometry designs show material saving potential of 19% and envelope volume saving potential of 34%.

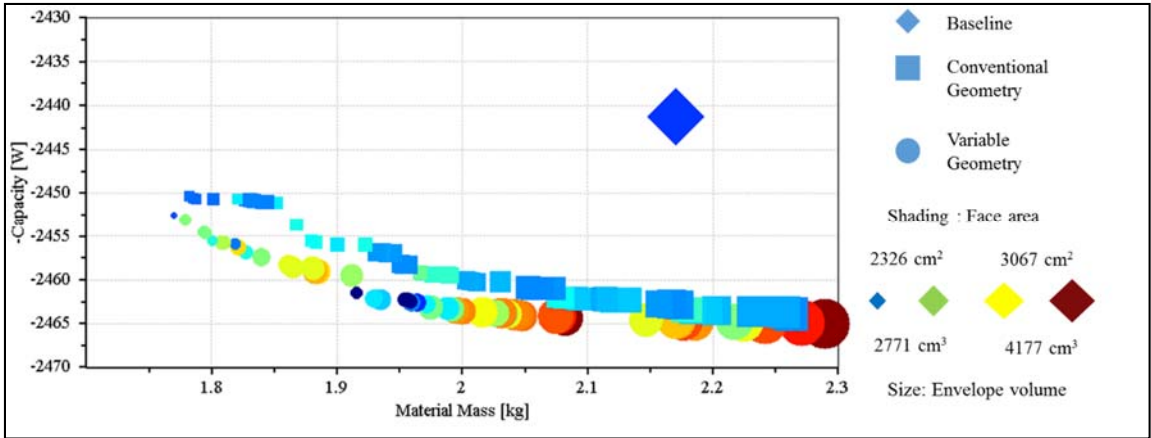


**Figure 5-4 Optimization results of R134a condenser under non-uniform air flow**

### 5.1.2 R290 condenser validation

Here, a R290 data point is selected to optimize the same heat exchanger and to study the effect of refrigerant used and the condition of working fluids. The objectives are to minimize material mass and to maximize capacity as shown in Equation (5-2). There are constraints on the capacity, refrigerant side pressure drop, material mass and heat exchanger envelope volume. The baseline MCHX's material mass is 2.17 [kg] with envelope volume of 4170 [cm<sup>3</sup>]. The baseline R290 condenser geometry parameters and the range of design variables used in the optimization are consistent with the R134a condenser optimization study in Table 5-2.

Objectives:

Minimize: Material mass

Maximize: Capacity

Subject to:

Capacity > 3570 [W] (uniform air flow) (5-2)

Capacity > 3380 [W] (non-uniform air flow)

Refrigerant pressure drop > 9 [kPa]

Material mass < 2.3 [kg]

Envelope volume < 4200 [cm<sup>3</sup>]

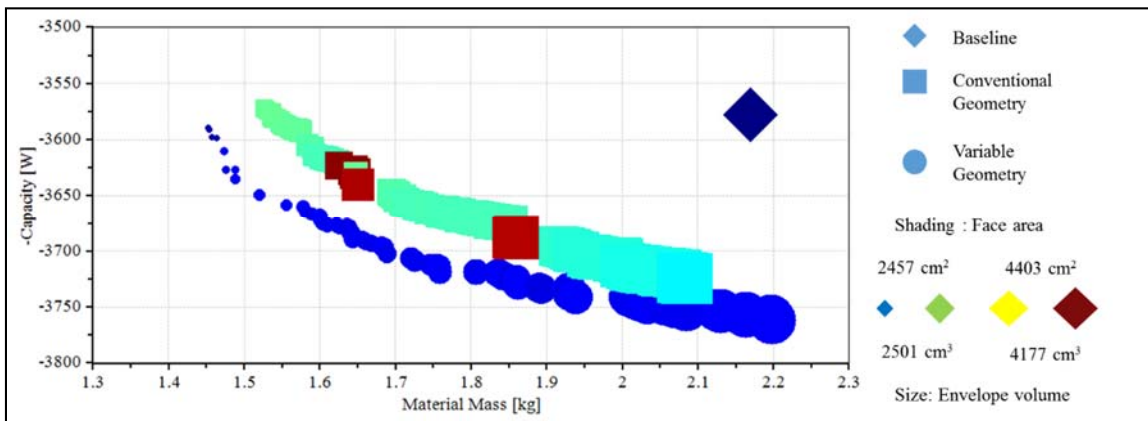


Figure 5-5 Optimization results for R290 condenser under uniform air flow

As shown in Figure 5-5, it is clear that the VG-MCHX design concept pushed the optimum design boundary further as compared to CG-MCHX optimum solutions. As indicated by the shading of the symbols, the face area of the variable geometry designs can be up to 42% lower than the optimum designs of conventional MCHX. Compared to the baseline design, the maximum material mass and envelope volume savings found in the variable geometry designs are 33% and 40% respectively. Table 5-4 presents an example of optimized VG-MCHX design and the comparison with baseline. It can be seen that, for the same capacity, the optimized design has significant reduction in the material mass, envelope volume while maintaining the same level of pressure drops and face area.

**Table 5-4 Comparison of baseline and optimized R290 variable geometry condenser design**

	<b>Baseline</b>	<b>Optimized Design</b>
Capacity [W]	3578	3589 (+0.3%)
Refrigerant pressure drop [kPa]	8.3	8.9 (+7.2%)
Air side pressure drop [Pa]	9.9	10.2 (+3%)
Material mass [kg]	2.17	1.45 (-33.2%)
Envelope volume [cm <sup>3</sup> ]	4177	2504 (-40%)
Face area [cm <sup>2</sup> ]	2457	2536 (+3.2%)

From optimization results for R290 condenser designs under non-uniform air flow shown in Figure 5-6, VG-MCHX shows even more advantage compared to the CG-MCHX designs. This is because the variable geometry design adapts the air flow configuration in this case for been able to have 4 different geometric combinations in the 4 different passes. As compared to the baseline case, the variable geometry designs show material saving potential of 35% and envelope volume saving potential of 43%.

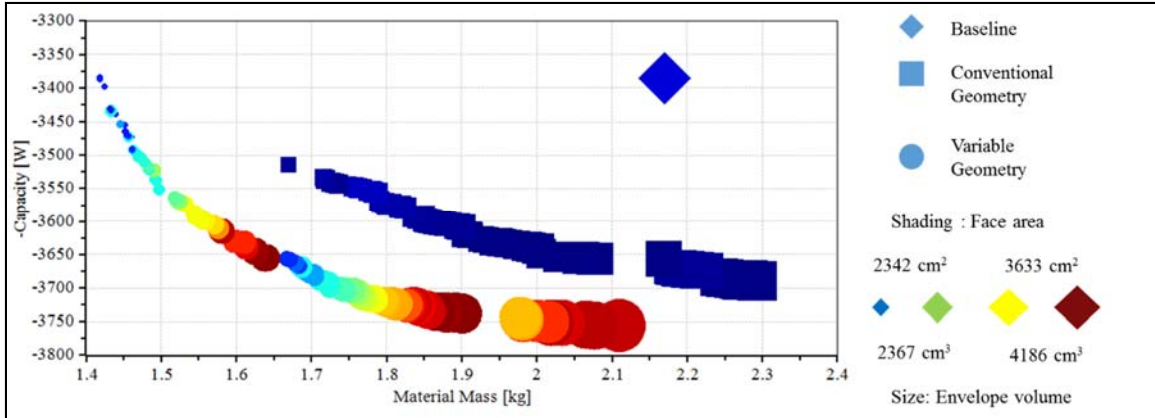


**Figure 5-6 Optimization results of R290 condenser under non-uniform air flow**

Based on the optimization results presented for the two fluids, the variable geometry design concept has greater advantage over the conventional designs for the R290 case than the R134a case studied here. Thus, while evaluating the benefit of variable geometry concept, it is important to study various working conditions and possible applications.

## 5.2 CO<sub>2</sub> Gas Cooler Optimization

The CO<sub>2</sub> gas cooler studied by Yin *et al.*, (2001) is taken as the baseline in the gas cooler optimization study. Forty-seven experimental data points are validated using Huang *et al.*, (2014a) VG-MCHX model and one of the testing conditions is selected in the presented optimization study. The selected correlations are presented in Table 5-5. The comparison between measured capacity and simulated capacity is as shown in Figure 9.

**Table 5-5 Summary of selected heat transfer and pressure drop correlations**

<b>Heat transfer coefficient</b>	
Air-side	Chang & Wang (1997)
Supercritical region	Liao & Zhao (2002)
<b>Frictional pressure drop</b>	
Air-side	Chang & Wang (1997)
Supercritical region	Churchill (1977)

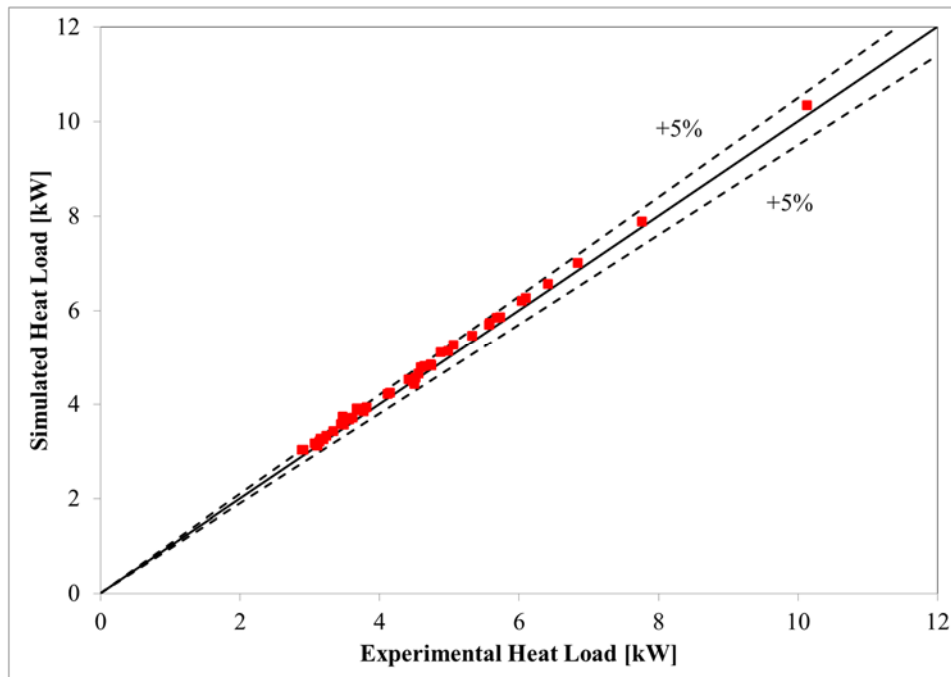


**Figure 5-7 Capacity validation for conventional geometry CO<sub>2</sub> gas cooler**

As shown in equation (5-3), the two objectives of the optimization problem are capacity and heat exchanger material mass are. The formulation includes constrains on capacity, refrigerant side pressure drop, material mass and heat exchanger envelope volume. Similar to the automotive condenser optimization study, the design optimization is conducted with both conventional geometry concept and variable geometry concept in order to compare the two different designs.

Objectives:

Minimize:Material mass

Maximize:Capacity

Subject to:

Capacity > 5600 [W]

Refrigerant pressure drop < 120 [kPa]

Material mass < 2 [kg]

Envelope volume < 3300 [cm<sup>3</sup>]

(5-3)

The baseline values for the design variables and their limits for optimization are tabulated in Table 5-6. The microchannel port is circular port in this case. In both design optimization studies, the distance between microchannels and the distances between the microchannel and the tube surface are kept the same as the baseline cases. There are 8 different pass configurations studied in this case.

**Table 5-6 Design variables of CO<sub>2</sub> microchannel gas cooler**

	<b>Baseline</b>	<b>Lower Limit</b>	<b>Upper Limit</b>
Vertical Spacing [mm]	10.51	6	20
Fins Per Inch	22	12	27
Port Count	11	5	20
Port Diameter[mm]	0.79	0.3	2

As shown in Figure 5-8, the baseline design falls on the Pareto set of conventional geometry designs. This indicates that the baseline design was itself optimized. The Pareto solutions for conventional geometry designs are grouped into five clouds. This is due to the fact that the pass configuration is considered as the discrete variable in the study. Each cloud, i.e., group of designs, represents a set of designs with the same pass configuration. However, the Pareto solutions for variable geometry designs are continuous because there is always a best possible geometric combination for different pass configurations. For each pass configuration, there is always a best combination of design variables that optimizes both objectives. Comparing the two sets of optimum designs, the variable geometry designs generally require at least 10% less material than the conventional geometry designs. Under the same performance as compared to the baseline design, the material savings is 13% and the envelope volume savings is 18%.

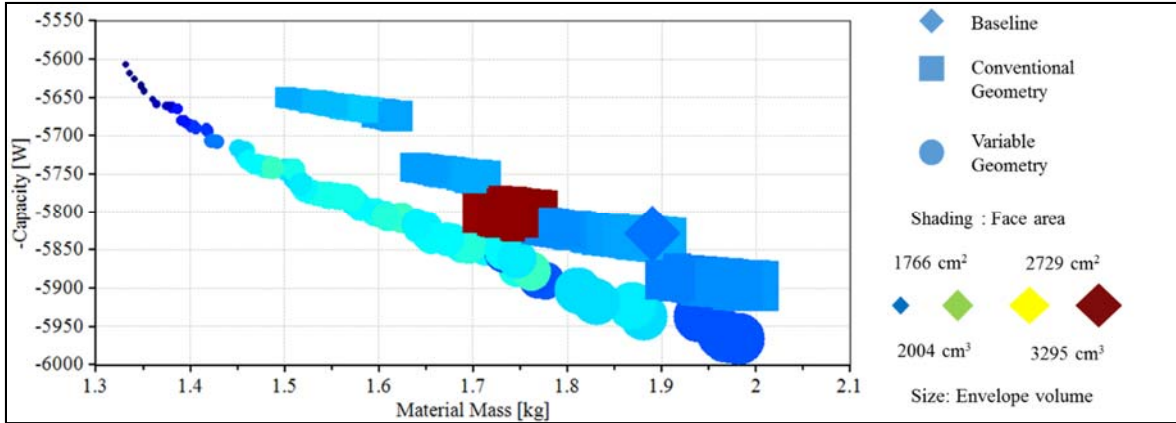


**Figure 5-8 Optimization results of CO<sub>2</sub> gas cooler under uniform air flow**

One of the best material saving examples is tabulated and compared to the baseline design in Table 5-7. With a minor performance degradation and an increased face area, the optimized design achieved 23% reduction in material mass and 28% savings in envelope volume.

**Table 5-7 Comparison of baseline and optimized CO<sub>2</sub> variable geometry gas cooler design**

	<b>Baseline</b>	<b>Optimized Design</b>
Capacity [W]	5828	5716 (-1.9%)
Refrigerant pressure drop [kPa]	110	114 (+4%)
Air side pressure drop [Pa]	22.5	12.83 (-43%)
Material mass [kg]	1.89	1.45 (-23%)
Envelope volume [cm <sup>3</sup> ]	3295	2376 (-28%)
Face Area [cm <sup>2</sup> ]	1995	2098 (+5%)

Figure 5-9 presents the CO<sub>2</sub> gas cooler optimization results under non-uniform air flow scenario. Similar to previous findings in the automotive condenser optimization, the VG-MCHX consistently yield to better designs as compared to the conventional MCHXs. At the same capacity, the material saving and envelope volume saving of variable geometry design are 17% and 26% respectively.

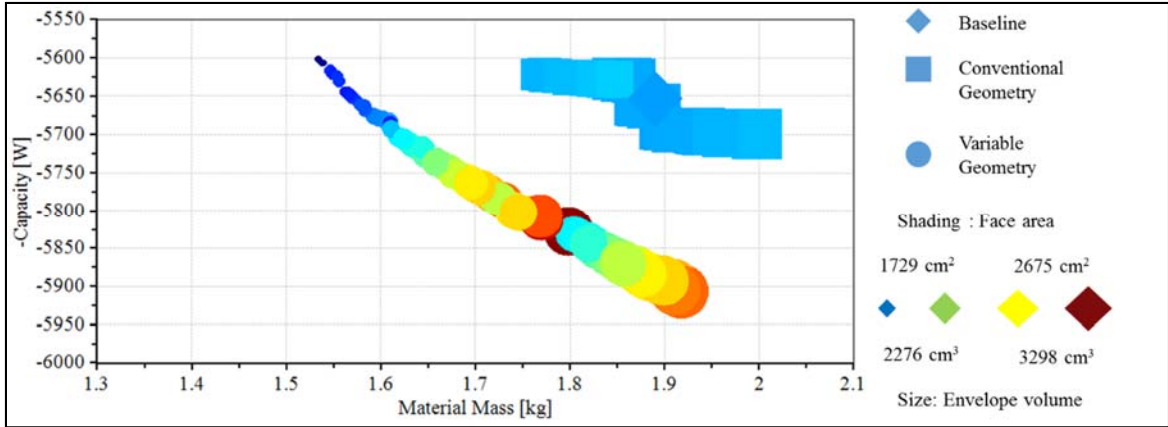


**Figure 5-9 Optimization results of CO<sub>2</sub> gas cooler under non-uniform air flow**

### 5.3 Prediction of Air Flow Mal-distribution

There are many causes for air flow mal-distribution, such as duct design, heat exchanger orientation, variation in geometry (e.g., staged fins) and fan position. With the aid of Computational Fluid Dynamic (CFD) modeling or experimental measurement, velocity profiles on coil face can be generated as inputs for use in the heat exchanger models. Variable geometry microchannel heat exchangers have non-uniform geometry facing the air. This variation in geometric characteristics can lead to different air flow resistances causing air flow mal-distribution. Considering that CFD analysis and experimental measurements are expensive in the design process in terms of computational resources and time, it is desired to have a computationally inexpensive method to understand the impact of variable geometric parameters in VG-MCHX. Similar to the solving methodology of refrigerant mal-distribution problem, the air-side distribution can be obtained in an iterative manner.

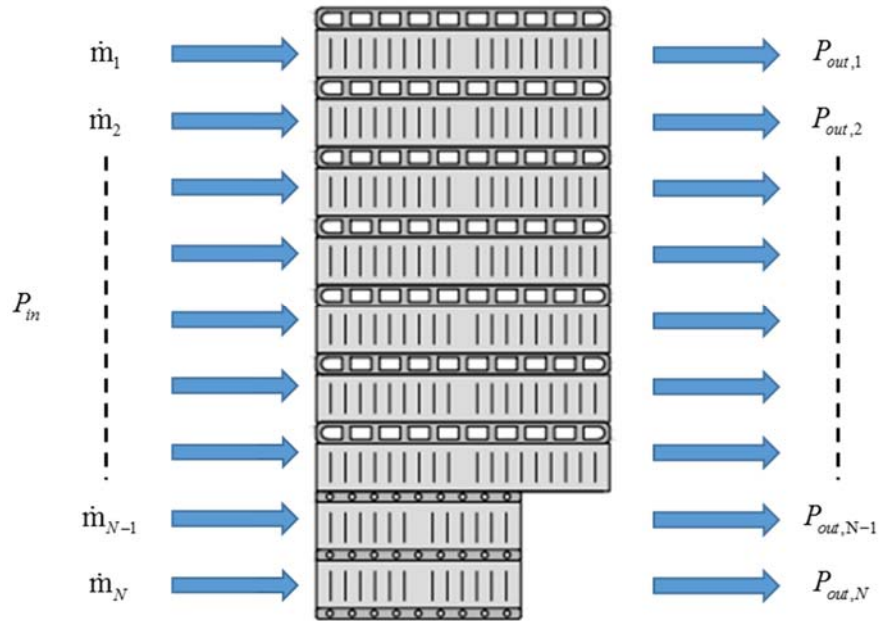


**Figure 5-10 Air flow distribution for variable geometry microchannel heat exchanger**

As presented in Figure 5-10, the air streams are separated by flow channels. The outlet pressure of each air flow channel can be calculated using air-side pressure drop correlations. The model will then calculate the outlet pressure and then assign new inlet flow distribution. I present the solving methodology in Figure 5-11.

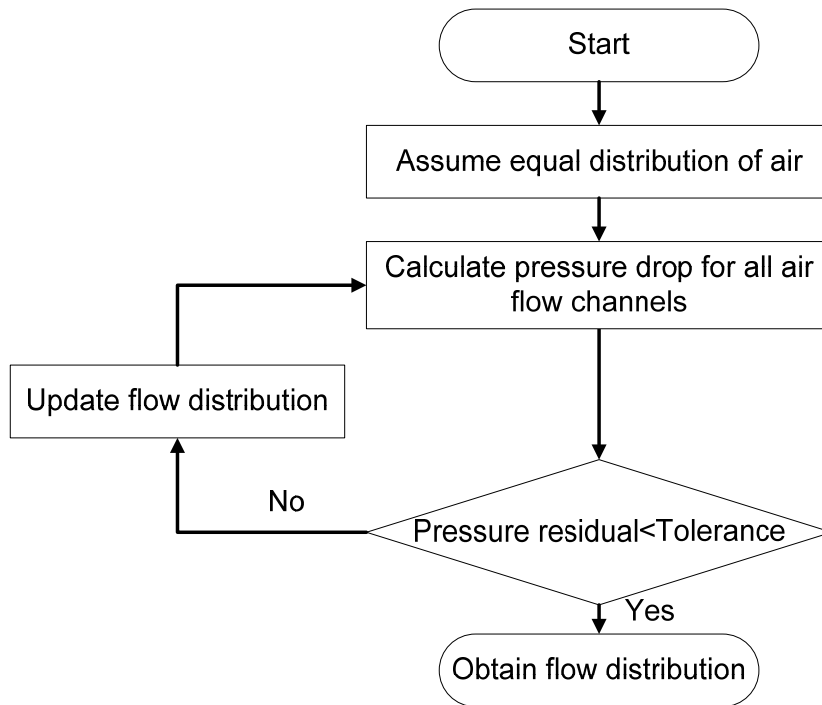


**Figure 5-11 Air distribution solving methodology**

In previous studies presented in this paper, the air flow distribution is treated as an input, either uniform or non-uniform. In order to better understand the impact of air flow distribution on variable geometry, we studied the CO<sub>2</sub> gas cooler optimization using the above mentioned approach. In this study, we assume that the only cause of air flow maldistribution is the difference in air flow resistance due to geometry variation. Given the fixed air flow rate, the new optimum designs based on calculated air distribution are compared to the previous cases that assumed uniform air flow distribution as presented in Section 5.2.

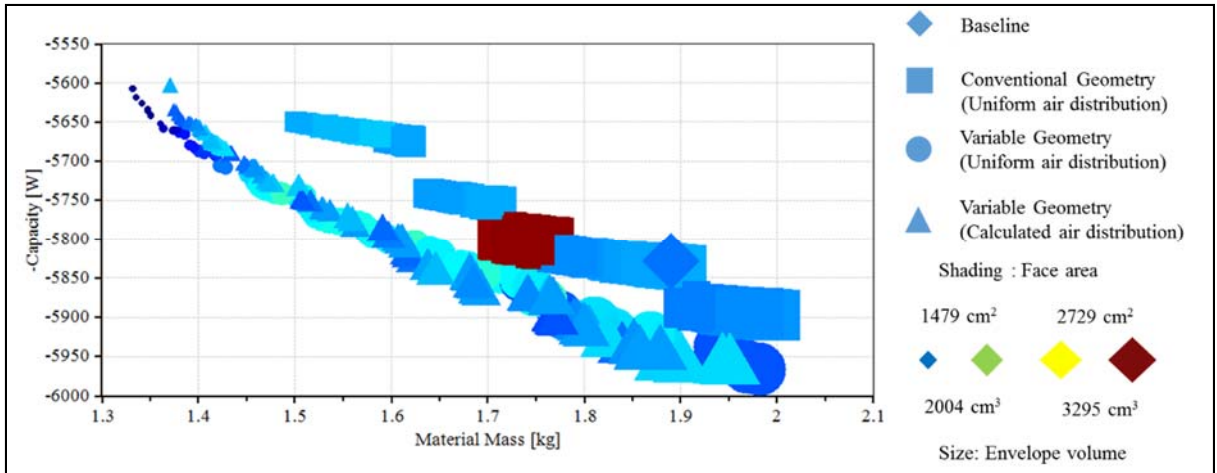


**Figure 5-12 Optimization results of CO<sub>2</sub> gas cooler under uniform and non-uniform air flow distribution**

In Figure 5-12, the optimum variable geometry designs using calculated air distribution are represented by triangular shape. As presented in the figure, even when the air maldistribution issue is considered, the optimum designs based on the variable geometry cases are consistently better than the conventional designs in terms of material mass and capacity. For the cases with 5700 [W] or more capacity, the Pareto solutions of variable geometry designs under uniform air distribution or calculated air distribution yield the same level of material savings. The optimum geometry itself is different for the uniform and the non-uniform air flow cases. This highlights the potential of the VG-MCHX to achieve optimal designs under various air flow distributions. For the cases with lower capacity and smaller heat exchanger size, the optimum designs are more sensitive to air flow distribution. With calculated air flow distribution, the least material mass consumption is 1.37 [kg]. Comparing to the best material savings case at 1.33 [kg] assuming uniform velocity distribution, 3% more material is required. This study shows that, air flow distribution is an important factor to consider while evaluating variable geometry designs. It is worthwhile to investigate

the combined effect of duct design, heat exchanger orientation and fan position as well as heat exchanger geometry variation via CFD simulation and experimental testing.

#### **5.4 Summary**

This paper presented optimization studies on variable geometry microchannel heat exchanger designs to investigate their performance potential. The motivation for the use of variable geometry designs is discussed, including heat transfer enhancement and pressure drop reduction, air and refrigerant mal-distribution minimization, heat conduction effect minimization, material saving as well as application requirements. We validated and optimized an automotive R134a and R290 condenser and a CO<sub>2</sub> gas cooler. The material and envelope saving potential are revealed under both uniform air flow case and non-uniform air flow case. For both applications and for both air flow scenarios, the variable geometry design shows clear advantage compared to the conventional designs. The maximum material savings and envelope volume savings found in this study are 35% and 43% respectively. Besides material saving and capacity enhancement, different objectives can be applied to the optimization problem to investigate the potential benefits of variable geometry designs. Further analysis of system level investigations and life cycle climate performance analyses can be carried out to explore the impact of applying variable geometry designs. An iterative approach to calculate air flow mal-distribution caused by varying geometry was developed. The optimization results under uniform air flow assumption and using calculated air flow distribution are compared. The comparison showed the importance of considering the variable geometry impact on air flow distribution. Comparing the best material saving cases assuming uniform air distribution and using calculated air flow, 3% more mass is required when accounting for the difference in flow resistance. It is observed that

even under the non-uniform air flow distribution, the variable geometry designs are significantly better than the baseline designs. Further CFD analysis and experimental testing can be carried out to study the combined effect of duct design, heat exchanger geometry and orientation, as well fan position and design.

## 6 A FINITE VOLUME COAXIAL HEAT EXCHANGER MODEL WITH MOVING BOUNDARIES AND MODIFICATIONS TO CORRELATIONS FOR TWO-PHASE FLOW IN FLUTED ANNULI

This Chapter introduces a generalized CHX model that is capable of simulating various flow conditions, flow configurations, coil configurations and tube geometries. Detailed modeling methodology including four different segment insertion/subdivision approaches is illustrated. Modifications to existing correlations are proposed for the calculation of heat transfer coefficient and pressure drop correlations during two phase flow in fluted tube annulus. Finally, the numerical model using the proposed correlation formulations is validated against experimental data for fluted tube CHX operating as a condenser and an evaporator.

### **6.1 Model Description**

#### **6.1.1 Model overview**

The proposed model is capable of simulating single-phase and two-phase CHXs with smooth and enhanced surfaces, straight and helical configurations, as well as parallel and counter-flow arrangements. It is capable of estimating the overall performance based on geometric parameters and fluid inlet states and mass flow rates. It is also able to calculate the required mass flow rate for a specific outlet condition. The model provides various options to track the phase change point efficiently. Lastly, a set of newly developed and validated fluted tube annulus heat transfer and pressure drop correlations are implemented such that the performance fluted tube condenser and evaporator can be predicted with reasonable accuracy. The geometric parameters used in the model are shown in Figure 6-1.

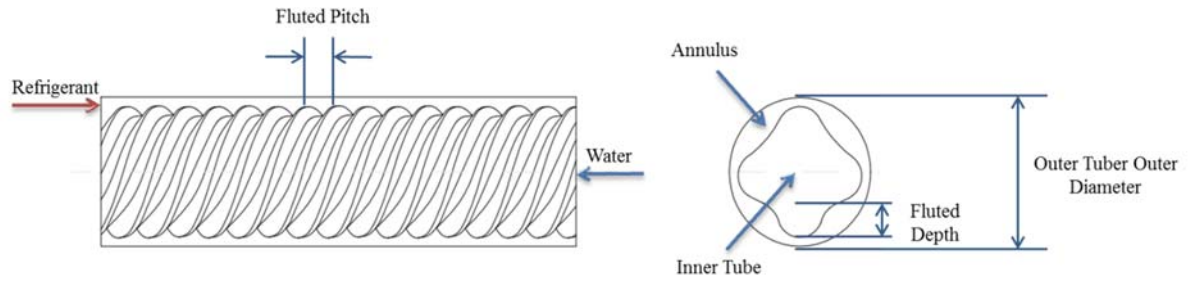


**Figure 6-1 Fluted tube geometry**

A finite-volume approach is adopted in the proposed model to track the fluid property change and the thermal and hydraulic performance variation along the length of flow channel. The entire heat exchanger length is divided into a given number of finite volumes, each termed as a segment. The number of finite volumes (aka segments) can be adjusted to change the speed and accuracy of the model. The inputs to the model are the inlet fluid conditions and flow rates (inner tube and annulus side), tube geometry, the flow configuration and material properties. The fluid outlet states, capacity, pressure drops and charge are predicted by this model. The proposed model is based on following assumptions:

- 1) Steady state
- 2) Thermally and hydro-dynamically fully developed flow
- 3) The thermophysical properties, heat transfer coefficients and pressure drops are evaluated based on the inlet of each segment
- 4) Heat exchanger is adiabatic (i.e., no heat transfer between the outer tube and the ambient)
- 5) No heat conduction in flow direction (i.e., no axial conduction)
- 6) Phase change occurs when bulk enthalpy reaches saturated enthalpy at given pressure level (i.e., no sub-cooled boiling; no superheated condensation)

It should be noted that assumption (3) is introduced to avoid additional iterations within the segment. Instead of using the inlet state for thermophysical property evaluation, the average state could be used to increase the accuracy, but that would require additional iterations and the calculation may not be as stable. The entire coaxial tube-in-tube heat exchanger is divided into a given number of segments along the length of the heat exchanger. The underlying solution algorithm of the proposed model is illustrated in Figure 6-2.

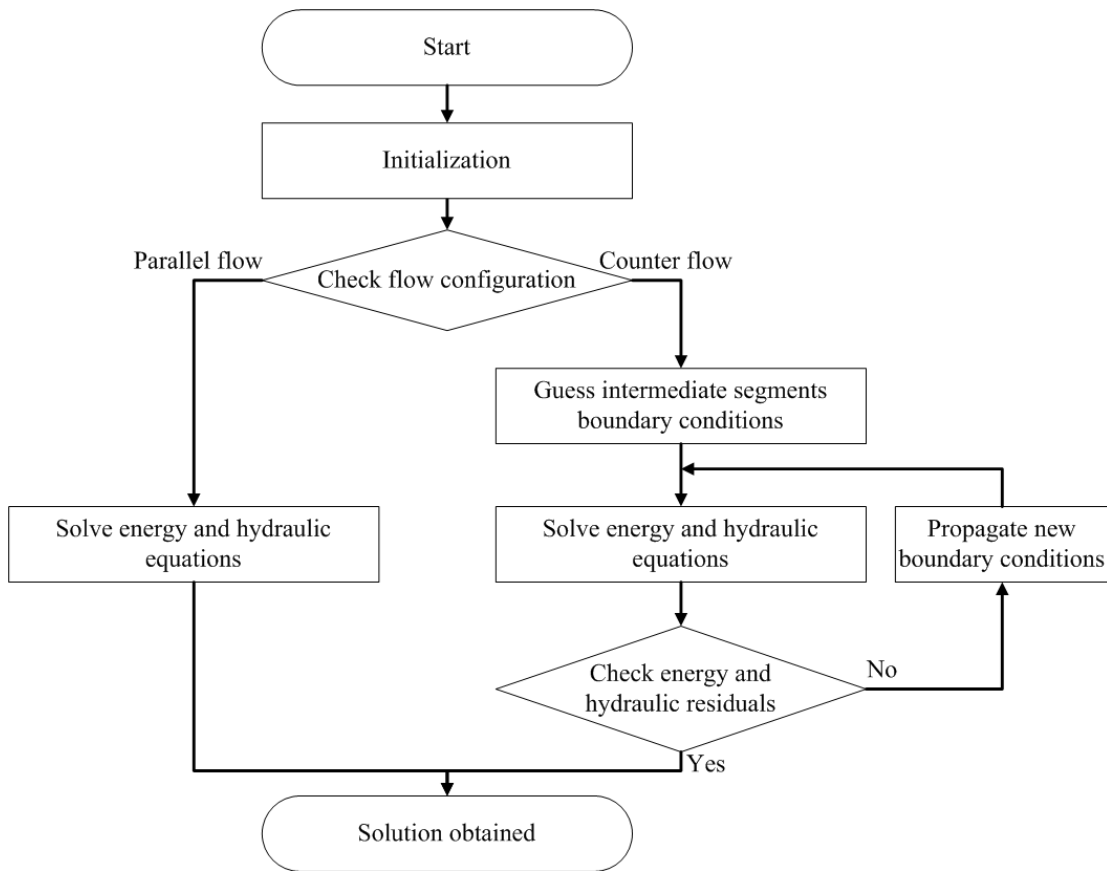


**Figure 6-2 Model main solving methodology**

Separate iteration schemes are developed to handle parallel flow and counter flow configurations. In the case of parallel flow configuration, the model solves energy and hydraulic equations for each segment sequentially from the first (i.e., inlet) segment

to the last (i.e., outlet) segment. For counter flow configuration, the initial conditions for all the unknown state points at each segment are guessed by the algorithm and then the outlet states for each segment are solved iteratively.

In most applications, when the CHX is serving as a condenser/evaporator, the outlet superheat/subcooling is fixed for design purposes. With the assistance of nonlinear equation solver, the proposed model can be used for design purposes such as solving for a specific outlet superheat/subcooling for one of the flow channel by varying inlet mass flow rate or geometry parameters of the respective flow channel.

### 6.1.2 Segment level heat transfer model

At the segment level, when at least one of the fluids is in single phase, the heat transfer between inner fluid and outer fluid is calculated based on Effectiveness-NTU (Kays & London, 1984) approach. In the case where there is two-phase flow on both sides, an energy balance approach is applied. The application of the two methods is explained below.

For Effectiveness-NTU approach

$$Q = \varepsilon C_{min} \Delta T \quad (6-1)$$

where  $C_{min}$  is the minimum heat capacity rate between the two fluids.  $\varepsilon$  is the effectiveness, which depends on number of transfer units, heat capacity ratio and flow arrangement. The temperature difference is calculated using arithmetical mean temperature difference.

$$\begin{aligned} \varepsilon &= \phi \left( \frac{UA}{C_{min}}, \frac{C_{min}}{C_{max}}, flow\ arrangement \right) \\ &= \phi (NTU, C^*, flow\ arrangement) \end{aligned} \quad (6-2)$$

Here  $C^*$  is the heat capacity rate ratio.

$$C^* = \frac{C_{\min}}{C_{\max}} \quad (6-3)$$

Effectiveness-NTU approach is applied to three different cases as shown below.

Case I: Single phase flow on both sides

$$C_{\max} = \max(\dot{m}_{\text{inner}} C_{p_{\text{inner}}}, \dot{m}_{\text{outer}} C_{p_{\text{outer}}}) \quad (6-4)$$

$$C_{\min} = \min(\dot{m}_{\text{inner}} C_{p_{\text{inner}}}, \dot{m}_{\text{outer}} C_{p_{\text{outer}}}) \quad (6-5)$$

For parallel flow configuration

$$\varepsilon = \frac{1 - e^{-NTU(1+C^*)}}{(1+C^*)} \quad (6-6)$$

For counter flow configuration

$$\varepsilon = \frac{1 - e^{-NTU(1-C^*)}}{(1-C^*) \cdot e^{-NTU(1-C^*)}} \quad (6-7)$$

Case II: Single phase flow in inner tube, two-phase flow in outer tube

When one of the fluids is changing phase (i.e., undergoing evaporation or condensation), heat capacity ratio is always 0 and minimum heat capacity is always calculated based on the single phase fluid. For these two cases, effectiveness of the segment is calculated by the following equation.

$$\varepsilon = 1 - e^{-NTU} \quad (6-8)$$

Case III: Single phase flow in outer tube, two-phase flow in inner tube

Same as Case II.

Case IV: Two-phase flow on both sides

Energy balance approach is used in this case. The total heat transfer rate is given as

$$Q = UA\Delta T \quad (6-9)$$

For both the Effectiveness-NTU approach and energy balance approach, the overall UA of the segment is calculated as

$$UA = \frac{1}{\frac{1}{UA_{inner}} + \frac{1}{UA_{outer}} + R_{material} + R_{fouling, inner} + R_{fouling, outer}} \quad (6-10)$$

The expression for the material resistance term is

$$R_{material} = \frac{\log\left(\frac{ID_{inner} + 2\delta}{ID_{inner}}\right)}{2\pi k_{tube} L} \quad (6-11)$$

### 6.1.3 Phase change tracking methods

The fluid properties, heat transfer coefficients and pressure drop in three different phases (liquid, two-phase and vapor) can be significantly different. Thus, it is important to track the exact phase change point, even within a segment. The traditional moving boundary technique only divide the entire heat exchanger into few control volumes. However, with limited number of control volumes, the accuracy is typically worse than finite volume approach. To further improve the accuracy and stability of the finite volume model proposed, the moving boundary approach is applied to segment level simulation. The remainder of this section proposed four different technique to locate the phase change point. By solving the energy (i.e., heat transfer) equations in each segment, the outlet enthalpy of each fluid can be obtained. The pressure drop within each segment is calculated based on correlations.

Finally, the outlet states for the two fluids are checked against their respective inlet states. If no phase change occurs in this segment, then the segment level calculation is completed. If there is phase change within this segment, the segment will be further divided in order to track the exact phase change point(s). In the literature, this approach is also referred to as the moving boundary heat exchanger model. Jiang *et al.* (2006) proposed an iterative segment subdivision approach for modeling a tube-fin heat exchanger used for air-to-refrigerant heat transfer. This approach was then adopted and investigated in different types of air-to-refrigerant heat exchanger models (Singh *et al.*, 2009, Huang *et al.*, 2012a, Huang *et al.*, 2012b). Jiang's approach is developed for an air-to-refrigerant segment where all the sub-segments are facing the same air inlet condition. Under such circumstance, the calculation in each sub-segment can be conducted successively to locate the phase change point(s) using the Golden Section Method (Kiefer, 1953). In the case of CHX, it is possible that both sides may have phase change. This is further complicated by the fact that the model needs to account for various fluid conditions and flow configurations. In such cases, the Golden Section Method may not have a viable starting point (i.e., guess value) to begin with. In order to address this issue, the authors propose three different segment insertion methods that deal with all the possible cases, including the most complex case in which there are phase changes happening on both sides in a counter flow configuration. The segment insertion techniques are in fact adaptively increasing the number of finite volumes to account for phase change. In addition, based on Jiang's concept, a new segment subdivision technique is developed for the most common design of CHX,

water/brine to refrigerant (i.e., one fluid is always single phase) counter flow configuration.

A counter flow CHX example with phase change on one side is shown in Figure 6-3 to explain the concept of segment insertion techniques. The sample heat exchanger case consists of two segments that are numbered from left to right. Fluid A flows from right (Segment-2) to left (Segment-1) while a single phase Fluid B flows in the opposite direction. Suppose the model finds that during the calculation of segment 2, Fluid A's inlet is vapor phase and outlet is in two-phase region? In that case the actual calculation for the enthalpy residual calculated based on outlet enthalpy and saturation enthalpy (i.e., saturated vapor enthalpy in this case) determines whether segment insertion or sub-division should be carried out. When phase change is observed and the calculated enthalpy residual is larger than an acceptable tolerance, segment insertion or sub-division function is triggered.

$$\left| \frac{(h_{out} - h_{sat})}{h_{sat}} \right| > Tolerance? \quad (6-12)$$

Different segment insertion methods for this sample case are also illustrated in Figure 6-3.

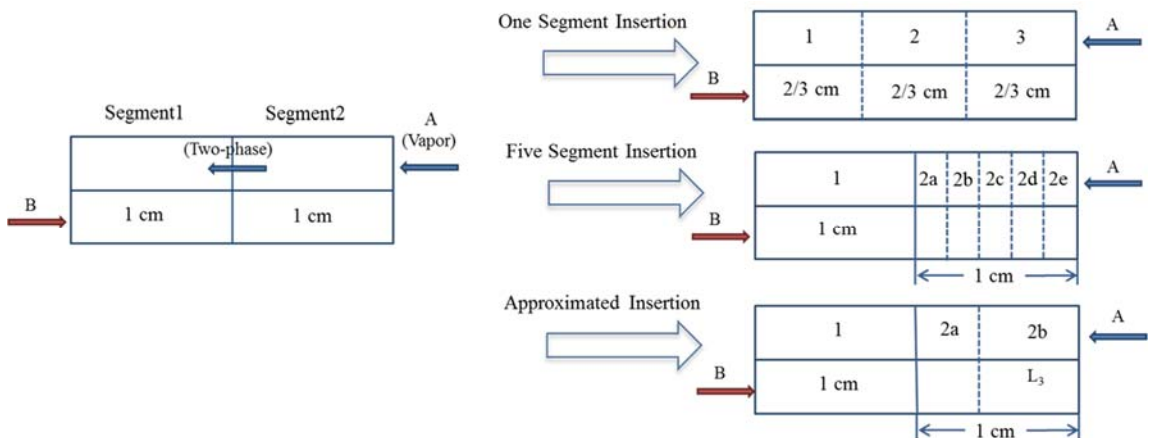


Figure 6-3 Segment insertion techniques

### Segment Insertion Method I, One segment insertion

This method inserts a new segment 3 for the example case, segment 1 and 2 are reconstructed such that segment 1, 2 and 3 have equal lengths.

### Segment Insertion Method II: Five segments insertion

This method replaces segment 2 with five new even length segments. The model chooses to use five new segments to avoid unnecessary additional iterations while maintaining a reasonable computational effort.

### Segment Insertion Method III: Segment insertion based on approximation of phase change point

This method calculates an approximated length from the inlet of Fluid A to the phase change point. The length of new segment 3 is approximated by the equation below

$$L_3 = \frac{\dot{m}(h_{in} - h_{sat})}{Q_{segment}} L_{segment} \quad (6-13)$$

It should be noted that  $Q_{segment}$  represents the heat load calculated in the original segment 2 that assumes that it is filled with vapor-phase Fluid A.

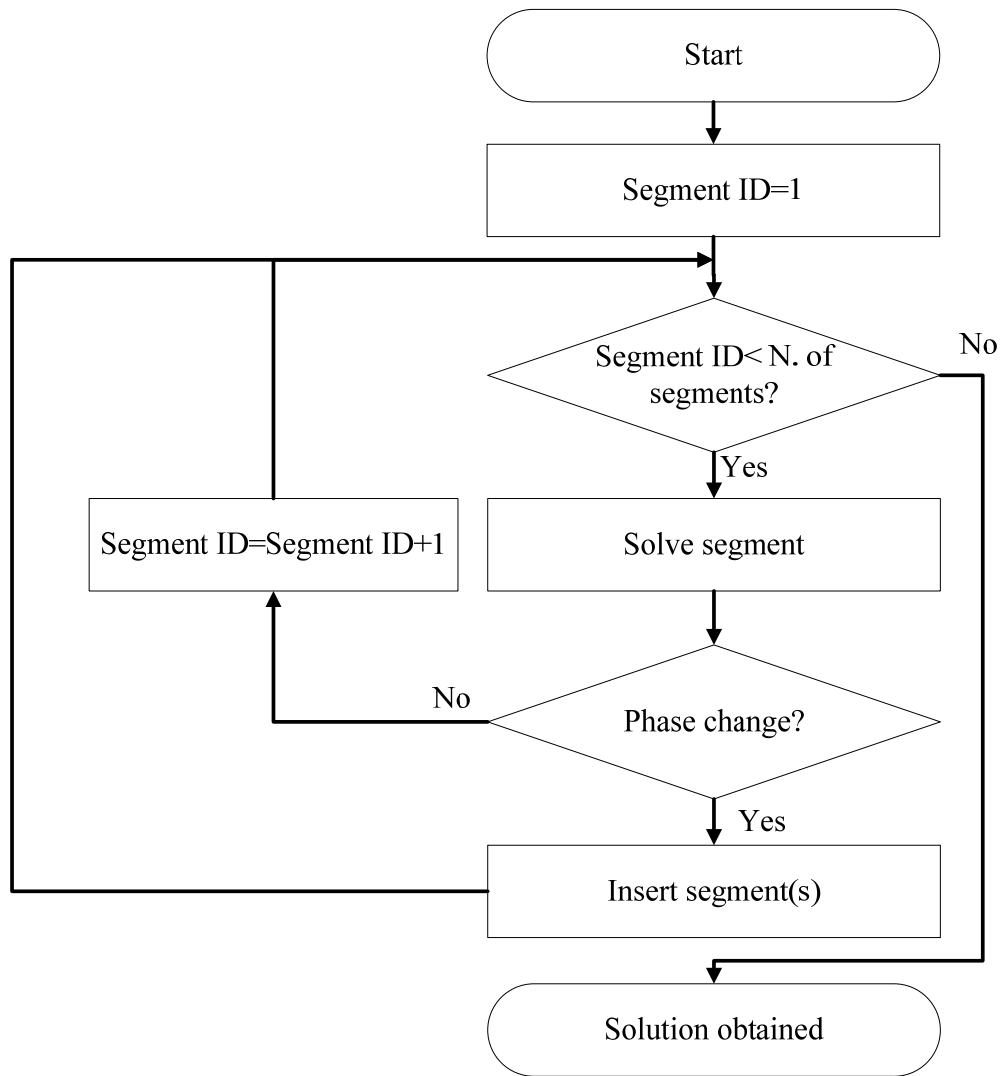


**Figure 6-4 Parallel flow configuration segment insertion method**

Based on different characteristics of parallel flow configuration and counter flow configuration, two different solving methodologies are developed. As shown in Figure 6-4, the parallel flow segments are solved successively. When phase change occurs, new segment(s) will be inserted and the solver will continue the calculation from newly inserted segments. Counter-flow configuration solving approach is presented in Figure 6-5. Upon completion of each iteration, the algorithm checks for all the phase change points within the heat exchanger, new segments are inserted near the phase change points and their boundary conditions are updated based on the flow conditions of

adjacent segments. The solver will continue its iteration until the overall enthalpy residual meets the convergence criterion.

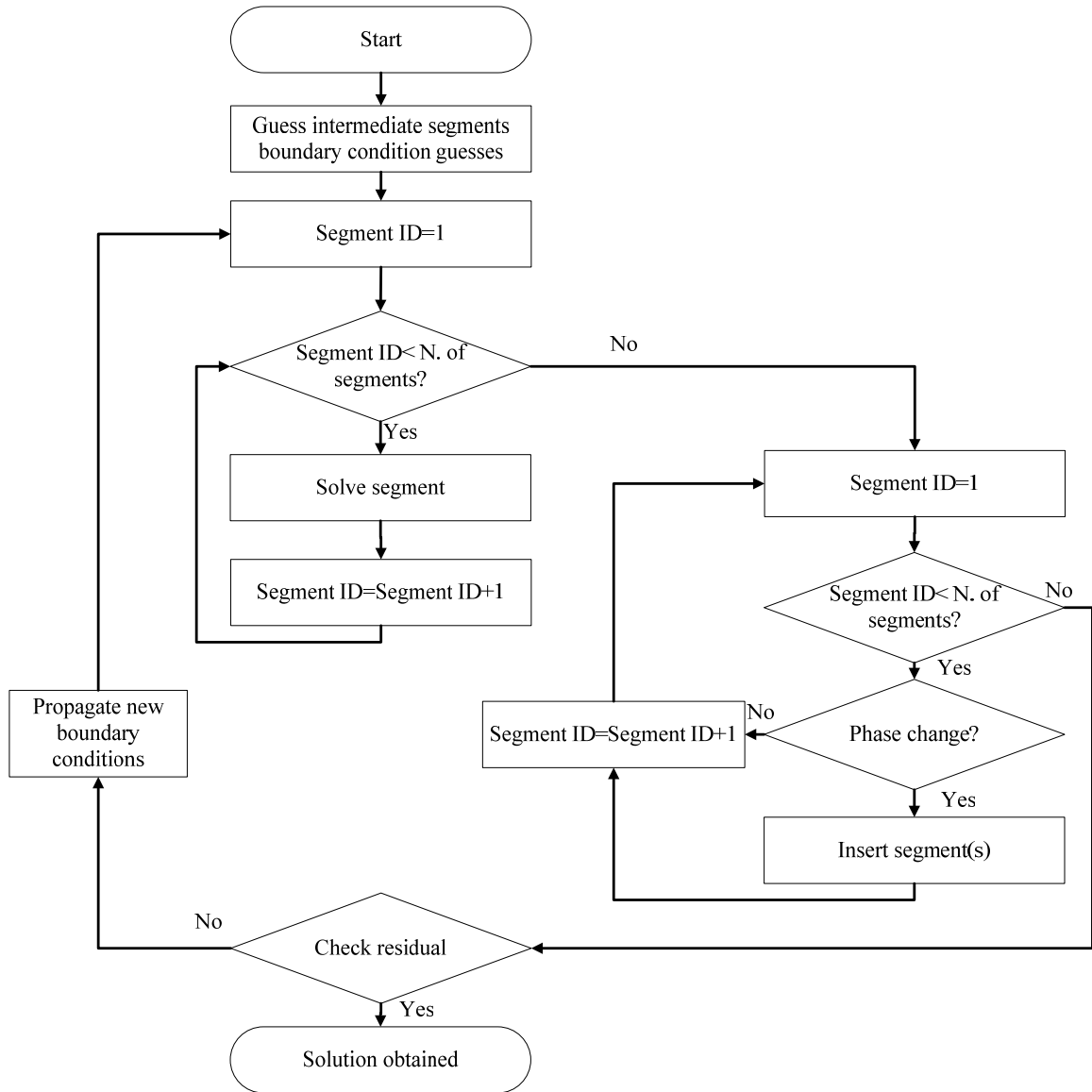


**Figure 6-5 Counter flow configuration segment insertion method**

Segment insertion methods require additional considerations in the main solution methodology. Segment sub-division technique resolves the phase change problem within the current solving segment. Figure 6-6 illustrates the strategy of the sub-division method at the segment level calculation. A full segment with phase change is first equally subdivided as the starting point for the nonlinear solver. The lengths of

each sub-segment can be obtained based on known overall segment inlet conditions and fluid conditions at each phase change point. Pressure drop is then calculated iteratively. Both energy and hydraulic criteria are met at the end of sub-division function.

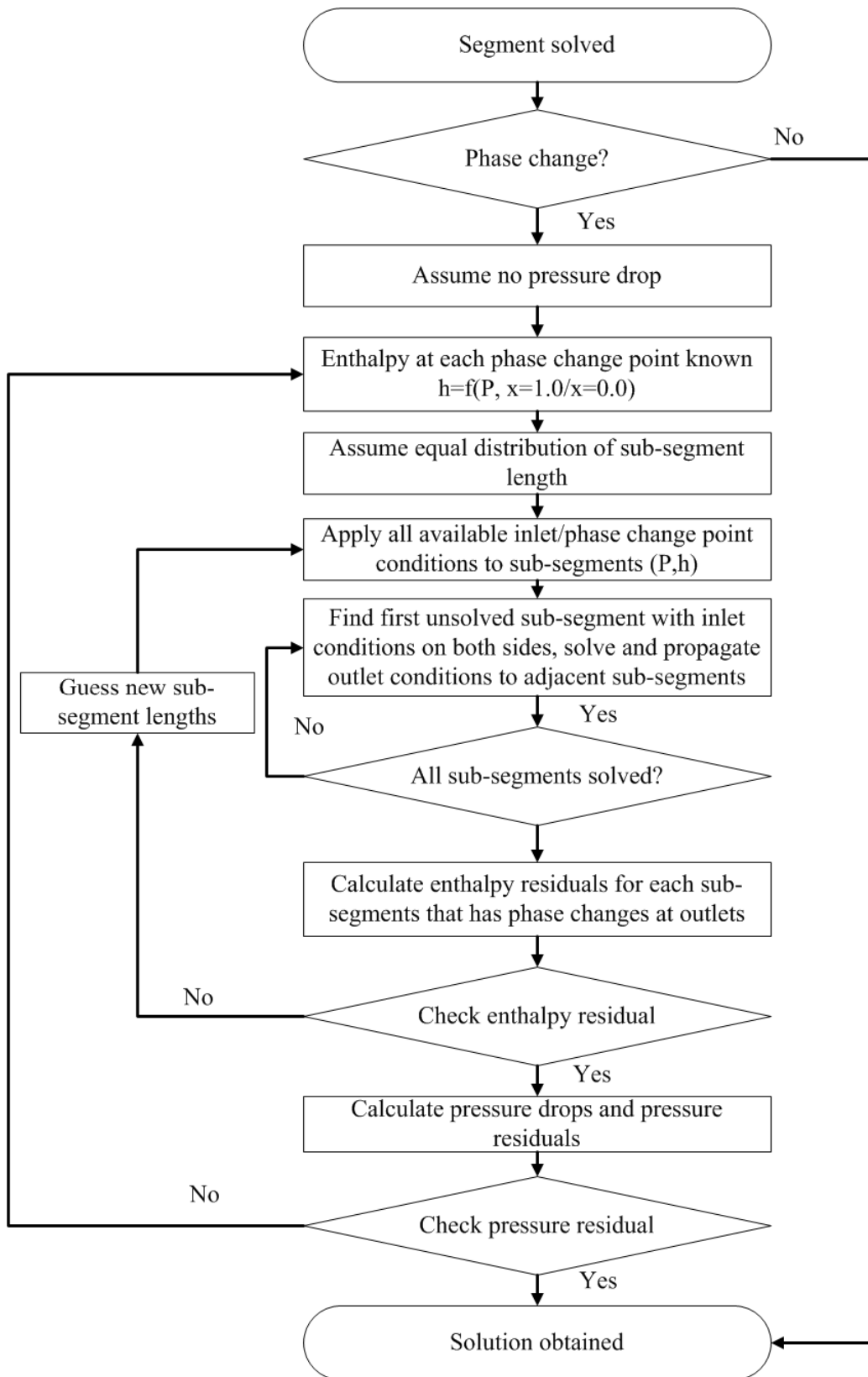


Figure 6-6 Segment subdivision method

## 6.2 Study on Segment Insertion/Sub-division Methods

In this section, a study is presented to evaluate the effect of the different segment-insertion methods and the effect of the number of segments. A water-to-refrigerant smooth tube CHX is selected to compare the performance of various segment insertion/sub-division techniques. Inlet conditions, geometric parameters and correlations selected for this study are tabulated in Table 6-1. The CHX is simulated with both parallel flow and counter flow configurations. Water flows through the inner tube and the evaporating refrigerant flows through the annulus. The refrigerant inlet is two-phase and the outlet is expected to be superheated vapor.

**Table 6-1 Parameters of water-to-refrigerant CHX**

<b>Parameter</b>	<b>Value</b>
Tube length (m)	5
Tube surface type	Smooth
Inner tube outer diameter(mm)	16.9
Inner tube wall thickness(mm)	2
Inner tube refrigerant	water
Inner tube inlet pressure (bar)	1.3
Inner tube inlet temperature (K)	312.2
Inner tube mass flow rate (g/s)	40
Outer tube outer diameter(mm)	30.9
Outer tube wall thickness(mm)	1
Outer tube refrigerant	R134a
Outer tube inlet pressure (bar)	3.5
Outer tube inlet quality (K)	0.8
Outer tube mass flow rate (g/s)	20
Single phase HTC correlation	Dittus & Boelter (1985)
Single phase DP correlation	Churchill (1977)
Two-phase HTC correlation	Jung & Radermacher (1989a)
Two-phase DP correlation	Jung & Radermacher (1989b)

Firstly, a sensitivity study on the number of segments is conducted in order to find the reference heat load for the parallel flow case. Segment insertion method is not applied in this calculation. The sensitivity study result is shown in Figure 6-7. Note that

the scale on the Y-axis has a very narrow range. The heat loads for the number of segments greater than 100 have a standard deviation of 0.04W. Thus, average heat load of this region is selected as the reference heat load for further investigations. To compare different segment insertion techniques, the initial number of segments was varied from 10 to 30. The initial number of segments matters, because a higher number of initial segments will have a more accurate prediction and location of phase change point during initial iterations. Figure 6-8 shows the comparison of various methods in terms of heat load deviations as compared to the reference heat load. The three methods yield an average deviation lower than 0.13%. Figure 6-9 presents the normalized computational time based on the calculation speed of 200 segment baseline case with no segment insertion. Amongst the three methods, the approximated-segment insertion method requires the least computational effort as shown in Figure 9. We note that these deviations are relatively minor for this parallel flow case, compared to those for the counter flow case, discussed next.

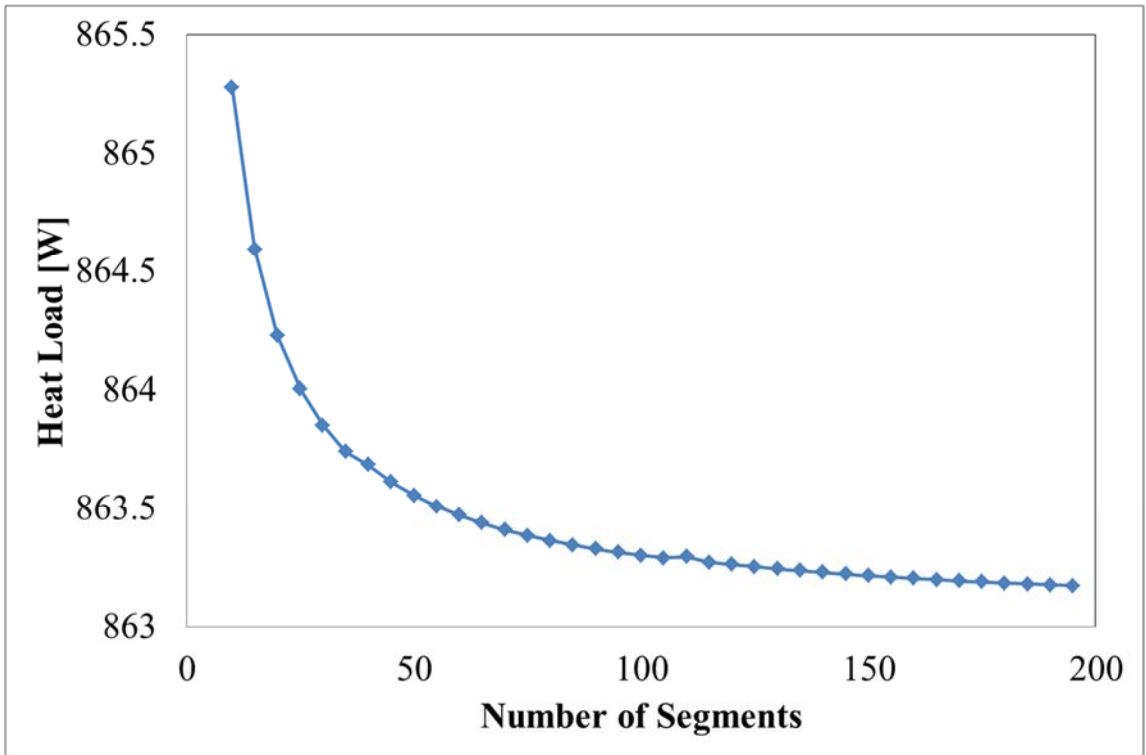


Figure 6-7 Sensitivity study of heat load on number of segments, parallel flow case (No segment insertion/subdivision)

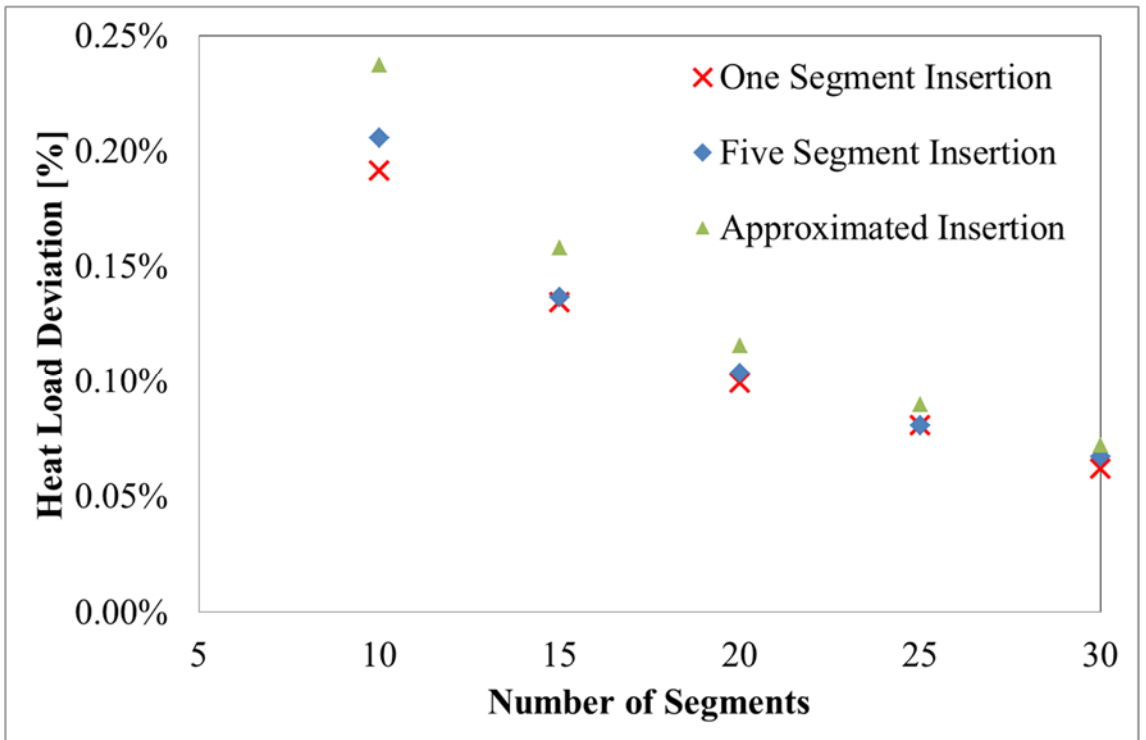
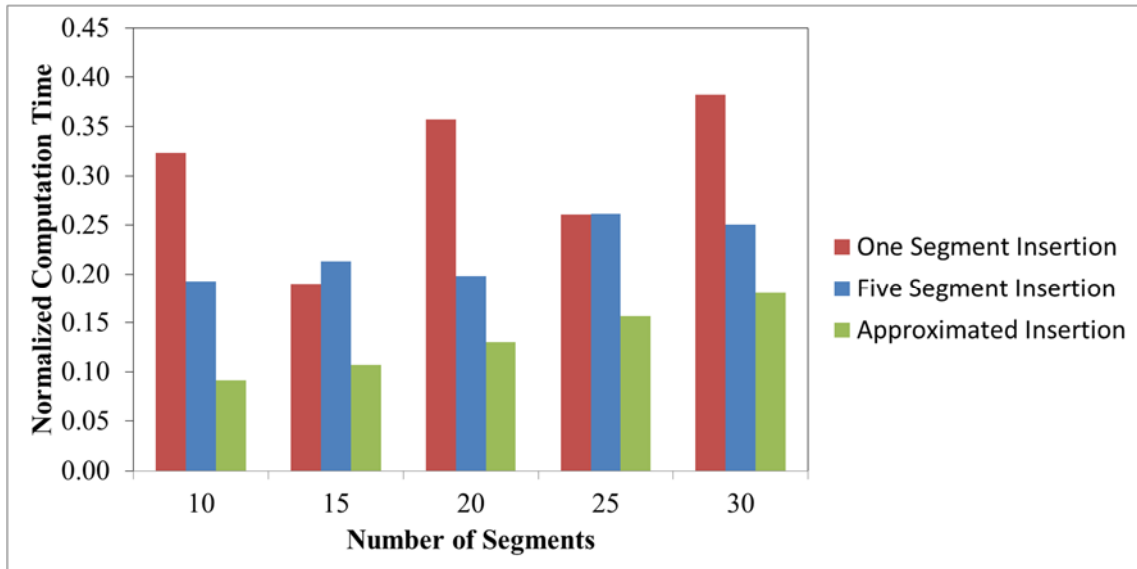


Figure 6-8 Comparison of segment insertion methods on heat load deviations, parallel flow case



**Figure 6-9 Comparison of segment insertion methods on computation time, parallel flow case**

The previous sensitivity study is repeated for the case of a counter-flow heat exchanger and the results are shown in Figure 6-10. All the segment insertion/subdivision functions are disabled at first and the average of the heat load for number of segments from 100 to 200 is selected as the reference heat load. From Figure 6-10, several jumps are observed when increasing the number of segments. This is due to the fact that different number of segments would result in different phase distribution along the heat exchanger when the model is not forced to find the phase change point. That is why segment insertion/sub-division is necessary in such a detailed model in order to obtain consistent and accurate results.

As shown in Figure 6-11, segment subdivision method is superior to the approximated insertion method, but has larger deviations compared to five segments insertion method and one segment insertion methods. The computational costs presented in Figure 6-12 are normalized based on 200 segment baseline case with no segment insertion or sub-division. Segment subdivision method is computationally

more expensive than the other methods. This is mainly due to the fact that segment sub-division method calculates a single segment with phase change iteratively (i.e., another iteration within a segment). At the same time, all the boundary conditions for each segment keep changing at the solver level iterations. Thus, the overall calculation time with segment sub-division is more than other insertion methods. However, as the geometric parameters, inlet conditions and flow configurations differ depending upon different applications, one of these methods can be chosen to achieve the best computational efficiency and accuracy under various conditions. Overall, five segment insertion method costs least amount of time.

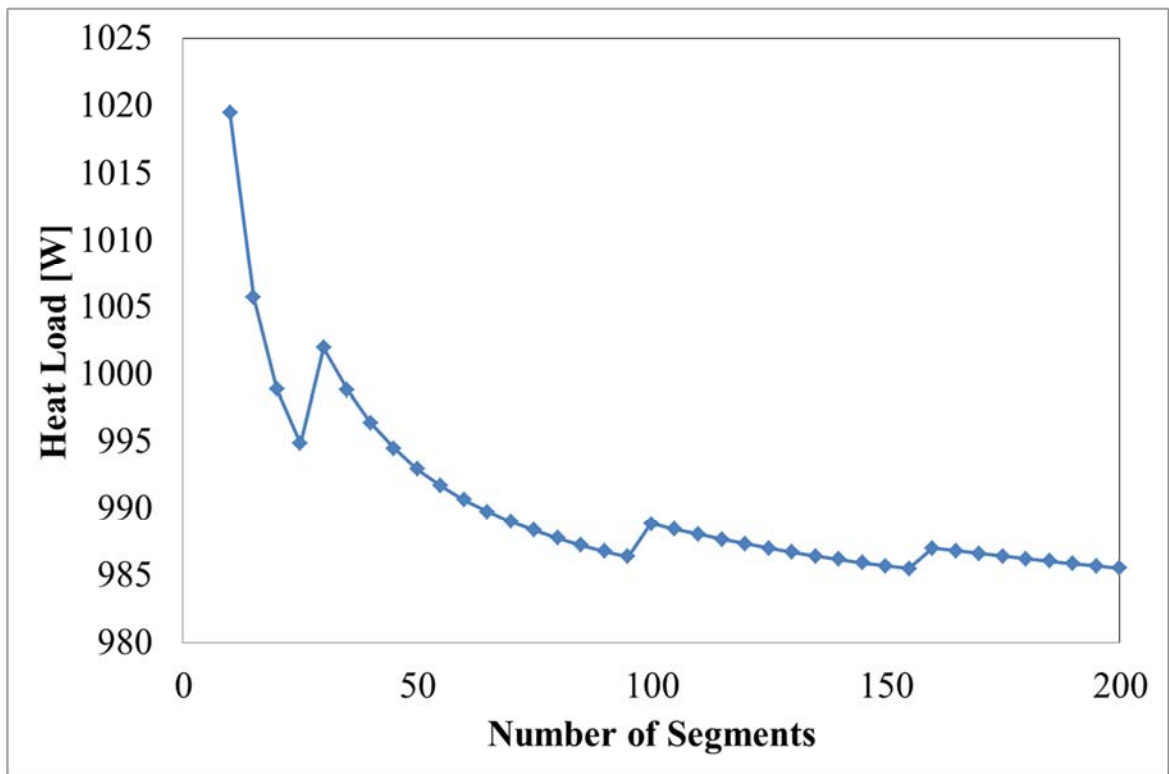


**Figure 6-10 Sensitivity study of heat load on number of segments, counter flow case (No segment insertion/subdivision)**

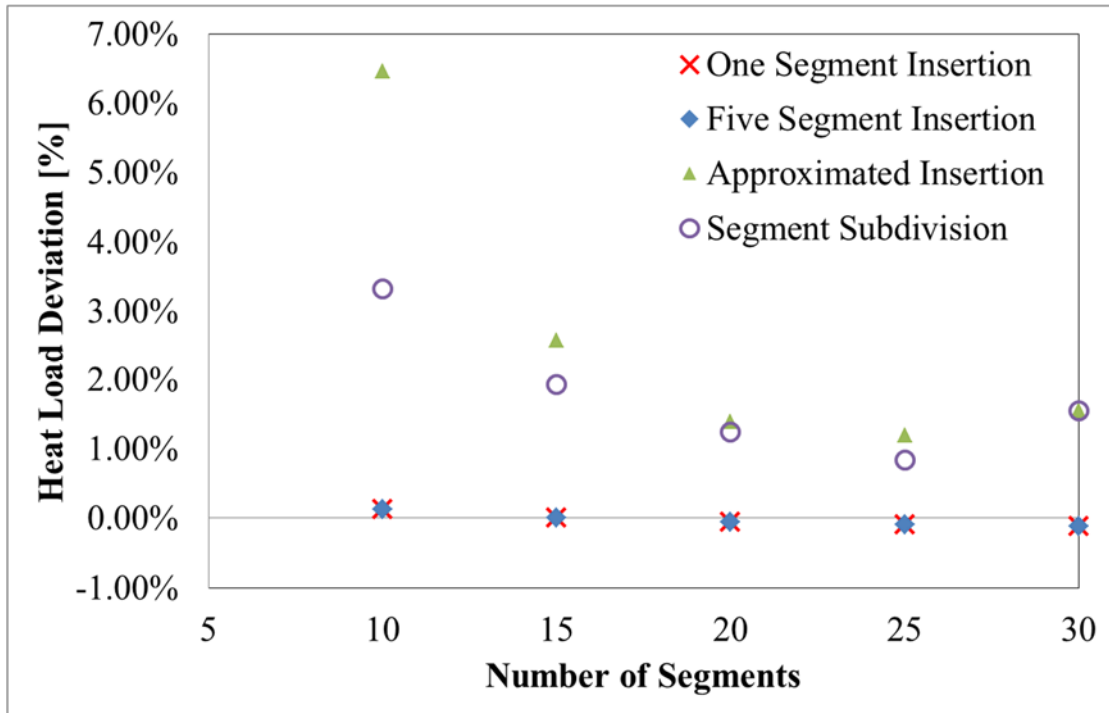


Figure 6-11 Comparison of segment insertion/subdivision methods on heat load deviations, counter flow case

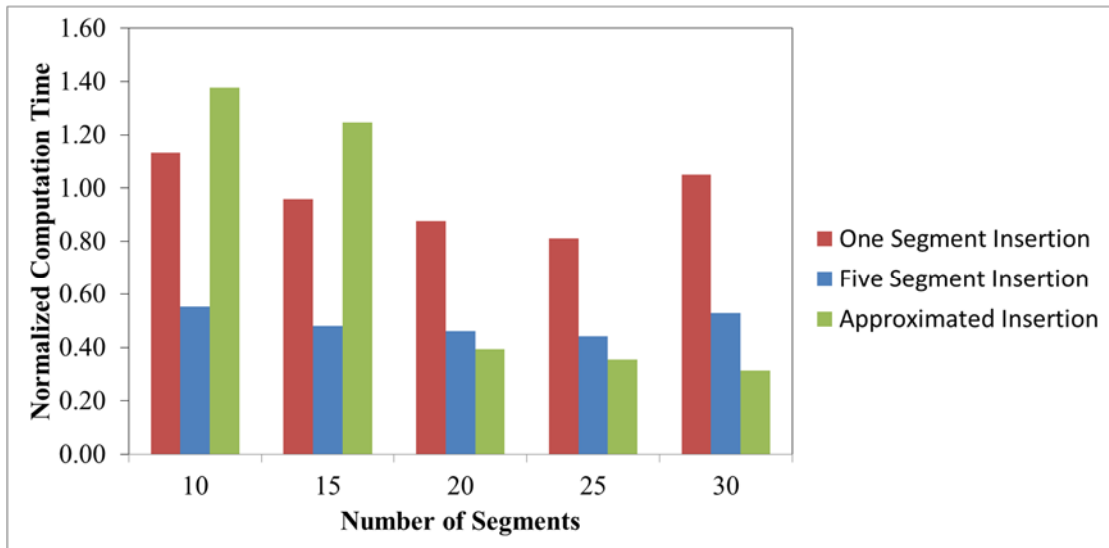


Figure 6-12 Comparison of segment insertion methods on computation time, counter flow case

### 6.3 Two-Phase Fluted Tube Annuli Correlation

As stated previously, there are no correlations in the open literature for calculating two-phase heat transfer coefficient and pressure drop for flow in fluted tube

CHX. Previous study on single phase heat transfer and pressure drop characteristics on fluted tube stated that both heat transfer and frictional loss increase significantly as compared to smooth tube surface. The enhancement factor ranges from 1.1 to 20. In this case, it is not practical to simulate a fluted tube CHX by simply using enhancement factors. Reviewing the popular empirical two-phase correlations, it is found that condensation heat transfer correlation by Shah (1979), boiling heat transfer correlation by Kandlikar (1991) and the two-phase pressure drop correlation by Friedel (1979) have one common basis in the correlation formulation. These empirical correlations apply a two-phase multiplier on the single phase heat transfer and friction terms to calculate the corresponding two-phase heat transfer coefficient and friction factor respectively.

In these correlations, the single phase heat transfer coefficient (or pressure drop) equation is related to the tube geometry while two-phase multipliers are calculated based on fluid quality and other thermophysical properties. The single phase fluted tube heat transfer and pressure drop correlations are available in Arnold *et al.* (1993) and the two-phase multipliers are only a function of the fluid properties and not related to any geometric parameters. Based on these facts, the authors propose to apply two-phase multipliers developed by Shah (1979), Kandlikar (1991) and Friedel (1979) over the single phase correlations provided in Arnold *et al.* (1993). For most of the CHXs in HVAC&R applications such as condenser or evaporator, two-phase refrigerant flows on the annulus side. In this paper, based on the two-phase multipliers and fluted tube single phase flow correlations in open literature, the authors propose a condensation heat transfer correlation formulation, an evaporation heat transfer correlation

formulation and a two-phase pressure drop correlation formulation for the flow in fluted tube annuli.

### 6.3.1.1 Fluted tube geometry

Several parameters are introduced here in order to describe the geometric characteristics of fluted type tube. Firstly, the volumetric diameter of inner tube is defined as the diameter that leads to the actual cross-section area using the following equation for circular tube.

$$D_{vi} = \sqrt{\frac{4V}{\pi L}} \quad (6-14)$$

While the inner volumetric diameter is obtained, outer volumetric diameter can be calculated as

$$D_{vo} = D_{vi} + 2\delta \quad (6-15)$$

The radius ratio is then defined as the ratio of outer volumetric diameter to the smooth outer tube inner diameter.

$$r^* = \frac{D_{vo}}{D_{o,i}} \quad (6-16)$$

The annulus side hydraulic diameter is defined as the difference between smooth outer tube inner diameter and outer volumetric diameter of inner fluted tube.

$$Dh = D_{o,i} - D_{vo} \quad (6-17)$$

Effective flow area is calculated as

$$A_{eff} = \frac{4}{\pi} (D_{o,i}^2 - D_{vi}^2) \quad (6-18)$$

The helix angle of the fluted is defined as follows:

$$\theta = \arctan\left(\frac{\pi D_{vo}}{N_s p}\right) \quad (6-19)$$

Non-dimensional forms of flute depth and flute pitch are applied by dividing by outer volumetric diameter. The helix angle is divided by 90° in order to be dimensionless.

### 6.3.1.2 Two-phase pressure drop correlation

According to Arnold *et al.* (1993), single phase friction factor term for annulus tube can be expressed as follows:

$$f_{lo} = \frac{96r^{*0.035}}{Re_{lo}} \left(1 + 101.7 Re_{lo}^{0.52} e^{*1.65+2\theta^*} r^{*5.77}\right) \quad Re_{lo} \leq 800 \quad (6-20)$$

$$f_{lo} = 4 \left[ 1.7372 \ln\left(\frac{Re_{lo}}{1.964 \ln(Re_{lo}) - 3.8215}\right) \right]^{-2} (1 + 0.0925r^*) e_f \quad (6-21)$$

$$800 \leq Re_{lo} \leq 40,000$$

Where

$$e_l = \left(1 + 222 Re_{lo}^{0.09} e^{*2.4} p^{*-0.49} \theta^{*-0.38} r^{*2.22}\right) \quad (6-22)$$

Here  $Re_{lo}$  is defined as Reynolds number assuming the flow is all in liquid phase.

$$Re_{lo} = \frac{G \cdot D_h}{\mu_l} \quad (6-23)$$

From this point, single phase pressure loss term can be obtained.

$$DP_{lo} = \frac{f_{lo} L \rho u^2}{2D_h} \quad (6-24)$$

Friedel (1979) proposed the formulation of two-phase pressure drop multiplier

as

$$\varphi_{lo}^2 = E + \frac{3.24FH}{Fr^{0.045}We^{0.035}} \quad (6-25)$$

Friedel (1979) defined the associated parameters (E, F and H) in above equation as follows

$$E = (1+x)^2 + x^2 \frac{\rho_l}{\rho_g} \frac{f_g}{f_l} \quad (6-26)$$

Here  $f_g$  is calculated based on Equation (6-27) and (6-28) using  $Re_v$ .

$$F = x^{0.78} (1+x)^{0.24} \quad (6-27)$$

$$H = \left( \frac{\rho_l}{\rho_g} \right)^{0.91} \left( \frac{\mu_g}{\mu_l} \right)^{0.19} \left( 1 - \frac{\mu_g}{\mu_l} \right)^{0.7} \quad (6-28)$$

Froude number and Weber number (Carey, 2008) can be obtained by the following equations

$$Fr = \frac{G^2}{gD_h \rho_{tp}^2} \quad (6-29)$$

$$We = \frac{G^2}{gD_h \rho_{tp}^2} \quad (6-30)$$

Finally, the proposed two-phase annulus pressure drop correlation for the fluted tube is represented as follows:

$$DP_{tp} = \varphi_{lo} * DP_{lo} \quad (6-31)$$

### 6.3.1.3 Two-phase heat transfer correlation

The liquid phase heat transfer coefficient for both condensation and boiling correlations are calculated based on Arnold *et al.* (1993). First, the liquid phase Nusselt number is evaluated using the following equation

$$Nu_{lo} = \left[ \frac{\frac{f_{lo}}{8} RePr}{1 + 9.77 \sqrt{\frac{f_{lo}}{8}} \left( P_r^{\frac{2}{3}} - 1 \right)} \right] \left( Re_{lo}^{-0.20} e^{*-0.32} p^{*-0.28} r^{*-1.64} \right) \quad (6-32)$$

$800 \leq Re_{lo} \leq 40,000$

Then the corresponding single phase heat transfer coefficient can be calculated as:

$$\alpha_{lo} = \frac{Nu_{lo} k_l}{D_h} \quad (6-33)$$

The condensation heat transfer multiplier proposed by Shah (1979) is:

$$C_{cond} = (1-x)^{0.8} + \frac{3.8x^{3.76} (1-x)^{0.4}}{\left( \frac{P}{P_{cr}} \right)^{0.38}} \quad (6-34)$$

Thus, the fluted tube annulus condensation heat transfer coefficient correlation can be obtained as follows

$$\alpha_{cond} = C_{cond} \alpha_{lo} \quad (6-35)$$

Kandlikar (1991) presented a general smooth tube correlation where boiling heat transfer coefficient is determined by the larger value between heat transfer coefficient in nucleate boiling dominant region and convective boiling dominant region.

$$\alpha_{evap} = \max(\alpha_{NBD}, \alpha_{CBD}) \quad (6-36)$$

The formulations of nucleate boiling and convective boiling heat transfer coefficients are given as

$$\alpha_{NBD} = 0.6683 Co^{-0.2} (1-x)^{0.8} \alpha_{lo} + 1058 Bo^{0.7} (1-x)^{0.8} F_{fl} \alpha_{lo} \quad (6-37)$$

$$\alpha_{CBD} = 1.136 Co^{-0.9} (1-x)^{0.8} \alpha_{lo} + 667.2 Bo^{0.7} (1-x)^{0.8} F_{fl} \alpha_{lo} \quad (6-38)$$

Here,  $Co$  is convection number,  $Bo$  is boiling number.

$$Co = (1-x)^{0.8} \left( \frac{\rho_g}{\rho_l} \right)^{0.5} \quad (6-39)$$

$$Bo = \frac{q}{Gh_{fg}} \quad (6-40)$$

$F_{fl}$  is the fluid-dependent parameter provided by Kandlikar (1991). A list of available fluids and their corresponding fluid-dependent parameters are summarized in Table 6-2.  $F_{fl} = 1$  is applied for all other fluids.

**Table 6-2 Fluid-dependent parameter based on Kandlikar (1991)**

<b>Fluid</b>	<b>Value</b>
Water	1.00
R-11	1.30
R12	1.50
R13B1	1.31
R22	2.20
R113	1.30
R114	1.24
R134a	1.63
R152a	1.10

#### **6.4 Experimental Validation of Numerical Model and Proposed Correlation Formulations**

A fluted tube brine-to-refrigerant CHX was tested as a component of a heat pump system. The dual mode system is tested for both cooling and heating cases. The energy balance in cooling mode test was within three percent. The CHX is serving as the condenser in the cooling condition, and as the evaporator under heating condition. The geometric parameters are given in Table 6-3. Test conditions are as shown in Table 6-4. It should be noted that the evaporator cases are not the conventional test conditions. The inlet temperature of the brine is actually lower than that of the refrigerant. However,

significant pressure drop along the outer tube decreases the saturation temperature below the temperature of the brine and therefore leads to temperature difference between the two working fluids, which leads to evaporation. McElligott (1948) investigated the pressure drop enhancement in helical tube. According to the comparison, the enhancement of pressure drop in helical tube is 10 percent to approximately 100 percent as compared to straight tube. Enhancement factors are applied on the pressure drop correlations in both cases as stated in Table 6-5 while no correction factors are applied over the heat transfer correlations. In total, 15 test points are validated for condenser cases and 15 test points for evaporator cases. Five segment insertion method is used for all validation case as it is proved to be the most accurate and efficient method for counter flow case. Initial number of segment is 20 for all the validation cases.

**Table 6-3 Geometric parameters of brine-to-refrigerant fluted tube CHX**

<b>Parameter</b>	<b>Value</b>
Tube length (m)	6.797
Tube surface type	Fluted
Inner tube refrigerant	Methanol-Water (Concentration: 15%, 16% and 17%)
Outer tube refrigerant	R410A
Volume based inner diameter (mm)	28.4
Inner tube wall thickness (mm)	1
Flute depth	6.3
Flute pitch	8
Flute starts	6
Inner tube unit heat transfer area (mm)	173.5
Outer tube outer diameter(mm)	44.4
Outer tube wall thickness(mm)	0.5
Outer tube unit heat transfer area (mm)	183.7

**Table 6-4 Test conditions of brine-to-refrigerant fluted tube CHX**

<b>Parameter</b>	<b>Range</b>
<b>Condenser</b>	
Inner tube inlet temperature (K)	288.1-303.3
Inner tube mass flow rate (g/s)	742.2-987.2
Outer tube inlet pressure (bar)	16.1-24.4
Outer tube inlet temperature (K)	313.4-332.1
Outer tube mass flow rate (g/s)	77.5-110.4
<b>Evaporator</b>	
Inner tube inlet temperature (K)	273.19-293.19
Inner tube mass flow rate (g/s)	736.7-992.1
Outer tube inlet pressure (bar)	20.2-25.8
Outer tube inlet temperature (K)	303.8-310.9
Outer tube mass flow rate (g/s)	48.9-102.4

**Table 6-5 Selected correlations for brine-to-refrigerant fluted tube CHX**

<b>Parameter</b>	<b>Correlation</b>	<b>Enhancement Factor</b>
<b>Single Phase</b>		
Heat transfer	Arnold <i>et al.</i> (1993)	1
Pressure drop	Arnold <i>et al.</i> (1993)	2.0
<b>Two-Phase</b>		
Condensation heat transfer	Proposed condensation correlation	1
Evaporation heat transfer	Proposed evaporation correlation	1
Condensation pressure drop	Proposed two-phase DP correlation	2.0

The comparison between simulation result and experimental data for condenser cases is shown in Figure 6-13 and Figure 6-14. Nearly all the predictions for both heat transfer and pressure drop fall within  $\pm 5\%$  of the experimental data. The validation results for the evaporator case are shown in Figure 6-15 and Figure 6-16. The heat load for most of the test points (12 out of 15) is predicted within  $\pm 5\%$  error. The authors recorded the values of heat transfer resistance components of two-phase segments. For evaporator cases, the two-phase fluid side's heat transfer resistance is 44%~72% of the overall heat transfer resistance. As for condenser cases, this value ranges from 47%~87%. Thus, the annulus side heat transfer resistance is a major component of the

overall heat transfer resistance. Although there are not enough experimental data to validate the proposed two-phase heat transfer correlations themselves, it can be seen that the heat transfer and pressure drop predictions using these correlations are reasonably accurate for simulation and design purposes. In the pressure drop comparison for evaporator cases, most points are within  $\pm 10\%$  of the measured data. As stated previously, the heat transfer potential for the evaporator cases actually come from the pressure drop of annulus side. Thus, if the pressure drop estimation accuracy can be further improved, the heat transfer performance prediction can also be improved.

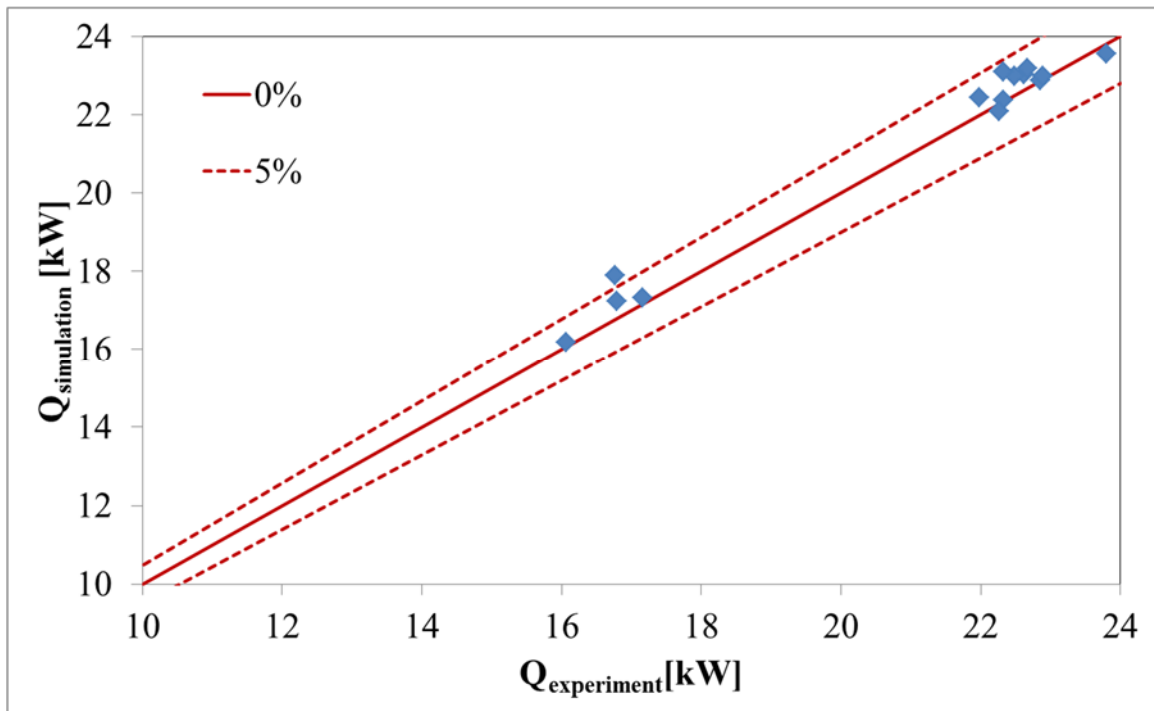


**Figure 6-13 Comparison between simulation and experimental heat load for brine-to-refrigerant condenser**

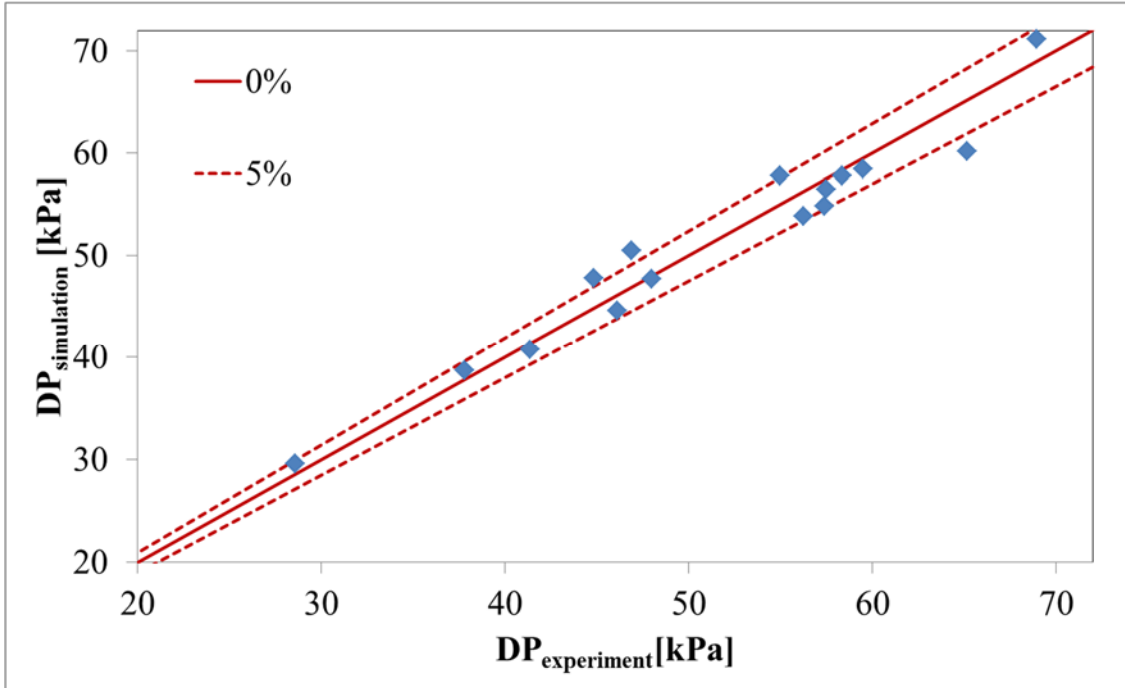


Figure 6-14 Comparison between simulation and experimental pressure drop for brine-to-refrigerant condenser

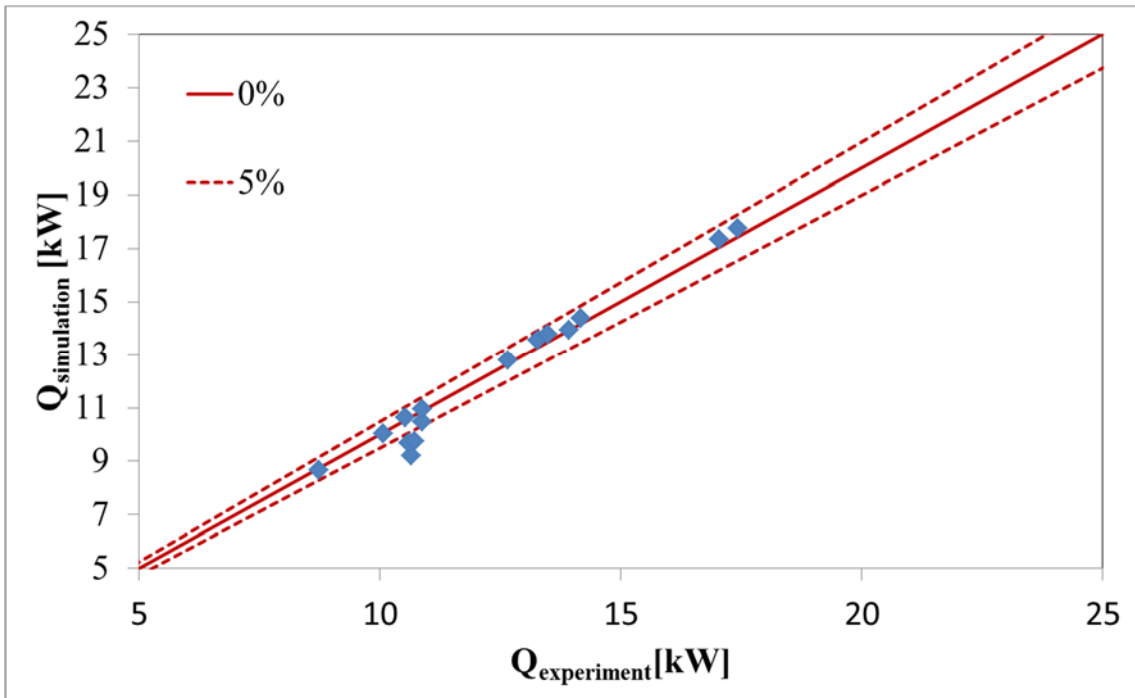
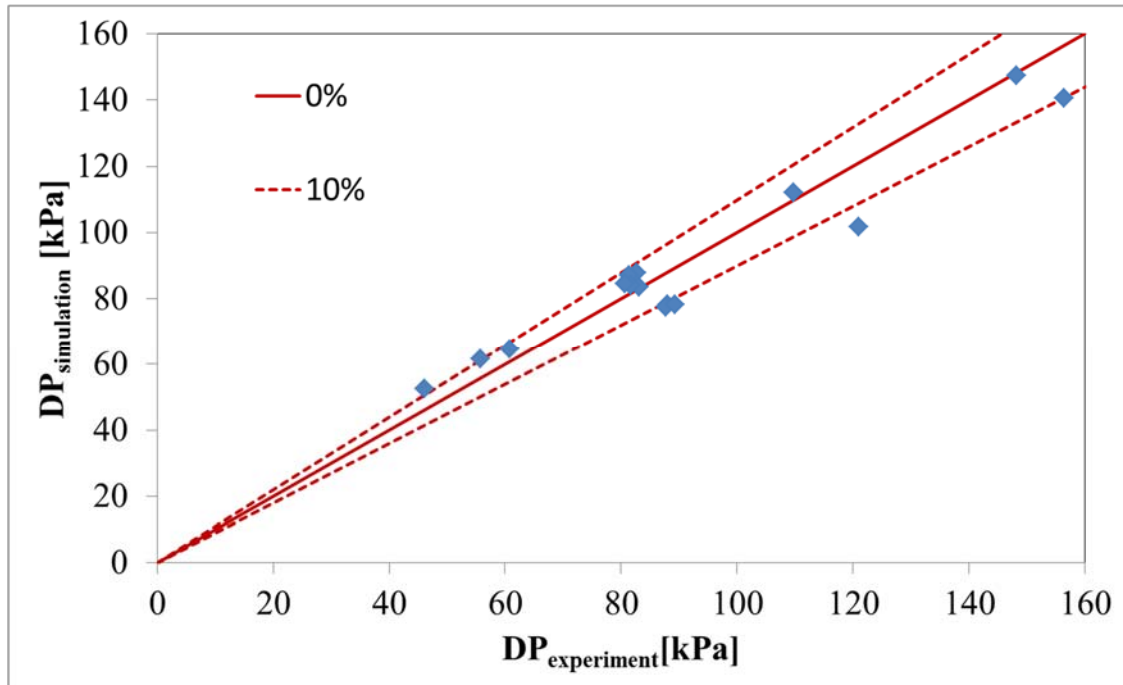


Figure 6-15 Comparison between simulation and experimental heat load for brine-to-refrigerant evaporator



**Figure 6-16 Comparison between simulation and experimental pressure drop for brine-to-refrigerant evaporator**

## 6.5 Summary

A new model was developed for the design and analysis of coaxial heat exchangers with flexible flow configurations, multiple surface types as well as the capability to model simultaneous phase change on both sides. The finite volume model divides the heat exchanger into multiple segments in order to track the fluid property, heat transfer and pressure drop variations due to phase change and heat transfer. The model is capable of handling both single-phase and two-phase flow. Segment insertion and subdivision methods were developed such that the solver can track the exact phase change point. Numerical studies showed that the five-segment-insertion approach worked best. Empirical correlations were implemented along with the modeling effort to predict heat transfer coefficients and pressure drop over different surfaces. Three new correlation modifications are proposed in this paper to fill in the gap of fluted tube

annulus side condensation heat transfer correlation, evaporation heat transfer correlation as well as two-phase pressure drop correlation. The model is validated against experimental data for condenser and evaporator. The validation shows that the model predictions using proposed correlations matched the experimental results very well. The model is able to predict the thermal and hydraulic performance of fluted tube condenser within  $\pm 5\%$ . For fluted tube evaporator, the model's accuracy is within  $\pm 5\%$  for heat load prediction and  $\pm 10\%$  for pressure drop calculation. It should be noted that the heat exchanger model presented in this paper can be generally applied to various coaxial heat exchanger geometries, fluid conditions and flow arrangements. Since the proposed model is dependent upon correlations for local heat transfer and pressure drop calculations, they need to be properly selected in order to accurately simulate the coaxial heat exchangers.

## 7 LIST OF MAJOR CONTRIBUTIONS AND FUTURE WORK

### 7.1 Major Contributions

The major contributions of this research are the development of comprehensive air-to-refrigerant and refrigerant-to-refrigerant heat exchanger models, with novel capabilities. These contributions are summarized below.

1. First-principle microchannel heat exchanger model with the following contributions:

- Allows evaluation of variable geometry microchannel heat exchangers which offer tremendous potential in terms of cost versus performance tradeoff for a given application. This model will help engineers to develop more sophisticated microchannel heat exchangers ultimately resulting in improved systems efficiency and lower cost.
- Accounts for tube-to-tube conduction in heat exchanger core, thereby facilitating the improvement of heat exchanger performance through better geometry design and selective fin cuts
- Allows detailed heat transfer prediction under dry, wet and partially wet surfaces which will allow the users to analyze heat exchanger performance under these conditions
- A new co-simulation approach that allows simulation of complex flow behavior in header while accounting for heat transfer and pressure drop in microchannel tubes, therefore extending the potential of MCHX simulation tools on improving header designs

- Enhanced the understanding of variable geometric impact on air flow mal-distribution
2. Finite-volume coaxial heat exchanger simulation tool:
    - A detailed and comprehensive model that allows the engineer to accurately model coaxial heat exchangers thus pursuing optimum designs
    - Improved prediction of two-phase heat transfer and pressure drop of fluted tube annuli, thus providing confident results for heat exchanger design and system level simulation
  3. Comprehensive experimental validation
    - The proposed work presents the most comprehensive comparison between simulation results and experimental data in open literature, thus confirms the validity of the mathematical models
    - Validated against 247 microchannel heat exchanger data points from 7 data sources, 18 geometries and 8 fluids. The validation includes 4 different variable geometry microchannel heat exchanger for both condenser and evaporator applications
    - 30 fluted tube coaxial heat exchanger data points for both evaporators and condensers validated
  4. Design optimization of variable geometry microchannel heat exchangers
    - The development of the advanced simulation tools enables further expanding the design domain of current heat exchanger designs. Optimization studies based on the proposed model proved the

necessity of the proposed work and can reveal the potential improvement of new generation of heat exchanger designs

## 7.2 List of Publications

The following peer-reviewed journal papers were published or submitted as outcomes of the research conducted in this dissertation.

- 1) L. Huang, V. Aute, R. Radermacher. “A Model for Air-to-Refrigerant Microchannel Condensers with Variable Tube and Fin Geometries”, *International Journal of Refrigeration*, 2014 (40), 269-281
- 2) L. Huang, M.S. Lee, K. Saleh, V. Aute, R. Radermacher. “A Computational Fluid Dynamics and Effectiveness-NTU Based Co-Simulation Approach for Flow Mal-Distribution Analysis in Microchannel Heat Exchanger Headers”, *Applied Thermal Engineering*, 2014 (65), 447-457
- 3) L. Huang, V. Aute, R. Radermacher. “A Finite Volume Coaxial Heat Exchanger Model with Moving Boundaries and Modifications to Correlations for Two-phase Flow in Fluted Annuli”, *International Journal of Refrigeration*, 2014 (40), 11-23
- 4) L. Huang, D. Bacellar, V. Aute, R. Radermacher. “Variable Geometry Microchannel Heat Exchanger Modeling Under Dry, Wet and Partially Wet Surface Conditions Accounting for Tube-to-Tube Heat Conduction”, Submitted to *HVAC&R Research*
- 5) L. Huang, V. Aute, R. Radermacher. “Air flow Distribution and Design Optimization of Variable Geometry Microchannel Heat Exchangers”, Submitted to *HVAC&R Research*

- 6) S. Qian, L. Huang, V. Aute, Y. Hwang, R. Radermacher. “Applicability of Entransy Dissipation Based Thermal Resistance for Design Optimization of Two-Phase Heat Exchangers”, Applied Thermal Engineering, 2013 (55), 140-148

The following peer-reviewed conference papers were published or accepted and resulted from this research conducted in this dissertation.

- 1) L. Huang, V. Aute, R. Radermacher. “A Mass Flow Based Generalized Microchannel Heat Exchanger Model”, 10th IIR Gustav Lorentzen Conference, 2012
- 2) L. Huang, V. Aute, R. Radermacher. “A Generalized Effectiveness-NTU Based Variable Geometry Microchannel Heat Exchanger Model”, International Refrigeration and Air Conditioning Conference at Purdue. Purdue University, West Lafayette, 2012
- 3) L. Huang, V. Aute, R. Radermacher. “Design Optimization of Variable Geometry Microchannel Heat Exchangers”, International Refrigeration and Air Conditioning Conference at Purdue. Purdue University, West Lafayette, 2014
- 4) L. Huang, V. Aute, R. Radermacher. “Refrigerant Property Uncertainty Analysis on Prediction of Heat Transfer Coefficient and Pressure Drop in Heat Exchangers”, International Refrigeration and Air Conditioning Conference at Purdue. Purdue University, West Lafayette, 2014
- 5) L. Huang, D. Bacellar, V. Aute, R. Radermacher. “Fin Performance Analysis for Microchannel Heat Exchangers Under Dry, Wet and Partial

Wet Conditions”, International Refrigeration and Air Conditioning Conference at Purdue. Purdue University, West Lafayette, 2014

- 6) L. Huang, V. Aute, R. Radermacher. “Design Optimization of Microchannel Heat Exchangers with Variable Geometry for Natural Refrigerants”, 11th IIR Gustav Lorentzen Conference, 2014
- 7) L. Huang, V. Aute, R. Radermacher. “A Survey of Optimization Formulations and Techniques for the Design of Heat Exchangers Using Lower GWP Refrigerants”, Accepted to ASHRAE 2015 Winter Conference
- 8) S. Qian, L. Huang, V. Aute, Y. Hwang, R. Radermacher. “Effectiveness of Entransy Dissipation Metric and Entropy Generation Units in The Design of Fin-Tube Heat Exchangers”, International Refrigeration and Air Conditioning Conference at Purdue. Purdue University, West Lafayette, 2012
- 9) J. Ling, S. Qian, S. Li, L. Huang, Y. Hwang, R. Radermacher. “The Winner Design of the Max Tech and Beyond Competition: A High-efficient Residential Air-conditioning System”, ASHRAE Winter Conf. 2013

### **7.3 Future Work**

The research work presented in this thesis represents the cutting edge modeling of microchannel heat exchangers and coaxial heat exchangers. The following research task could further improve the understanding of heat exchanger designs

- Analytical model for two-phase refrigerant distribution in microchannel heat exchanger headers. This will allow fast analysis of two-phase refrigerant maldistribution effect, especially for evaporators.
- Ability to account for liquid accumulation in condenser outlet headers. This will provide the researchers ability to analysis the performance degradation due to liquid back flow for condensers.
- Conduct further numerical analysis and experimental validation for two-phase flow within fluted inner tube. Such research would further expand the usability of coaxial heat exchanger model on applications with two-phase refrigerant within the inner tube.

## REFERENCES

- [1] Abdelaziz, O., V. Aute, S. Azarm, and R. Radermacher. 2010. "Approximation-assisted optimization for novel compact heat exchanger designs." *HVAC&R Research* 16: 707-728.
- [2] Aganda, A.A., J.E.R. Coney, and C.G.W. Sheppard. 200. "Airflow maldistribution and the performance of a packaged air conditioning unit evaporator." *Applied Thermal Engineering* 20: 515-528.
- [3] ANSYS, Inc. 2006. "Fluent version 6.3.26. ."
- [4] ANSYS, Inc. 2011. "Gambit version 2.3.16."
- [5] Arnold, J.A., S. Garimella, and R. N. Christenen. 1993. "A Manual For Heat Exchanger Design Using Spirally Fluted Tubes."
- [6] Asinari, P., L Cecchinato, and Fornasieri. 2004. "Effects of thermal conduction in microchannel gas coolers for carbon dioxide." *International Journal of Refrigeration* 27: 577-586.
- [7] Aute, V., and R. Radermacher. n.d. *TSIOP-Thermal systems integration and optimization platform, IS-2005-062*. Platform documentation code, University of Maryland.
- [8] Baclic, B. S., D. P. Sekulic, and D. Gvozdenac. 1982. "Performances of three-fluid single pass crossflow heat exchanger." *Heat transfer* 40 (3): 167-172.
- [9] Bankoff, S.G. 1960. "On the mechanism of subcooled nucleate boiling." *Chemical Engineering Progress Symposium Series* 57 (32): 156-172.
- [10] Brix, W., M.R. Kærn, and B. Elmegaard. 2010. "Modelling distribution of evaporating CO<sub>2</sub> in parallel minichannels." *International Journal of Refrigeration* 33: 1086-1094.
- [11] Brix, W., M.R. Kærn, and B. Elmegaard. 2009. "Modelling refrigerant distribution in microchannel." *International Journal of Refrigeration* 32: 1736-1743.
- [12] Broyden, C.G. 1965. "A class of methods for solving nonlinear simultaneous equations." *Mathematics of Computation* 19 : 577–593.
- [13] Byun, H.W., and N.H. Kim. 2011. "Refrigerant distribution in a parallel flow heat exchanger having vertical headers and heated horizontal tubes." *Experimental Thermal Fluid Science* 35: 920-930.

- [14] Carey, V.P. 2008. *Liquid-vapor phase-change phenomena*. 2nd. New York: Taylor & Francis Group.
- [15] Carey, V.P. 2008. *Liquid-vapor phase-change phenomena*. 2nd. New York: Taylor & Francis Group, LLC.
- [16] Castiglia, F., and M. Giardina. 2002. "Modelling two-phase flow discharge through lateral branches in large horizontal pipes with stratified flow." Alba (Cueno), Italy September: Eight International Conf. Multiphase flow in Industrial Plants.
- [17] Chang, Y.J., and C.C. Wang. 1997. "A generalized heat transfer correlation for louver fin geometry." *International Journal of Heat and Mass Transfer* 40: 533-544.
- [18] Chen, J.C. 1963. "A correlation for boiling heat transfer to saturated fluids in convective flow." Boston: 6th National Heat Transfer Conference.
- [19] Chiou, J.P. 1978. "The effect of longitudinal heat conduction on crossflow heat exchanger." *ASHRAE Transaction* 100: 346-351.
- [20] Chisholm, D. 1983. *Two-phase flow in pipelines and heat exchangers*. Longman Higher Education.
- [21] Cho, H., K. Cho, and Y.S. Kim. 2003. "Mass flow rate distribution and phase separation of R22 in multi-microchannel tubes under adiabatic condition." ASME Conference Proceeding.
- [22] Churchill, S.W. 1977. "Frictional equation spans all fluid flow regimes." *Chemical Engineering* 84: 91-92.
- [23] Dittus, F.W., and L.M.K Boelter. 1985. "Heat Transfer in Automobile Radiators of the Tubular Type." *International Communications in Heat and Mass Transfer* 12 (1): 3-22.
- [24] Domanski, P.A. 2003. *EVAP-COND, simulation models for finned tube heat exchangers*. Gaithersburg, MD, USA: National Institute of Standards and Technology Building and Fire Research Laboratory.
- [25] Eisele, M. 2012. "Transient performance evaluation of automotive secondary loop systems." Ph.D Thesis, University of Maryland, College Park.
- [26] Fei, P., and P.S. Hrnjak. 2004. "Adiabatic developing two-phase refrigerant flow in manifolds of heat exchangers in manifolds of heat exchangers." Technical Report 225, ACRC, University of Illinois.

- [27] Friedel, L. 1979. "Improved friction pressure drop correlations for horizontal and vertical two phase pipe flow." Ispra, Italy: . European Two Phase Flow Group Meeting.
- [28] Fronk, B.M., and S. Garimella. 2010. "Water-coupled carbon dioxide microchannel gas cooler for heat pump water heaters: Part II – Model development and validation." *International Journal of Refrigeration* 34: 17-28.
- [29] García-Cascales, J.R., F. Vera-García, J. González-Maciá, J.M. Corberán-Salvador, M.W Johnson, and G.T Kohler. 2010. "Compact heat exchangers modeling: condensation." *International Journal of Refrigeration* 33: 135-147.
- [30] Garimella, S., and R. N. Christensen. 1995a. "Heat Transfer and Pressure Drop Characteristics of Spirally Fluted Annuli, Part I: Hydrodynamics." *Journal of Heat Transfer* 117: 54-60.
- [31] Garimella, S., and R. N. Christensen. 1995b. "Heat Transfer and Pressure Drop Characteristics of Spirally Fluted Annuli, Part II: Heat Transfer." *Journal of Heat Transfer* 117: 61-68.
- [32] Garimella, S., and R. N. Christensen. 1997. "Performance Evaluation of Spirally Fluted Annuli: Geometry and Flow Regime Effects." *Heat Transfer Engineering* 18 (1): 34-46.
- [33] Garimella, S., R. N. Christensen, M. A. Garrabrant, and M. E. Boos. 1990. "An Experimental Investigation of Heat Transfer Characteristics of Spirally-Fluted Tubes in Confined Crossflow." *ASHRAE Transactions* 96 (2): 450-455.
- [34] Gnielinski, V. 1976. "New equations for heat and mass transfer in turbulent pipe and channel flow." *Chemical Engineering* 16: 359-368.
- [35] Gossard, J.J., X. Han, M. Ramalingam, and A.D. Sommers. 2013. "Investigating the thermal-hydraulic performance of new refrigerant mixtures through numerical simulation of minichannel and microchannel evaporators." *Applied Thermal Engineering* 50: 1291-1298.
- [36] Gregorig, R. 1954. "Film Condensation on Finely Waved Surfaces with Consideration of Surface Tension." *Zeitschrift fur Angewandte Math, und Physik* 5: 36.
- [37] Habib, M.A., R. Ben-Mansour, S. A. M. Said, J. J. Al-Bagawi, and K. M. Al-Mansour. 2008. "Correlations of flow mal-distribution parameters in an air cooled heat exchanger." *International Journal for Numerical Methods in Fluids* 56: 143-165.

- [38] Herman, P.J. 1962. "Simulation of steam generation in a heat exchanger." *Institute of Ratio Engineers Transactions on Electronic Computers* 53-57.
- [39] Heun, M.K., and R.R. Crawford. 1994. "Longitudinal fin conduction in multipass cross-counterflow finned-tube heat exchangers." *ASHRAE Transaction* 100 (11): 382-389.
- [40] Hoehne, M. R, and P. S. Hrnjak. 2004. *Charge minimization in systems and components using hydrocarbons as a refrigerants*. ACRC TR-224.
- [41] Hrnjak, P.S. 2004. "Developing adiabatic two phase flow in headers—distribution issue in parallel flow microchannel heat exchangers." *Heat Transfer Engineering* 25: 61-68.
- [42] Hrnjak., Litch. A. D and. 1999. *Condensation of ammonia in microchannel heat exchangers*. ACRC CR-22.
- [43] Huang, L., V. Aute, and R. Radermacher. 2014. "Uncertainty analysis on prediction of heat transfer coefficient and pressure drop in heat Exchangers due to refrigerant property prediction error." *International Conference of Air Conditioning and Refrigeration*. Purdue University.
- [44] Hwang, Y., D.H. Jin, and R. Radermacher. 2007. "Refrigerant distribution in minichannel Evaporator Manifolds Minichannel Evaporator Manifolds." *HVAC&R Research* 13: 543-555.
- [45] Incropera, F.P., D.P. Dewitt, T.L. Bergman, and Lavine. A.S. 2011. *Fundamental of heat and mass transfer*. Wiley.
- [46] Jiang, H. 2003. *Development of a simulation and optimization tool for heat exchanger design*. Ph.D. Thesis, University of Maryland, College Park.
- [47] Jiang, H., V. Aute, and R. Radermacher. 2006. "CoilDesigner: A general-purpose simulation and design tool for air-to-refrigerant heat exchangers." *International Journal of Refrigeration* 29: 601-610.
- [48] Jiji, L.M., and J.A. Clark. 1964. "Bubble boundary layer and temperature profile for forced convective boiling in channel flow." *Journal of Heat Transfer* 76: 50-58.
- [49] Jin, D.H. 2006. *Investigation on refrigerant distribution in evaporator manifolds (Ph.D Thesis)*. University of Maryland, College Park.
- [50] Jin, J., J. Chen, and Z. Chen. 2011. "Development and validation of a microchannel evaporator model for a CO<sub>2</sub> air-conditioning system." *Applied Thermal Engineering* 31: 137-146.

- [51] Jung, D.S., and R. Radermacher. 1989. "A study of flow boiling heat transfer with refrigerant mixtures." *International Journal of Heat and Mass Transfer* 32 (9): 1751-1764.
- [52] Jung, D.S., and R. Radermacher. 1989. "Prediction of pressure drop during horizontal annular flow boiling of pure and mixed refrigerants." *International Journal of Heat and Mass Transfer* 21 (12): 2435-2446.
- [53] Kandlikar, S.G. 1991. "A Model for Correlating Flow Boiling Heat Transfer in Augmented Tubes and Compact Evaporators." *Transactions of the ASME, Journal of Heat Transfer* 113: 966-972.
- [54] Kandlikar, S.G. 2007. "A roadmap for implementing microchannels in refrigeration and air-conditioning systems-current status and future directions." *Heat Transfer Engineering* 28 (12): 973-985.
- [55] Kays, W.M., and A.L. London. 1984. *Compact heat exchangers*. New York: McGraw-Hill.
- [56] Kiefer, J. 1953. "Sequential minimax search for a maximum." *Proceedings of the American Mathematical Society* 4 (3): 502-506.
- [57] Kim, J.H., J.E. Braun, and E.A. Groll. 2009. "A hybrid method for refrigerant flow balancing in multi-circuit evaporators: Upstream versus downstream flow control." *International Journal of Refrigeration* 32: 271-282.
- [58] Kim, M.H, and Bullard. 2001. "Development of a microchannel evaporator model for a CO<sub>2</sub> air-conditioning system." *Energy* 26: 931-948.
- [59] Kirby, E.S., C.W. Bullard, and W.E.D Dunn. 1988. "Effect of airflow nonuniformity on evaporator performance." *ASHRAE Transactions* 104 (2): 755-762.
- [60] Kondou, C., and P. Hrnjak. 2010. "Heat rejection from R744 near the critical point." West Lafayette, IN: International Refrigeration and Air Conditioning Conference.
- [61] —. 2012. "Heat rejection in condensers: desuperheating, condensation in superheated region and two phase zone." West Lafayette, IN: International Refrigeration and Air Conditioning Conference.
- [62] Kou, G.S., and P. Yuan. 2007. "The effect of longitudinal wall conduction on the crossflow heat exchanger with nonuniform inlet temperatures." *Heat Transfer Engineering* 19 (2): 54-63.
- [63] Kumar, V., S. Saini, Sharma M., and K. D. P. Nigam. 2006. "Pressure drop and heat transfer study in tube-in-tube helical heat exchanger." *Chemical Engineering Science* 61: 4403-4416.

- [64] Kutateladze, S.S. 1961. "Boiling heat transfer." *International Journal of Heat and Mass Transfer* 4: 31-45.
- [65] Lalot, S., P. Florent, S.K. Lang, and A.E. Bergles. 1999. "Flow mal-distribution in heat exchangers." *Applied Thermal Engineering* 19: 847-863.
- [66] Lee, M.S., V. Aute, and R. Radermacher. 2012. "A review on direct two-phase, phase change flow simulation methods and their applications." Purdue, IN: International Refrigeration and Air Conditioning Conference.
- [67] Lemmon, E.W., M.L. Huber, and M.O. McLinden. 2007. *NIST reference fluid thermodynamic and transport properties (REFPROP), Version 8.0*. NIST Standard Reference Database.
- [68] —. 2013. *NIST reference fluid thermodynamic and transport properties (REFPROP), Version 9.1*. National Institute of Standard and Technology.
- [69] Liao, S. M., and T. S. Zhao. 2002. "Measurements of heat transfer coefficients from supercritical carbon dioxide flowing in horizontal mini/micro channels." *Journal of Heat Transfer* 124 (3): 413-420.
- [70] Ling, J., S. Qian, S. Li, L. Huang, Y. Hwang, and Radermacher. R. 2013. "The winner design of the Max Tech and Beyond competition: A high-efficient residential air-conditioning system." ASHRAE Winter Conference.
- [71] Litch, A. D and Hrnjak, P.S. 1999. *Condensation of ammonia in microchannel heat exchangers*. Air Conditioning and Refrigeration Center.
- [72] Lockhart, R.W., and R.C. Martinelli. 1949. "Proposed correlation of data for isothermal two-phase, two-component flow in pipes." *Chemical Engineering Progress* 45 (1): 39-48.
- [73] Maciaszek, T., and J.C. Micaelli. 1990. "CATHARE phase separation modeling for small breaks in horizontal pipes with stratified flow." *Nuclear Engineering and Design* 124: 247-256.
- [74] Martínez-Ballester, S., J. Corberán, and J. González-Maciá. 2013a. "Numerical model for microchannel condensers and gas coolers: Part I - Model description and validation." *International Journal of Refrigeration* 36: 173-190.
- [75] Martínez-Ballester, S., J. Corberán, and J. González-Maciá. 2013b. "Numerical model for microchannel condensers and gas coolers: Part II-simulation studies and model comparison." *International Journal of Refrigeration* 36: 191-202.

- [76] Martínez-Ballester, S., J.M Corberán, J. González-Maciá, and P.A. Domanski. 2011. "Impact of classical assumptions in modelling a microchannel gas cooler." *International Journal of Refrigeration* 34: 1898-1910.
- [77] McElligott, R, H. 1948. *Investigation of pressure drop through helical coils*. Ph.D Thesis. California Institute of Technology, Pasadena, California.
- [78] McQuiston, F., and J. Parker. 1994. *Heating, ventilating and air conditioning analysis and design*. 4th. New York: Wiley.
- [79] McQuiston, F.C. 1975. "Fin efficiency with combined heat and mass transfer." *ASHRAE Transactions* 81 (1): 350-355.
- [80] Mueller, A.C., and J. Chiou. 1988. "Review of various types of flow mal-distribution in heat exchangers." *Heat Transfer Eng.* 9: 36-50.
- [81] Müller-Steinhagen, H., and K. Heck. 1986. "A simple friction pressure drop correlation for two-phase flow in pipes." *Chemical Engineering Process* 20: 297-308.
- [82] Oberkampf, W.L, and C.J. Roy. 2010. *Verification and validation in scientific computing*. New York: Cambridge University Press.
- [83] Payne, W.V, and P.A. Domanski. 2002. *Potential benefits of smart refrigerant distributors*. Arlington, VA: ARTI.
- [84] Pethkool, S., S. Eiamsa-ard, S. Kwankaomeng, and P. Promvonge. 2011. "Turbulent heat transfer enhancement in a heat exchanger using helically corrugated tube." *International Communications in Heat and Mass Transfer* 38 (3): 340-347.
- [85] Poggi, F., A. Bontemps, H. Macchi-Tejeda, A. Marechal, and D. Leducq. 2009. "Experimental and numerical study of the distribution of a single phase in a small channel heat exchanger." *IIR 1st workshop on refrigerant charge reduction*. Cemagref Antony, France.
- [86] Ranganayakulu, C., K.N. Seetharamu, and K.N. Sreevatsan. 1997. "The effects of longitudinal heat conduction in compact plate-fin and tube-fin heat exchangers using a finite element method." *International Journal of Heat and Mass Transfer* 40 (6): 1261-1277.
- [87] Ren, T., G. Ding, T. Wang, and H. Hu. 2013. "A general three-dimensional simulation approach for micro-channel heat exchanger based on graph theory." *Applied Thermal Engineering* 59: 660-674.

- [88] Rennie, T. J. 2004. *Numerical and experimental studies of a double-Pipe helical heat exchanger*. Ph.D. Thesis, Department of Bioresource Engineering, McGill University, Montreal.
- [89] Rennie, T. J., and G. S. V. Raghavan. 2006. "Experimental studies of a double-pipe helical heat exchanger." *Experimental Thermal and Fluid Science* 29: 919-924.
- [90] Roache, P.J. 1997. "Quantification of uncertainty in computational fluid dynamics." *Annual Reviews of Fluid Mechanics* (29): 123-160.
- [91] Romero-Mendez, R., M. Sen, K.T. Yang, and R.L McClain. 1997. "Effect of tube-to-tube conduction on plate-fin and tube heat exchanger performance." *International Journal of Heat and Mass Transfer* 40 (16): 3909-3916.
- [92] Rousseau, P. G., M. V. Eldik, and G. P. Greyvenstein. 2000. ". Detailed simulation of fluted tube water heating condensers." West Lafayette, IN: International Refrigeration and Air Conditioning Conference.
- [93] Rousseau, P. G., M. V. Eldik, and G. P. Greyvenstein. 2003. "Detailed simulation of fluted tube water heating condensers." *International Journal of Refrigeration* 26: 232-239.
- [94] Saba, N., and R.T. Lahey. 2984. "The analysis of phase separation phenomena in branching conduits." *International Journal of Multiphase Flow* 10: 1-20.
- [95] Saleh, K., O. Abdelaziz, V. Aute, and R. Radermacher. 2012. "New Generation of Air Cooled Heat Exchanger 1 kW Module Design Optimization." Purdue, IN: International Refrigeration and Air Conditioning.
- [96] Saraireh, M. 2012. *Heat transfer and condensation of water vapour from humid air in compact heat exchangers*. Ph.D Thesis. Melbourne, Australia: Victoria University.
- [97] Schmidt, J., and L. Friedel. 1997. "Two-phase pressure drop across sudden contractions in duct areas." *International Journal of Multiphase Flow* 23: 283-299.
- [98] Schwentker, R., and Winkler. 2005. "A simulation and design tool for flat tube, louvered-fin heat exchangers." SAE Technical Paper.
- [99] Schwentker, R.A., V.C Aute, R. Radermacher, and K.B. Mercer. 2005. "Simulation and design tool for microchannel heat exchangers." Hoboken,NJ: Proceedings of Fifth International Conference on Enhanced, Compact and Ultra-Compact Heat Exchangers: Science, Engineering and Technology.

- [100] Seeger, W., J. Reimann, and U. Müller. 1985. "Phase separation in a T-junction with horizontal inlet." London, England : The 2nd International Conf. Multi-phase Flow.
- [101] Seeger, W., J. Reimann, and U. Müller. 1987. "Two-phase flow through small breaks in a horizontal pipe with stratified flow." *Nuclear Engineering and Design* 99: 117-130.
- [102] Shah, M.M. 1979. "A general correlation for heat transfer during film condensation inside pipes." *International Journal of Heat and Mass Transfer* 22: 547-556.
- [103] Shah, M.M. 1982. "Chart correlation for saturated boiling heat transfer: equations and further study." *ASHRAE Transactions* 88 (1): 185-196.
- [104] Shah, R.K., and D.P. Sekulic. 2003. *Fundamental of heat exchanger design*. 1st. Hoboken, NJ: John Wiley & Sons.
- [105] Shah, R.K., and D.P. Sekulic. 2003. *Fundamentals of Heat Exchanger Design*. 2nd. New Jersey: John Wiley & Sons.
- [106] Shao, L.L., L. Yang, C.L. Zhang, and B. Gu. 2009. "Numerical modeling of serpentine microchannel condensers." *International Journal of Refrigeration* 1162-1172: 32.
- [107] Singh, V., V. Aute, and R. Radermacher. 2009. "A heat exchanger model for air-to-refrigerant fin-and-tube heat exchanger with arbitrary fin sheet." *International Journal of Refrigeration* 32 (7): 1724-1735.
- [108] Singh, V., V. Aute, and R. Radermacher. 2008. "Numerical approach for modeling air-to-refrigerant fin-and-tube heat exchanger with tube-to-tube heat transfer." *International Journal of Refrigeration* 31: 1414-1425.
- [109] Srinivasan, V., and R.N. Christensen. 1992. "Experimental investigation of heat transfer and pressure drop characteristics of flow through spirally fluted tubes." *Experimental Thermal and Fluid Science* 5: 820-827.
- [110] Steiner, H., A. Kobor, and L. Gebhard. 2005. "A wall heat transfer model for subcooled boiling flow." *International Journal of Heat and Mass Transfer* 4161-4173: 48.
- [111] Thome, J. 2006. *Engineering Data Book*. 3rd. Wolverine Tube, Inc.

- [112] Tompkins, D.M., T. A. Newell, and Hrnjak P. S. 2002. *Single phase, two-phase modeling; X-ray visualization for a microchannel manifold distribution system*. ACRC, University of Illinois, Technical Report 206.
- [113] Traviss, D.P, W.M. Rohsenow, and A.B. Baron. 1973. "Forced convection condensation inside tubes: a heat transfer equation for condenser design." *ASHRAE Transactions* 79 (1): 157-165.
- [114] Tuo, H., A. Bielskus, and P. Hrnjak. 2012. "An experimentally validated modeling of refrigerant distribution in a parallel microchannel evaporator." Chicago, IL: ASHRAE Winter Conference.
- [115] Tuo, H., A. Bielskus, and P.S. Hrnjak. 2012. "An experimentally validated model of refrigerant distribution in a parallel microchannel evaporator." ASHRAE Winter Conference.
- [116] Vist, S. 2003. "Two-phase flow distribution in heat exchanger manifolds." Ph.D. Thesis, Norwegian University of Science and Technology.
- [117] Vist, S., and J. Pattersen. 2004. "Two-phase flow distribution in compact heat exchanger manifolds." *Experimental Thermal Fluid Science* 28: 209-215.
- [118] Watanabe, M., M. Katsuta, and K. Nagata. 1995. "Two-phase flow distribution in multi-pass tube modeling serpentine type evaporator." Proceedings of the ASME/JSME Thermal Engineering Conference.
- [119] Yashar, D.A., P.A. Domanski, and H.H. Cho. 2011. "An experimental and computational study of approach air distribution for a finned-tube heat exchanger." *HVAC&R Research* 17: 76-85.
- [120] Yashar, D.A., P.A. Domanski, and H.H. Cho. 2014. "An experimental and computational study of approach air distribution for slanted and A-shaped finned-tube heat exchangers." *HVAC&R Research* (20): 498-507.
- [121] Yin, J.M., C.W. Bullard, and P.S. Hrnjak. 2001. "R-744 gas cooler model development and validation." *International Journal of Refrigeration* 24: 692-701.
- [122] Yun, R., Y. Kim, and C. Park. 2007. "Numerical analysis on a microchannel evaporator designed for CO<sub>2</sub> air-conditioning systems." *Applied Thermal Engineering* 27: 1320-1326.
- [123] Zhang, Z., and Y.Z. Li. 2003. "CFD simulation on inlet configuration of plate-fin heat exchangers." *Cryogenics* 43: 673-678.

- [124] Zhao, Y., M.M. Ohadi, and R. Radermacher. 2001. *Microchannel heat exchangers with carbon dioxide*. ARTI-21CR/10020-01.
- [125] Zhu, D., H. Xu, Y. Sun, and B. Qi. 2010. "Numerical heat transfer analysis of laminar film condensation on a vertical fluted tube." *Applied Thermal Engineering* 30: 1159-1163.
- [126] Zilio, C, L. Cecchinato, M. Corradi, and G. Schiochet. 2007. "An assessment of heat transfer through fins in a fin-and-tube gas cooler for transcritical carbon dioxide cycles." *HVAC&R Research* 13 (3): 457-469.
- [127] Zou, Y., and P.S. Hrnjak. 2013. "Experiment and visualization on R134a upward flow in the vertical header of microchannel heat exchanger and its effect on distribution." *International Journal of Heat and Mass Transfer* 62: 124-134.
- [128] Zou, Y., and P.S. Hrnjak. 2013. "Refrigerant distribution in the vertical header of the microchannel heat exchanger -measurement and visualization of R410A flow." *International Journal of Refrigeration*. doi:10.1016/j.ijrefrig.2013.04.021.